Quantum Mechanical and Synthetic studies of Coordination and Organometallic Complexes of Lanthanides and other Heavy Metals

Maria Rosa Russo

University College London

Thesis submitted for the degree of Ph.D. in Chemistry

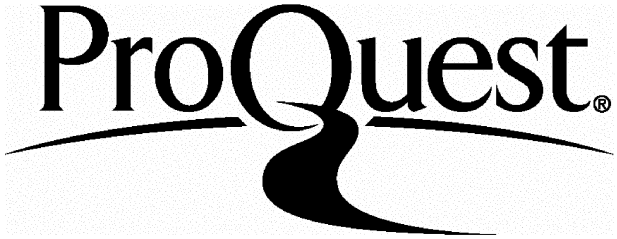

Abstract

This thesis presents an investigation of the structure and bonding of heavy element complexes. In particular, the thesis contains computational analyses of the steric and electronic factors influencing the structure and bonding of complexes containing the lanthanides or other heavy metals. In addition the thesis presents synthetic investigations related to some of these computational issues.

Density Functional Theory, with the inclusion of scalar-relativistic corrections, has been used to investigate the bonding of Lanthanides and other heavy metals in a series of complexes with ligands ranging from polihapto-π-donors such as cyclopentadienyls, to monodentate σ-bonding ligands such as chalcogenolates and cyanides. These calculations provide a rationalization of the previously proposed/determined geometries of $[(CN)_5PtTl(CN)_n]^{n-}$ (chapter 3) and lanthanide chalcogenolates (chapter 4). These latter studies provide a detailed insight into the nature and bonding of lanthanide metals and allow rationalization of observed structural features in simple electrostatic terms.

Chapter 5 describes laboratory experiments aimed at the preparation of lanthanide complexes containing 1,3 dialkylated calix[4]arenes as ancillaries. Spectroscopic and structural evidence for a number of complexes is presented together with several attempts to develop improved starting materials for lanthanide chemistry including alkyl, aryls and amides.

Acknowledgement

Time has come eventually to express my thanks to all the people which have contributed, in one way or another, to my Ph.D. experience.

I wish to thank my supervisors Nik and Andrea for their unconditional support, a huge number of good advices and, among other things, for rescuing me from the alluring prospect of a 100% computational project. I have greatly enjoyed the interesting discussions and appreciated the effort they have made to make my Ph.D. project as successful as it has been.

Many thanks to my fellow group mates (also known as 'the ladies', i.e. Katherine, Linnea, Emma, Natalie and, special addition from upstairs lab, Sarah) for being always there, in good and bad times!

Dickon's loud and cheerful music has definitely made a difference to my life in G25 (especially on a boring friday afternoon) and will be utterly missed (not to talk about his singing). There's only one Dickon (...and I'm glad about it!).

I owe a special token of gratitude to Gisela... who has pointed me the way to the light (latex) and saved me from darkness (word).

My heartfelt thanks to Erasmo for his support and for being special to me in many different ways.

Contents

1 The Rare Earth Elements **1**

1.1 General Overview 2

1.2 Physical Properties 3

1.3 Chemistry 7

1.4 Description of following chapters 11

2 Theoretical Considerations **12**

2.1 General Overview 13

2.2 *Ab Initio* Methods 15

2.3 Density Functional Theory (DFT) 19

2.4 The Kohn-Sham Method 21

2.5 Exchange-Correlation Functionals 24

2.6 Relativity in Chemistry 30

3 Computational Investigation of an unsupported Pt-Tl bond. **36**

3.1 Introduction 37

3.2 Computational Details 40

3.3 Results and discussion 41

3.3.1 Unsolvated Complexes 41

3.3.2 Solvated complexes 44
3.3.3 Other Factors affecting the Pt-Tl Bond Length 47
3.3.4 Position of CN_A 49
3.4 Conclusions 52

4 Bonding and Bending in Lanthanide Chalcogenolate Complexes. 53
4.1 Introduction 54
4.2 Computational Details 59
4.3 Results and Discussion 61
4.3.1 The equilibrium structures 61
4.3.2 Analysis of bending at the chalcogen atom in $[LaCp_2ER]$ (E = O, S; R = H, Me, Ph) 67
4.3.3 Analysis of bending at the chalcogen atom in $[LuCp_2EPh]$ (E = O, S). 78
4.4 Conclusions 81

5 Exploratory studies on the synthesis of functionalizable trivalent lanthanide complexes with calix[4]arene ligands 84
5.1 Introduction 85
5.1.1 The Calixarenes 85
5.1.2 Coordination chemistry of the calixarenes 87
5.1.3 Aspects of the coordination and organometallic chemistry of lanthanides 94
5.2 Results and Discussion 99
5.2.1 Synthesis of tBu-calix[4]arene and calix[4]arene derivatives . . 101
5.2.2 Synthesis of lanthanide starting materials 102

5.2.3 Synthesis of Calixarene complexes 108
5.3 Conclusions 121
5.4 Experimental 123
5.4.1 Reagents and apparatus 123
5.4.2 Synthesis of starting materials 123
5.4.3 Synthesis of Lanthanide Amides 127
5.4.4 Synthesis of Lanthanide Organometallics 130
5.4.5 Synthesis of Calixarene Complexes 133

List of Figures

1.1 Ionization energies for the oxidation of lanthanide atoms to +3 and +4 ions. . . 4

1.2 Ionization energies for the oxidation of Ln^{+2} to Ln^{+3}. 5

3.1 Proposed structures for complexes **I-IV**. These structures were used as starting points in our geometry optimisations. 38

3.2 Calculated structures for complexes **I-IV** 41

3.3 Calculated structures for solvated complexes **Ih-IIIh** 44

3.4 Calculated structures for complexes **Is** 48

3.5 Schematic representation of complexes **I'** and **Ih'**. 50

4.1 Schematic representation of the bis-trispyrazolylborate-lanthanide-chalcogenolate complexes (ref 39). 56

4.2 Schematic representation of the bis-cyclopentadienyl-lanthanide-chalcogenolate complexes. α is the Cp ring centroid-lanthanide-ring centroid angle; β is the angle subtended by the lanthanide, the chalcogen and the carbon atom bound to the chalcogen (or the hydrogen atom bound to the chalcogen for the model compounds with terminal EH). Potential energy curves were calculated for vertical (v) and horizontal (h) bending of the R group in the x-z and x-y planes respectively. 58

4.3 Valence molecular orbital energy level diagram for [$LaCp_2EMe$] (E =O, S). . . . 65

4.4 Total molecular bonding energy for [$LaCp_2OPh$] as a function of the torsional angle φ, corresponding to rotation of the OPh fragment around the La–O axis. Energy curve is scaled to an arbitrary value of 0 kJ/mol at 0^o. 67

4.5 Total molecular bonding energy as a function of the La–E–C(H) angle β for [$LaCp_2ER$] (E = O, S; R = H, Me, Ph). Energy curves are scaled to an arbitrary value of 0 kJ/mol at 180^o. 68

4.6 La–C(H) electrostatic interaction energy as a function of the La–E–C(H) angle β for [$LaCp_2ER$] (E = O, S; R = H, Me, Ph). Energy curves are scaled to an arbitrary value of 0 kJ/mol at 180^o. 74

4.7 La–C(H) electrostatic interaction energy as a function of the La–E–C(H) angle β for [$LaCp_2ER$] (E = O, S; R = Me, Ph), where all atoms have basis set III except La which has basis set IV. Energy curves are scaled to an arbitrary value of 0 kJ/mol at 180^o. 76

4.8 La–C(H) electrostatic interaction energy as a function of the La–E–C(H) angle β for [$LaCp_2ER$] (E = O, S; R = Ph), where atomic charges have been evaluated via Hirshfeld and Voronoi analysis. Energy curves are scaled to an arbitrary value of 0 kJ/mol at 180^o. 77

5.1 One pot synthesis of calixarenes (n = 4-8). 85

5.2 Cone conformation of t-butylcalix[4]arene (R = ^{t}Bu). The phenolic oxygens constitute the lower rim of the cone, while the ^{t}Bu groups are at the upper rim. . . 86

5.3 Schematic representation of the first reported lanthanide calixarene complexes, ref 177 and 178 (the drawing is simplified by omitting coordinating solvent molecules and the phenolic units of the ligand). 89

5.4 Schematic representation of a lower rim substituted calix[4]arene bimetallic complex (ref 202). Note that the pendant tridentate groups are rejected by the metal in favour of bridging phenoxide and solvent o-donors. (The drawing is simplified by omitting the phenolic units of the ligand.) 90

5.5 Typical lanthanide bimetallic complex with bridging calixarene ligands (ref 190). (The drawing is simplified by omitting the phenolic units of the ligand.) 91

5.6 Schematic representation of mononuclear lanthanide calixarene complexes (ref 174 and 203) (the drawing is simplified by omitting the phenolic units of the ligand). 92

5.7 Schematic representation of the first mononuclear functionalizable lanthanide cali[4]xarene complex, ref 207 (the drawing is simplified by omitting the phenolic units of the ligand). 93

5.8 Schematic representation of a 2:1 functionalizable lanthanide calix[6]arene complex, ref 208 (the drawing is simplified by omitting the phenolic units of the ligand). 93

5.9 Metathesis reaction of an alkaline metal salt of the calix[4]arene ether with a lanthanide halide (M = Na, K; X = Cl, Br, I). 100

5.10 Protonolysis reaction of protonated calix[4]arene ether with lanthanide complex (L′ = amide, alkyl, aryl). 100

5.11 Synthesis of tBu-calix[4]arene. 101

5.12 Synthesis of 1,3-dialkyl-tBu-calix[4]arene ether (R = Me, ^{i}Pr). 102

5.13 **a)** X-ray crystal structure and **b)** schematic representation of $[Na_2L^{iPr}]_2$. 110

5.14 Schematic representation of the 1:2 complex $LnH\{L^R\}_2$ and the 2:3 complex $Ln_2L^R_3$. 117

5.15 Schematic representation of the 1:1 complex $Y\{L^{Me}NPh_2\}$. 118

5.16 Schematic representation of the 1:1 complex LnL^RCp. 120

List of Tables

1.1 Crystallographic radii (Å) for 6-coordinate lanthanides and related ions. 6

1.2 Typical reaction pathways for the synthesis of lanthanide complexes. 7

3.1 Selected bond lengths in optimised complexes **I-IV** and comparison with experimental Pt-Tl distance. 42

3.2 Selected experimental and calculated vibrational wavenumbers for complexes **I-IV**. 43

3.3 Selected bond lengths for optimised complexes **Ih-IIIh** and vibrational wavenumbers for complex **Ih**. 45

3.4 Selected bond lengths in optimised complex **Is** and comparison with experimental Pt-Tl distance. 48

3.5 Calculated bond lengths and total molecular bonding energies for complexes **I**, **Ih**, **I'** and **Ih'**. 50

4.1 Optimised geometric parameters for the calculated equilibrium structures. See Fig. 4.2 for definition of α and β. d is the metal-Cp ring centroid distance. . . . 62

4.2 Experimental bond lengths and angles for some selected bis-cyclopentadienyl-lanthanide-chalcogenolate complexes. 63

4.3 Calculated Mulliken charges on the lanthanide and chalcogen atom, and Mulliken overlap populations for the Ln–E bond. 64

4.4 Values of the Cp–La–Cp angle α at $\beta = 180$ and 120^o, in [$LaCp_2ER$] (E = O, S; R = H, Me, Ph) 70

4.5 Values of the Mulliken overlap population (e) of the La–E bond at $\beta = 180$ and 120^o. 72

4.6 Values of Mulliken charges of the lanthanum, chalcogen and carbon (hydrogen) atom bound to the chalcogen, at $\beta = 180$ and 120^o 72

5.1 Elemental microanalysis found and calculated for $Y\{NPh_2\}_3$, $Y\{NPh_2\}_3(thf)_2$ and $Y\{NPh_2\}_3(thf)_3$. 104

5.2 Attempts to transmetallation reactions. 108

5.3 Summary of reactions between lanthanide trimethylsilyl amides and calixarene ligands 113

5.4 Comparison of ^1H NMR spectra of H_2L^{Me} and the product obtained from reaction **a**=**b**. 114

5.5 Comparison of ^1H NMR spectra of H_2L^{iPr}, and the products of reactions **c** and **e**. 115

5.6 Elemental microanalysis (found and calculated) for the products of reactions **a** and **d** (see Table 5.3) 116

5.7 Summary of reactions between lanthanide trimethylsilyl amides and calixarene ligands 119

5.8 Comparison of ^1H NMR spectra of H_2L^{iPr}, and the products of reactions **b** and **c**. 120

Chapter 1

The Rare Earth Elements

1.1 General Overview

Being lanthanides the main target of the work presented in this thesis, a general introduction on their physical and chemical properties is given in this chapter.

The lanthanides (or rare earth metals) are a series of 14 elements, following lanthanum and up to lutetium, whose position in the periodic table corresponds to the filling of the $4f$ electronic shell. Although the members of the lanthanide series were isolated and identified at the beginning of the 19^{th} century it is only in the past few decades that the attention of chemists has been focused on this area of the periodic table. Despite the initial idea that lanthanide chemistry would not be as interesting as transition metal chemistry it was in fact realized that the rare earth elements have a combination of physical properties (including size, type of valence orbitals, ionization potential and predisposition to high magnetic anisotropy) which make their chemistry a unique and fascinating area of research for both experimentalists[1–7] and theoreticians.[7–14]

Due to the peculiarities of the f electronic functions, the lanthanides display a chemical and physical behaviour which is quite distinct from main group and transition metals, whereas they show some similarities with the actinide metals, whose atomic configuration involves the filling of the $5f$ shell. Even though the group III metals scandium, yttrium and lanthanum are not properly f elements, their electronic structure and ionic radii are such that their chemical behaviour resembles quite closely that of the f elements and they are therefore generally included in discussions regarding lanthanide chemistry.

1.2 Physical Properties

Ionization Potentials and Oxidation States

There are two typical ground state electronic configurations for the lanthanide atoms, $[Xe]4f^{n+1}5d^{0}6s^{2}$ and $[Xe]4f^{n}5d^{1}6s^{2}$ (n=0-14 from La to Lu), the first being most favourable for all elements except for Ce, Gd and Lu.

Among the possible oxidation states the trivalent (with electronic configuration $[Xe]4f^{n}5d^{0}6s^{0}$) is the most stable for all lanthanides, although divalent and tetravalent states are also possible for some elements. The relative stability of the lanthanides as 3+ ions is normally explained by their ionization potentials. The ionization potentials for the two processes:

$$Ln(g) \longrightarrow Ln^{+3} + 3e^{-} \tag{1.1}$$

$$Ln(g) \longrightarrow Ln^{+4} + 4e^{-} \tag{1.2}$$

are shown in Fig 1.1, and comparing the two curves it is clear that while oxidation to the trivalent state requires an amount of energy which is recoverable through chemical bond formation, oxidation to tetravalent state requires a much higher energy. The tetravalent state is however accessible for cerium, and in particular conditions for praseodymium, neodymium and terbium, whose value for the energy of process 1.2 is smaller than that of the other lanthanides.

The possibility of isolating a divalent lanthanide ion is related to the ionization potential for the process

$$Ln^{+2}_{(aq)} \longrightarrow Ln^{+3}_{(aq)} + 1e^{-} \tag{1.3}$$

The solvation energy of the 2+ and 3+ ions are much smaller than the energy

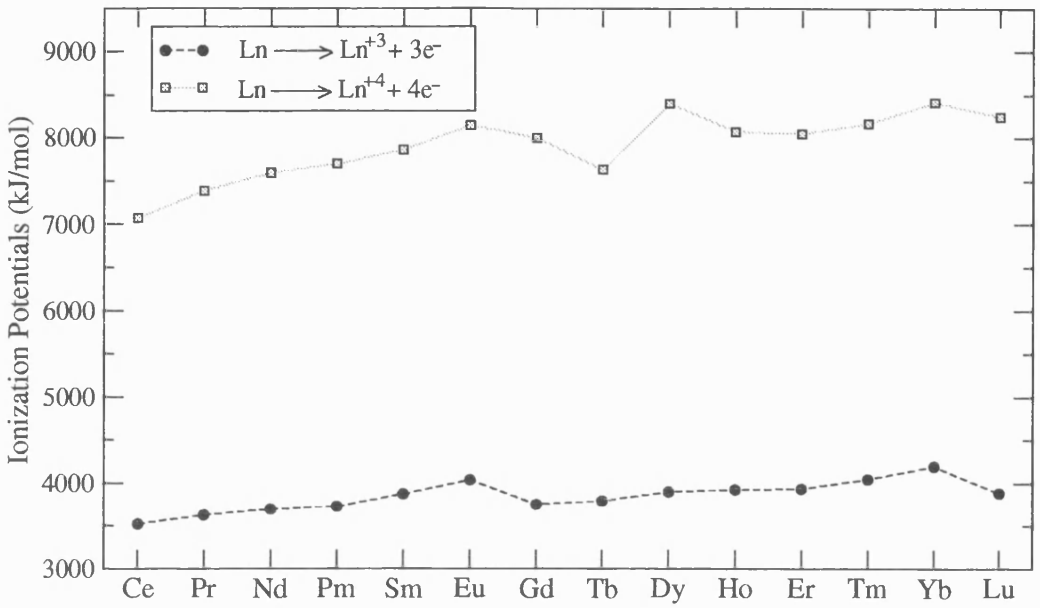

Figure 1.1: Ionization energies for the oxidation of lanthanide atoms to +3 and +4 ions.

associated with the ionization process,

$$Ln^{+2} \longrightarrow Ln^{+3} + 1e^{-} \tag{1.4}$$

therefore, to a good degree of approximation, it is the 2+ → 3+ ionization potential in the gas phase which determines the oxidation state of the lanthanide ion. The trend of this ionization potential within the lanthanide series is illustrated in Fig 1.2, and shows that the values are higher for europium and ytterbium, and (to a smaller extent) also for samarium and thulium. As a consequences these elements will be less easily oxidized to 3+ ions and therefore more easily isolated in the 2+ state.

Lanthanide Contraction

A striking difference between transition metals and lanthanides is the trend of metal sizes going across the series. For transition metals the size of the elements does not decrease monotonically with increasing atomic number. By contrast, the lanthanides

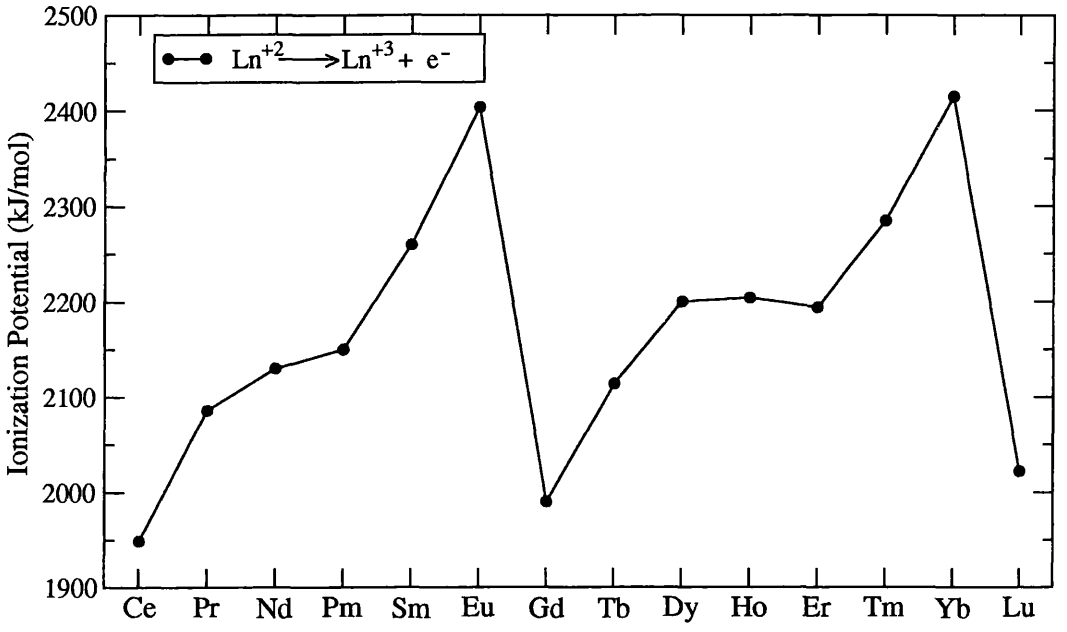

Figure 1.2: Ionization energies for the oxidation of Ln^{+2} to Ln^{+3}.

exhibit a steady decrease in atomic* and ionic radius on going through the series from La to Lu. This phenomen is known as the lanthanide contraction. One of the consequences of the lanthanide contraction is its effect on the radii of third row transition metals, which are comparable in size to their second row analogues, and often exhibit similar chemistry.

The ionic radii of the trivalent lanthanides and related ions given by Shannon,[15] are summarized in Table 1.1. A recent analysis of experimental and theoretical Ln-O bond length for several trivalent lanthanide complexes has found that the best empirical fit to describe the lanthanide contraction is a quadratic decay of the ionic radius with atomic number.[16] However, no physical explanation has yet been found for such observed correlation.

The lanthanide contraction has been explained classically by the failure of the

*Europium and ytterbium metals exhibit somewhat greater atomic radii with respect to the other lanthanides. However this is rather due to the fact that these two metals are best regarded as Ln^{2+} ions with two electrons per atom devoted to metallic bonding, instead of Ln^{3+} ions as it is the case for the other lanthanide metals.

Table 1.1: Crystallographic radii (Å) for 6-coordinate lanthanides and related ions.

Sc^{3+}	Y^{3+}	La^{3+}	Ce^{3+}	Pr^{3+}	Nd^{3+}	Pm^{3+}	Sm^{3+}	Eu^{3+}
0.745	0.901	1.132	1.010	0.990	0.983	0.970	0.958	0.947
Gd^{3+}	Tb^{3+}	Dy^{3+}	Ho^{3+}	Er^{3+}	Tm^{3+}	Yb^{3+}	Lu^{3+}	
0.938	0.923	0.912	0.901	0.890	0.880	0.868	0.861	

$4f$ orbitals to effectively shield the outer electron shells. Increasing atomic number therefore results in a higher effective nuclear charge and consequent smaller radius. However several papers dealing with the importance of relativity in the description of systems containing heavy metals have shown that relativistic effects have a significant influence on the properties of the f orbitals and therefore on the extent of the lanthanide contraction, which has been interpreted as a subtle combination of both relativistic effects and shell-structure effects.[13,17]

1.3 Chemistry

The increasing number of 4 f electrons as the lanthanide series is crossed does not generally result in a significant change of chemical properties, particularly for the Ln^{3+} ions. The $4f$ electrons are so well shielded from ligands by the outer $5s$ and $5p$ filled shells that the observed chemical behaviour is very similar going across the lanthanide series, despite the different electronic configurations of the elements. Furthermore, the limited radial extension of the $4f$ orbitals, and their consequent poor overlap with ligand-based orbitals is responsible for lanthanide chemistry being viewed as mainly ionic.[†] Thus the formation and structure of complexes is governed mostly by electrostatic and steric factors, with differences across the series due mainly to increasing charge over radius ratio of the metal ion. The chemistry of trivalent lanthanides can therefore be expected, to a first approximation, to be that of a large 3+ ion (in this respect showing many similarities to the chemistry of Sc^{3+}, Y^{3+}, and La^{3+}) with typical coordination numbers being around 8-12. Common reaction pathways used in the synthesis of lanthanide complexes are illustrated in Table 1.2.

Table 1.2: Typical reaction pathways for the synthesis of lanthanide complexes.

Reaction Type	Ln Starting Material	Ligand	Products
Metathesis	LnX_3 (X = Cl, I)	ML′ (M = Li, Na, K)	LnL'_3 + MX
Protonolysis	LnR_3 (R = basic ligand)	HL′ (HL′ = acidic ligand)	LnL'_3 + HR
Transmetallation	Ln (metal)	HL′ (HL′ = acidic ligand)	LnL'_3 + H_2

[†]Another consequence of the poor overlap between metal- and ligand-based orbitals is the small crystal field effects observed for lanthanide complexes compared to those observed for transition metal complexes.

Due to their large size, rather electropositive character, and quite high affinity for hard bases, the coordination chemistry of lanthanides with hard, oxygen and nitrogen donor ligands is well established, and a number of stable compounds are known with both neutral (water, ethers, ammonia) and negatively charged (aryloxides[6,18–20] and amides[6,21–24]) ligands. On the other hand the low affinity for less electronegative, softer ligands, and the difficulty of covalent interactions, make the lanthanides very inert with respect to neutral molecules like phosphines, alkenes and alkynes. Therefore for many years the synthesis of organolanthanide complexes has been dominated by the use of the negatively charged, polyhapto, π-donor cyclopentadienyl and cyclooctatetraenyl ligands.[3,25] However, whith improved techniques being developed for the synthesis of new negatively charged, soft ligands, it has been possible to isolate for example σ-bonded lanthanide alkyls,[26–30] and complexes with phosfides,[31–36] selenolate and tellurolate ligands.[37–47] Because organometallic species can undergo intramolecular decomposition via β-hydrogen elimination of alkenes, the choice of alkyls is usually limited to those without a β-hydrogen.

One problem often encountered in lanthanide chemistry (which arises from the highly polarized nature of the metal-ligand bond) is the high reactivity towards insertion of molecular oxygen. This most likely results in the formation of a peroxide intermediate species which can subsequently give rise to different decomposition products. Lanthanide complexes are also easily hydrolized by trace amounts of water and moisture which can protonate the strongly basic ligands and replace them with OH^-. These problems are usually overcome by handling lanthanide complexes in an inert nitrogen atmosphere, and by the use of perfectly dried solvents and starting materials.

The synthesis of both lanthanide neutral homoleptic compounds (i.e. where

the metal is surrounded by a number of equivalent ligands), as well as of complexes in which the metal is forced to be in a low coordination environment, is a rather challenging task. The metal tends to expand its coordination sphere either by further coordination of an anionic ligand (resulting in the anionic tetrakis lanthanide -ate complexes), by coordination of solvent molecules, or by formation of oligomers via bridging ligands. The stability of monomeric lanthanide homoleptic complexes has usually been achieved by use of bulky anionic ligands which satisfy the charge balance and block decomposition pathways by completely saturating the coordination sphere of the metal. With the bulky 2,6-di-t-butylphenoxide[18] and the bis-trimethylsilyl-amide[21] for example, the corresponding mononuclear homoleptic tris-aryloxide and tris-amide are easily formed, and no solvent coordination, oligomerization or contamination by -ate complexes have been reported. Similarly the first neutral homoleptic alkyl has been isolated as a monomeric species using the bulky bis-trimethylsilyl methyl ligands.[30] The use of trimethylsilyl (TMS) substituted alkyls and amides, has also proved to be a good strategy for stabilising lanthanide complexes by intramolecular Siβ–Cγ agostic interactions.[48]

While tetravalent lanthanide chemistry is mostly limited to a small number of cerium(IV) inorganic compounds, there is a growing interest in the synthesis of divalent and low valent[‡] lanthanide complexes.[2,5] They have in fact shown to have an unusual reactivity towards neutral molecules like dinitrogen,[49–53] isocarbonyl,[54,55] alkenes and alkynes.[56,57]

Beyond these most commonly observed oxidation states there has been in the recent years a sudden growth in the chemistry of the lanthanide in "non classical" oxidation states.[2,58] Some remarkable zerovalent lanthanide sandwich complexes

[‡]The usefulness of such species is indicated by the fact that divalent samarium iodide is routinely used as a selective reducing agent in organic synthesis.

with a surprising thermodynamical stability have been obtained with neutral η^6-arene ligands,[4,59,60] suggesting that some degree of covalency might indeed play a significant role in such low valent systems.

1.4 Description of following chapters

In chapter 2 I will give a description of the theoretical background and the computational methods used within this thesis, with particular emphasis on density functional theory and relativistic treatment of heavy elements. A brief account of computational investigations on lanthanide and actinide is also given in this chapter.

Chapter 3 describes the computational study of a series of Pt-Tl complexes. The calculated electronic and geometric structure of the complexes are compared with experimental observations in order to support the proposed structures. The platinum-thallium system was chosen at the beginning of the project in order to allow for training on the use of the program package and the computational techniques adopted.

The original aim of the Ph.D. project was to synthesize calixarene-supported lanthanide complexes (and in particular lanthanide bimetallics supported by encapsulating bis calixarene ligands) and investigate their electronic and geometric structures by means of spectroscopical and computational analysis. However, due to problems encountered with the experiments, it was decided to focus the computational analysis on other systems.

Chapter 4 presents therefore a computational investigation of several cyclopentadienyl-supported lanthanide chalcogenolates, with an analysis of the lanthanide-chalcogen bond and the factors influencing the geometric structures of these complexes.

Chapter 5 describes experimental work aimed at the synthesis of calixarene-supported lanthanide complexes. Several attempts at the synthesis of new tris homoleptic lanthanide starting materials are also presented.

Chapter 2

Theoretical Considerations

In this chapter a brief overview on the historical development of Density Functional Theory and its current state is presented. It follows a short description of *ab Initio* methods (for comparative purposes) and a more detailed discussion of different aspects of Density Functional Theory (principles, Kohn-Sham method, exchange-correlation functionals). The final section describes the effects of relativity at the atomic and molecular level and the different approaches to include relativity in the calculation of electronic properties, specifically those of the $4f$ elements.

2.1 General Overview

The origin of Density Functional Theory can be traced to the early part of the 20^{th} century when Fermi[61] and Thomas[62] proposed an approximate model to describe the electron distribution in space. This model, however, was unable to reproduce molecular properties (such as bonding between two atoms) and was less accurate than existing models in calculating the electronic structure of atoms. The first step towards the development of the density functional method, as it is known today,[63] was taken in 1964-65, when the theory and methodology of density functional calculations were published in the landmark papers by P. Hohenberg, W. Kohn, and L. J. Sham.[64,65] Although physicists soon applied the new theory using the local density spin approximation (LSDA) to study solids with considerable success,[66] it took a while for chemists to apply DFT to the calculation of molecular properties. This was partly due to failure of the LSDA to give accurate results for molecular dissociation energies, but with the introduction of gradient-corrected functionals in the mid-'80s[67] this problem was solved, and molecular DFT calculations experienced a huge growth over the next few years.

One of the reasons for the success of DFT and its wide application to the study of

chemical systems is its short computational time compared with other approaches. Comparison with correlated methods such as coupled cluster (CC) or configuration interaction (CI) shows that these methods generally achieve more accurate results than DFT, but being computationally very demanding, they are still limited to the study of comparatively small systems. Hartree-Fock calculations require roughly the same computational time, but unlike DFT electron correlation is not intrinsically included in the Hartree-Fock method and has to be computed separately.

The concept of electron density (which in the density functional approach replaces the many-electron wavefunction) is also particularly suited to the description of well established concepts in chemical structure and reactivity[68] (such as chemical potential, polarizability, hardness/softness and many others) and DFT is therefore appropriate for the investigation of chemical systems.

Although the Kohn-Sham equations (a set of equations which allows the self consistent calculation of the electron density for a given electronic system) are in principle exact, the insufficient knowledge on the form of the exchange-correlation potential for systems of interacting electrons leads inevitably to approximate solutions. However the currently available forms of exchange-correlation potential are in most cases accurate enough for the treatment of chemical systems, with errors of a few kcal/mol for binding energies.[69] Moreover there has been a recent interest in the search for exchange correlation functionals based on a deeper understanding of their nature and properties,[70–74] which if successful would reduce the level of approximation in density functional methods to the choice of basis functions.

2.2 *Ab Initio* Methods

The Schrödinger equation provides the basis for describing in principle any physical system at a non-relativistic* quantum mechanical level. Its time-dependent, and time-independent forms (in atomic units) are respectively:†

$$\hat{H}\Psi = i\frac{\delta\Psi}{\delta t} \tag{2.1}$$

$$\hat{H}\Psi = E\Psi \tag{2.2}$$

where $\hat{H}$ is the Hamiltonian energy operator, Ψ is the wavefunction associated to the system, and E is the energy of the system. The wavefunction has a central role in quantum mechanics since all the physical observables associated with a system can be calculated from its wavefunction through the corresponding operator (i.e. the observable is given by the expectation value of the associated operator over the wavefunction). An example is shown in equation 2.3, where the total energy is calculated from the corresponding Hamiltonian operator.

$$E[\Psi] = \frac{\langle\Psi|\hat{H}|\Psi\rangle}{\langle\Psi|\Psi\rangle} \tag{2.3}$$

The general form of the Hamiltonian operator for a molecular system is given by:

$$\hat{H} = \hat{T}_e + \hat{T}_n + \hat{V}_{ne} + \hat{V}_{ee} + \hat{V}_{nn} \tag{2.4}$$

where the terms on the right-hand side of the above equation are respectively the electronic kinetic energy operator, the nuclear kinetic energy operator, the potential

*In the following sections only non-relativistic methods will be treated, whereas relativistic effects and their possible treatment will be discussed in section 2.6.

†The following conventions will be adopted in mathematical equations: vectors will be represented as bold text, operators as $\hat{A}$, and square brackets will be used to designate functional dependency.

energy operator of nuclei-electron attraction, and the potential energy operator for electron-electron and nucleus-nucleus repulsion.

The Born-Oppenheimer approximation is generally applied to quantum mechanical calculations of electronic properties. Since the time scale of electron motion is much smaller than that of nuclei, it is assumed that electrons experience a field generated by fixed nuclei. This simplifies the form of the molecular Hamiltonian as it allows us to separate the motion of electrons from that of nuclei. Therefore the electronic Hamiltonian for a N-electron molecular system (in atomic units) has the following form.

$$\hat{H} = \hat{T} + \hat{V}_{ne} + \hat{V}_{ee} \tag{2.5}$$

The electronic kinetic energy operator has the form,

$$\hat{T} = \sum_{i=1}^{N} -\frac{1}{2}\nabla_i^2 \tag{2.6}$$

where ∇_i^2 is the Laplacian operator for electron i. The second term in equation 2.5 is the external potential operator, which if no other potential is present corresponds simply to the operator for the electrostatic nuclei-electron interaction:

$$\hat{V}_{ne} = \sum_{i=1}^{N} v(\mathbf{r}_i) = \sum_{i=1}^{N} \sum_{\alpha} \frac{Z_\alpha}{r_{i\alpha}} \tag{2.7}$$

where $v(\mathbf{r}_i)$ is the electrostatic potential experienced by electron i at point $\mathbf{r}$, Z_α is the nuclear charge of nucleus α and $r_{i\alpha}$ is the nucleus-electron distance. The operator for the electron-electron repulsion is given by.

$$\hat{V}_{ee} = \sum_{j} \sum_{i>j} \frac{1}{r_{ij}} \tag{2.8}$$

Note that in the formulation of the electronic Hamiltonian, the kinetic energy and electron repulsion operators are of a general form and are only determined by

the number of electron N. Therefore given the number of electrons, the Hamiltonian of the system is simply defined by the form of the electrostatic potential $v(\mathbf{r})$. Consequently N and $v(\mathbf{r})$ determine the Hamiltonian, the wavefunction, and all other properties of the system.

Unfortunately for systems of interacting electrons (i.e. many-electrons atoms and molecules) the time-independent Schrödinger equation can not be solved analytically, and only numerical approximate solutions are possible. Nevertheless, several *ab initio*[‡] computational methods have been devised, which provide increasingly more refined numerical solutions. All *ab initio* methods for the study of atomic and molecular systems (Hartree-Fock, Configuration Interaction, Coupled Cluster, etc.) are based on the calculation of an approximate wavefunction from which all other observables are derived.

The calculation of atomic and molecular wavefunctions depends crucially upon the definition of a trial many-electron wavefunction (usually constructed from many one-electron orbitals), and a suitable Hamiltonian. In the Hartree-Fock method for example, the Hamiltonian (known as Fock operator) contains a Coulomb and an exchange integral (K and J respectively) which depend on the basis set orbitals which define the wavefunction. The wavefunction is then optimized through a series of iterative processes following a Self-Consistent-Field procedure, so as to minimize the ground state energy of the system.[§]

There are different possible ways to approximate the Hamiltonian and different forms to express the wavefunction (according to the different *ab initio* methods) and these eventually determine the level of refinement of the corresponding numerical

[‡]i.e. from first principle, therefore without the use of empirical data.

[§]The Variational Principle ensures that the energy calculated with any trial wavefunction is always greater than the real ground state energy of the system.

solutions. For more details on typical *ab initio* methods see for example "Computational Chemistry"[75] and "Molecular Quantum Mechanics".[76]

2.3 Density Functional Theory (DFT)

In the same way that the electronic wavefunction plays a central role in *ab initio* methods, the electron probability density (or electron density) plays a central role in Density Functional Methods. Considering an electronic system, the electron density ρ for a given state is defined as the number of electrons per unit volume in that state. Integration over all space of the electron density for a given electronic system gives the total number of electrons for that system.

$$N = \int \rho(\mathbf{r}) d\mathbf{r} \tag{2.9}$$

The basic concepts on which Density Functional Theory is built are summarized in the first and second Hohenberg-Kohn theorems.[64] They quite simply demonstrate that:

1. The external potential $v(\mathbf{r})$ is determined, within a trivial additive constant, by the ground state electron density $\rho_0(\mathbf{r})$.

2. For a trial density $\tilde{\rho}(\mathbf{r})$, such that $\tilde{\rho}(\mathbf{r}) \geq 0$ and $\int \tilde{\rho}(\mathbf{r}) d\mathbf{r} = N$,

$$E_0 \leq E[\tilde{\rho}]$$

   where $E[\tilde{\rho}]$ is the energy calculated as a functional[¶] of $\tilde{\rho}(\mathbf{r})$.

We have already seen that the number of electrons in a system is uniquely determined by the electron density (see equation 2.9). Since the electrostatic potential $v(\mathbf{r})$ is also determined by the electron density, from the first Hohenberg-Kohn theorem it follows that the Hamiltonian, and therefore energy, wavefunction, and all

[¶]In analogy with a function, i.e. a rule for going from a variable x to a number $f(x)$, a functional is a rule for going from a variable function $f(x)$ to a number $F[f]$.

other electronic properties of the system, are uniquely determined by the ground-state electron density $\rho_0(\mathbf{r})$. We can therefore write:

$$E[\rho_0] = T[\rho_0] + V_{ne}[\rho_0] + V_{ee}[\rho_0] \tag{2.10}$$

to stress the point that the total energy, kinetic and potential energy terms must all be functionals of ρ_0.

The second Hohenberg-Kohn theorem is analogous to the Variational principle (with the only difference being that the ground state energy is expressed as a functional of the ground state electron density) and provides a tool for the numerical solution of the density functional problem.

There are however a few difficulties which have to be overcome in order to apply DFT to systems of interacting electrons, and these arise from finding suitable expressions for the energy functionals in equation 2.10. The potential energy $V_{ne}[\rho_0]$ due to an external field $v(\mathbf{r})$ is a simple functional of the density.

$$V_{ne}[\rho_0] = \int v(\mathbf{r})\rho_0(\mathbf{r})dr \tag{2.11}$$

However, the energy for electron-electron interaction V_{ee} has a classical part, the Coulomb potential energy $J[\rho_0]$,

$$J[\rho_0] = \frac{1}{2}\int\int \frac{\rho(\mathbf{r}_1)\rho(\mathbf{r}_2)}{|\mathbf{r}_2 - \mathbf{r}_1|} d\mathbf{r}_1 d\mathbf{r}_2 \tag{2.12}$$

and a non classical part which is not known.

Therefore the problem remains of how to evaluate the kinetic energy, $T[\rho_0]$, and the non classical part of the electron-electron interaction energy in terms of $\rho_0(\mathbf{r})$.

The Thomas-Fermi[61,62] and related models[77,78] are direct approaches which propose different ways to approximate $T[\rho]$ and the non classical part of $V_{ee}[\rho]$. However quite drastic assumptions have to be made and this leads inevitably to a great loss of accuracy.

2.4 The Kohn-Sham Method

Density Functional Theory was turned into a practical tool for rigorous calculations through the work of Kohn and Sham.[65] They devised an indirect approach which allows the exact evaluation of the kinetic energy for an electronic system, and provides a set of equations for the solution of the density functional problem.

Consider a system of N non interacting electrons (which from now on will be denoted by the subscript s). The Hamiltonian has the form:

$$\hat{H}_s = \sum_i^N (-\frac{1}{2}\nabla_i^2) + \sum_i^N v_s(\mathbf{r}_i) \tag{2.13}$$

and the corresponding ground state wavefunction is a single determinant wavefunction of the type:

$$\Psi_s = \frac{1}{\sqrt{N!}}|\psi_1, \psi_2, ..., \psi_N| \tag{2.14}$$

where ψ_i are one-electron spin orbitals which satisfy the time-independent Schrödinger equations below.

$$\{-\frac{1}{2}\nabla_i^2 + v_s(\mathbf{r}_i)\}\psi_i = \epsilon_i\psi_i \tag{2.15}$$

For such a non interacting system the exact kinetic energy can be easily calculated, and its form (in term of atomic orbitals) is shown below.

$$T_s = \sum_i^N \langle\psi_i| - \frac{1}{2}\nabla_i^2|\psi_i\rangle \tag{2.16}$$

Therefore for a system of non interacting electrons the ψ_i can be obtained by solving the N one-electron equations 2.15, and the electron density can be calculated simply by quadrature.

$$\rho_s(\mathbf{r}) = \sum_i^N |\psi_i(\mathbf{r})|^2 \tag{2.17}$$

The total energy for this non-interacting system is hence known exactly.

$$E_s[\rho] = T_s + \int v(\mathbf{r})\rho(\mathbf{r})d\mathbf{r} \tag{2.18}$$

If we now consider a real system of interacting electrons, the total energy,

$$E[\rho] = T[\rho] + V_{ee}[\rho] + \int v(\mathbf{r})\rho(\mathbf{r})d\mathbf{r} \tag{2.19}$$

has a rather more complicated form than 2.18, since it contains the electron-electron interaction energy, $V_{ee}[\rho]$, with a non classical term which is not known. Furthermore the kinetic energy of a real interacting-electron system is different from that shown in equation 2.16.

In order to simplify the problem, Kohn and Sham defined an exchange-correlation energy term (also known as exchange-correlation energy functional) $E_{xc}[\rho]$, which includes all the terms which cannot be easily calculated (i.e. the difference between $T[\rho]$ and $T_s[\rho]$ and the non classical part of V_{ee}).

$$E_{xc}[\rho] = (T[\rho] - T_s[\rho]) + (V_{ee} - J[\rho]) \tag{2.20}$$

The total energy for the interacting system (equation 2.19) can therefore be rewritten as:

$$E[\rho] = T_s[\rho] + J[\rho] + E_{xc}[\rho] + \int v(\mathbf{r})\rho(\mathbf{r})d\mathbf{r} \tag{2.21}$$

The central point in the Kohn-Sham method is considering that a real system of interacting electrons, with kinetic energy $T[\rho]$ and potential $v(\mathbf{r})$, is equal to a reference system of non interacting electrons having kinetic energy T_s but a modified external potential $v_{\text{eff}}(\mathbf{r})$ called the Kohn-Sham effective potential. With this clever assumption the total energy for the interacting system can be written as

$$E[\rho] = T_s[\rho] + \int v_{\text{eff}}(\mathbf{r})\rho(\mathbf{r})d\mathbf{r} \tag{2.22}$$

with $v_{\text{eff}}(\mathbf{r})$ defined as follows.

$$v_{\text{eff}}(\mathbf{r}) = v(\mathbf{r}) + \frac{\delta J[\rho]}{\delta\rho(\mathbf{r})} + \frac{\delta E_{xc}[\rho]}{\delta\rho(\mathbf{r})} \tag{2.23}$$

The last term in equation 2.23 is the exchange-correlation potential, $v_{xc}(\mathbf{r})$:

$$v_{xc}(\mathbf{r}) = \frac{\delta E_{xc}[\rho]}{\delta \rho(\mathbf{r})} \tag{2.24}$$

note that the exact expression for E_{xc}, and therefore v_{xc}, is not known. A more explicit form of $v_{\text{eff}}(\mathbf{r})$, obtained by substituting equations 2.12 and 2.24 in 2.23,

$$v_{\text{eff}}(\mathbf{r}) = v(\mathbf{r}) + \int \frac{\rho(\mathbf{r}')}{|\mathbf{r} - \mathbf{r}'|} d\mathbf{r}' + v_{xc} \tag{2.25}$$

highlights the fact that the only term in v_{eff} which is not known is the exchange-correlation potential.

The Kohn-Sham method is in principle exact in that, once $v_{xc}(\mathbf{r})$ is known, the electron density $\rho(\mathbf{r})$ can be calculated by solving the N Kohn-Sham equations,

$$\{-\frac{1}{2}\nabla_i^2 + v_{\text{eff}}(\mathbf{r}_i)\}\psi_i = \epsilon_i \psi_i \tag{2.26}$$

(where ψ_i are the one-electron Kohn-Sham orbitals) and substituting the obtained ψ_i in

$$\rho(\mathbf{r}) = \sum_i^N |\psi_i(\mathbf{r})|^2 \tag{2.27}$$

Since v_{eff} depends on ρ (see equation 2.25) the Kohn-Sham equations have to be solved iteratively i.e. choosing a trial ρ substituting in 2.25, solving 2.26 to obtain ψ_i, calculating a more accurate ρ from 2.27, and so on until self-consistency is reached.

However, the limitations on the knowledge of v_{xc}, and the consequent use of approximate semi-empirical expressions for its representation, introduce a further level of approximation which adds to the basis set truncation leading to inevitably approximate solutions.

2.5 Exchange-Correlation Functionals

The determination of improved exchange-correlation functionals is a continuing area of interest in Density Functional Theory, with more and more functionals being proposed every year.[79] In this section I describe some of the most commonly used exchange-correlation functionals. An exchange-correlation energy functional is considered 'local' when it is just a functional of the value of $\rho(\mathbf{r})$, while a 'gradient corrected' functional is one which depends also on the gradient of $\rho(\mathbf{r})$, indicated by $\nabla\rho(\mathbf{r})$.

Local Density Approximation

One of the simplest approximate forms of the exchange-correlation energy functional, is to treat the electrons locally as a uniform gas. This is known as the Local Density Approximation (LDA). The LDA method is most accurate for systems with slowly-varying electron densities however it also gives fairly useful results for chemical systems, in which the electron distribution is far from homogeneous.

The LDA exchange-correlation functional can be written as:

$$E_{xc}^{\mathrm{LDA}}[\rho] = \int \rho(\mathbf{r})\varepsilon_{xc}(\rho)d\mathbf{r} \tag{2.28}$$

where $\varepsilon_{xc}(\rho)$ is the exchange-correlation energy per particle of a uniform electron gas of density ρ, and can be separated in its two contributions.

$$\varepsilon_{xc}(\rho) = \varepsilon_x(\rho) + \varepsilon_c(\rho) \tag{2.29}$$

The set of Kohn-Sham equations within the LDA approach become:

$$\left[-\frac{1}{2}\nabla^2 + v(\mathbf{r}) + \int \frac{\rho(\mathbf{r}')}{|\mathbf{r}-\mathbf{r}'|}d\mathbf{r}' + v_{xc}^{\mathrm{LDA}}(\mathbf{r})\right]\psi_i = \epsilon_i\psi_i \tag{2.30}$$

where v_{xc}^{LDA} is:

$$v_{xc}^{\mathrm{LDA}}(\mathbf{r}) = \frac{\delta E_{xc}^{\mathrm{LDA}}}{\delta \rho(\mathbf{r})} = \varepsilon_{xc}(\rho(\mathbf{r})) + \rho(\mathbf{r}) \frac{\partial \varepsilon_{xc}(\rho)}{\partial \rho} \tag{2.31}$$

Solution of equations 2.30 is referred to as the LDA method.

The exact expression of the exchange functional per particle for a uniform electron gas has been developed by Dirac.[80]

$$\varepsilon_x(\rho) = C_x \rho(\mathbf{r})^{1/3} \qquad \text{with} \quad C_x = \left[-\frac{3}{4} \left(\frac{3}{\pi} \right)^{1/3} \right] \tag{2.32}$$

Possible approximate expressions for ε_c have also been proposed.[81,82]

Exchange-only LDA and the Xα Method

The simplest possible form of LDA is the exchange-only LDA. If one ignores correlation, the expression for the exchange-only functional is obtained,

$$E_x^{\mathrm{LDA}}[\rho] = C_x \int \rho(\mathbf{r})^{4/3} d\mathbf{r} \tag{2.33}$$

and differentiating with respect to ρ one can write the exchange-only LDA potential,

$$v_x^{\mathrm{LDA}}(\mathbf{r}) = -\left(\frac{3}{\pi} \rho(\mathbf{r}) \right)^{1/3} \tag{2.34}$$

and the corresponding exchange-only LDA Kohn-Sham equations.

$$\left[-\frac{1}{2}\nabla^2 + v(\mathbf{r}) + \int \frac{\rho(\mathbf{r}')}{|\mathbf{r} - \mathbf{r}'|} d\mathbf{r}' + v_x^{\mathrm{LDA}}(\mathbf{r}) \right] \psi_i = \epsilon_i \psi_i \tag{2.35}$$

Equation 2.35 shows many similarities with the Xα equation developed by Slater as an approximation to the Hartree-Fock equation:

$$\left[-\frac{1}{2}\nabla^2 + v(\mathbf{r}) + \int \frac{\rho(\mathbf{r}')}{|\mathbf{r} - \mathbf{r}'|} d\mathbf{r}' + v_{X\alpha}(\mathbf{r}) \right] \psi_i = \epsilon_i \psi_i \tag{2.36}$$

where $v_{X\alpha}$ is the Xα local potential,

$$v_{X\alpha} = -\frac{3}{2} \alpha \left(\frac{3}{\pi} \rho(\mathbf{r}) \right)^{1/3} \tag{2.37}$$

and α is a parameter which Slater set equal to 1.

Comparison of equations 2.35 and 2.34 with 2.36 and 2.37 shows in fact that the exchange-only LDA Kohn-Sham potential (2.34) corresponds exactly to the Xα potential (2.37) with $\alpha = 2/3$.

Within the Xα method, the exchange functional E_x^{LDA} is therefore rearranged into a more general form,

$$E^{X\alpha}[\rho] = \frac{3}{2}\alpha C_x \int \rho(\mathbf{r})^{4/3} d\mathbf{r} \tag{2.38}$$

and the parameter α is often treated as an adjustable quantity, varying between 2/3 and 1.

Because of the way it is constructed, the Xα solution does not include correlation effects.

Local Spin Density Approximation

One step beyond the simple LDA approach is the Local Spin Density Approximation (LSDA). This is an analogous approach to LDA (i.e. it approximates the electron distribution to that of an homogeneous spin-polarized electron gas) but applies to systems in which spin polarization is important (such as open shell systems, or systems in the presence of an external magnetic field) and for which Spin Density Functional Theory (SDFT) is used instead of Density Functional Theory.[‖] Due to its spin dependency, SDFT also allows the production of more accurate forms of the approximate exchange and correlation functionals. The energy functionals in the SDFT approach become in fact functionals of the α- and β-electron densities.

The exchange-correlation functional can be separated in its two contributions:

$$E_{xc}[\rho^\alpha, \rho^\beta] = E_x[\rho^\alpha, \rho^\beta] + E_c[\rho^\alpha, \rho^\beta] \tag{2.39}$$

[‖]For more details on Spin Density Functional Theory see Density-Functional Theory of Atoms and Molecules.[63]

where the exchange functional is,

$$E_x^{\mathrm{LSDA}}[\rho^\alpha, \rho^\beta] = 2^{1/3} C_x \int \left[(\rho^\alpha)^{4/3} + (\rho^\beta)^{4/3} \right] d\mathbf{r} \tag{2.40}$$

and the correlation functional has the form

$$E_c^{\mathrm{LSDA}}[\rho^\alpha, \rho^\beta] = \int \rho(\mathbf{r}) \varepsilon_c(\rho, \zeta) d\mathbf{r} \tag{2.41}$$

where $\varepsilon_c(\rho, \zeta)$ is the correlation energy per electron and ζ is the spin polarization parameter.

$$\zeta = \frac{\rho^\alpha - \rho^\beta}{\rho^\alpha + \rho^\beta} \tag{2.42}$$

Many possible forms have been developed for the correlation energy, $\varepsilon_c(\rho, \zeta)$.[82–84] The most commonly used is the one proposed by Vosko, Wilk and Nusair[82] (known as VWN correlation functional).

Generalized Gradient Approximation

The next level of approximation is given by the so called Generalized Gradient Approximation (GGA). Within this approach a gradient correction is applied to the local exchange-correlation functional so as to take into account the inhomogeneity of electron densities in atoms and molecules.

Since the major source of error in LDA is in the exchange energy, the simplest GGA approach, developed by Perdew and Wang,[85] consists of applying a gradient correction only to the exchange energy functional. This method, although quite simple, leads to a significant increase in the level of accuracy leaving only 1% error in the calculated exchange energy. The Perdew-Wang GGA-corrected exchange functional is shown below,

$$E_x^{\mathrm{GGA}}[\rho] = -\frac{3}{4} \left(\frac{3}{\pi} \right)^{1/3} \int \rho^{4/3} F(s) d\mathbf{r} \tag{2.43}$$

where

$$F(s) = \left(1 + 1.296s^2 + 14s^4 + 0.2s^6\right)^{1/15} \tag{2.44}$$

and

$$s = \frac{|\nabla\rho(\mathbf{r})|}{(2k_{\mathrm{F}}\rho)} \qquad \text{with} \qquad k_{\mathrm{F}} = (3\pi^2\rho)^{1/3} \tag{2.45}$$

A different form for the gradient expansion, F(s), was proposed by Becke.[67]

Analogous gradient corrections were also developed for the correlation functional; among the most used are the one proposed by Lee, Yang and Parr[86] and one proposed by Perdew.[87]

Other functionals have also been proposed which include gradient corrections both to the exchange and correlation terms. One such functional is the PW91[88] which uses the exchange and correlation corrections developed by Perdew and Wang in 1991. A more recent example is the PBE functional which uses the Perdew-Burke-Ernzerhof gradient corrected exchange and correlation terms.[89] The RPBE and revPBE also use the Perdew-Burke-Ernzerhof correlation correction while using a revised form of the Perdew-Burke-Ernzerhof exchange term, respectively the Hammer-Hansen-Norskov[90] and Zhang-Wang[91] exchange functionals.

Meta-GGA functionals

In order to improve the form of the GGA functionals there have been a few attempts to go beyond first-order approximation and introduce the second-order derivative of the electron density, i.e. the Laplacian of the density ($\nabla^2\rho$), or the kinetic energy density (τ). The form for a meta-GGA functional is therefore:

$$E_{xc}^{\mathrm{MGGA}}[\rho] = \int F_{xc}(\rho, \nabla\rho, \nabla^2\rho, \tau)d\mathbf{r} \tag{2.46}$$

where F_{xc} represents a general gradient expansion function for the exchange and correlation functionals.

Examples of such functionals are the B98[92] (which includes $\nabla^2\rho$, τ and exact exchange), PKZB[93] (based upon PBE but extended to include τ), and VS98[94] (based on second-order density matrix expansion). In general, the functionals which are dependent on the Laplacian of the density display a large variation with respect to basis set changes or numerical integration accuracy. Furthermore, testing these functionals together with their corresponding first-order analogues proved that they perform worse or comparably well, with the only exception being VS98 which performs similarly for energy calculation but shows improved geometrical predictions.[79]

2.6 Relativity in Chemistry

Relativistic Effects

Despite the initial belief that relativity would not affect atomic and molecular properties, the importance of relativistic effects in chemistry has now been widely accepted.[17,95]

The radial velocity v of an electron moving in the $1s$ shell and inner shells increases with increasing atomic number. Therefore, the relativistic mass correction for the core electrons

$$m = \frac{m_0}{\sqrt{1 - \left(\frac{v}{c}\right)^2}} \tag{2.47}$$

(where m_0 is the mass at rest and c is the speed of light) becomes increasingly important for heavy elements. As a result the s and, to a lesser extent, p shells are contracted and stabilized. This effect is referred to as direct relativistic orbital contraction. On the other hand, d and f orbitals are destabilized by the increased shielding of the nuclear charge by the s and p electrons of similar radial distribution. This effect is known as indirect relativistic orbital expansion, and is generally less marked than the previous one.

The inclusion of relativistic corrections in the computational analysis of systems containing heavy elements generally leads to a significant shortening of covalent bonds with respect to analogous non-relativistic calculations. Although this was first thought to be a consequence of the reduced radial extension of the valence atomic orbitals, it was proved to be an independent effect rather due to the form of the relativistic Hamiltonian operator.[96–98]

Another aspect of relativity, which is related to the existence of electron spin (and is correctly predicted by the Dirac equation), is spin orbit coupling. In an atom

or molecule the electron spin angular momentum couples with the orbital angular momentum, leading to a total angular momentum. There are two qualitative spin orbit coupling schemes that can be used to evaluate the spin orbit coupling, namely L-S (or Russell-Saunders) and j-j approaches. The first is more appropriately used when spin orbit coupling is weak with respect to interelectronic repulsion, the second is more appropriate when spin-orbit coupling becomes stronger than electrostatic interactions. Since spin orbit coupling depends on Z^4 (Z being the atomic number) it becomes very effective for heavy elements.** In the second case, spin orbit coupling results in the splitting of a shell into subshells characterized by non integral quantum number j, which is reflected in the observed electronic absorption spectra. Since the use of single point symmetry is not sufficient to describe states with non integral quantum number, the rather less familiar double point symmetry groups have to be used for a rigorous treatment of relativity.

Relativistic Computational Methods

I will now describe the possible computational approaches to treat relativity at quantum mechanical level. All of these approaches are in principle applicable to both *ab initio* and DFT methods.

A precise relativistic description of electrons in atomic and molecular systems is given by the 4-component Dirac equation:

$$\hat{H}_{\mathrm{DC}}\Psi = i\frac{\partial\Psi}{\partial t} \tag{2.48}$$

where $\hat{H}_{\mathrm{DC}}$ is the electronic Dirac-Coulomb operator,

$$\hat{H}_{\mathrm{DC}} = -\sum_i \left[c\alpha_i\hat{p}_i + \beta_i c^2 + v(\mathbf{r}_i) + \sum_{i>j}\frac{1}{r_{ij}} \right] \tag{2.49}$$

**The Russell-Saunders approach describes very well the electronic structures of lanthanide atoms and the corresponding 3+ ions, but becomes unappropriate for heavier elements.

c is the speed of light, α and β are 4x4 constant matrices, and $\hat{p}$ is the linear momentum operator. The solution of Dirac equations is a 4-component wavefunction. It has two positive energy states corresponding to α and β spin electrons, and two negative energy states corresponding to α and β spin positrons. The Dirac equation has several conceptual advantages over the Schrödinger equation; first electron spin and spin orbit coupling are intrinsically defined rather than being added as an extra, second it is symmetric with respect to space and time, therefore obeying Einstein's special theory of relativity. However the computational effort associated to the solution of the full Dirac equation is such that calculations are currently restricted to atoms and very small molecules.

One way to simplify the Dirac-Coulomb operator is by elimination of the positronic states. This leads to approximate 2-component methods such as n-ORA (n^{th} order regular Hamiltonian approximation, with n = 0, 1, 2...).[99,100] Among these approximations one of the most commonly used is ZORA (zero-order regular approximation) which can be combined to single or double point group symmetry to give scalar-relativistic or spin orbit coupled results respectively[††].

A different way to treat relativity is the Pauli formalism. This approach uses the Schrödinger equation instead of Dirac equation, and a form of the Hamiltonian (the Pauli Hamiltonian[101,102]), which contains first-order relativistic corrections. The Pauli Hamiltonian has corrective terms for the kinetic and potential energy (called respectively the mass-velocity and Darwin corrections), and, if necessary, an extra term to account for the spin-orbit contribution. In chemical applications, it has been found that a Pauli treatment is of acceptable accuracy for all electron calculations of $3d$ and $4d$ transition-metal systems, but can be unreliable where heavier elements

[††]As implemented in Amsterdam Density Functional, version 2002.01

are involved. The use of frozen cores gives however reasonable results for all but the very heavy elements.‡‡

Another less sophisticated approach to introduce relativistic corrections is the so called relativistic pseudopotential method. This consists of replacing the wave-function associated with the core electrons with relativistic effective core potentials (ECP),[104] therefore highly reducing the computational effort, particularly for heavy elements. The ECP are usually generated from very accurate relativistic atomic calculations, and calculation of molecular properties often involves no further relativistic treatments.

Relativity and the *f* block

The way in which relativity affects the geometric and electronic properties of lanthanide and actinide complexes has been widely investigated.[8–10,105,106] A series of fully relativistic density functional calculations of the ionization energies and *d-f* charge transfer energies for the whole series of lanthanide atoms and comparison with analogous results using a quasirelativistic *ab initio* pseudopotential method has shown that both density functional and *ab initio* methods give equally accurate results.[10] Electron correlation effects turn out to be very important, while spin-orbit coupling contributions were found to be generally small for the lanthanide atoms, suggesting that the use of scalar-relativistic Hamiltonians might lead to sufficiently accurate results for many purposes.[10]

In one of the earlier attempts to evaluate the effects of relativity for lanthanide molecules the electronic structures of several lanthanide mono-hydrides, mono-fluorides, and monoxides were calculated by nonrelativistic and quasirelativistic gradient-

‡‡Theoretical deficiencies of the Pauli Hamiltonian are due to its singular behavior at the nucleus, and therefore it performs worse with a complete basis set[103]

corrected density functional theory.[106] Nonrelativistic calculations showed significant discrepancies from experimental data, while the quasirelativistic results were found to be in good agreement with experimental bond length values, even for the open shell gadolinium molecules with high spin multiplicity. The quasirelativistic bond lengths obtained for the gadolinium molecules are also in excellent agreement with recent fully relativistic density functional calculations on Gd diatomics,[105] although the agreement was not as good for binding energies (calculated to be somewhat lower than the fully relativistic values).

The effect of relativity on the lanthanide and actinide contraction has also been investigated.[13,17,107,108] A comparison between fully relativistic Dirac-Fock (DF), and non relativistic Hartree- Fock (HF) calculations on a series of lanthanide and actinide hydrides and fluorides has shown an increase in the calculated contraction of 10-30% for the lanthanides and 40-50% for the actinides, when relativity is included.[107]

With the implementation of fast computing resources, the study of real systems is becoming ever more accessible and there are already many examples in which a theoretical investigation successfully predicted and/or helped to understand the nature of the metal-ligand bonding in lanthanide and actinide complexes. For example an *ab initio* self consistent field (SCF) plus configuration interaction study has been carried out for the ground state and low lying excited states of cerocene, $Ce(C_8H_8)_2$, and thorocene, $Th(C_8H_8)_2$. Theoretical results suggested that in such complexes, while the thorium ion can be represented as Th(IV), the cerium ion should be best regarded as Ce(III).[12] This surprising prediction was later confirmed experimentally by X-ray absorption measurements.[109]

Another successful example is given by a series of *ab initio* calculations on the bis-η^6-benzene complexes of zerovalent lanthanide and actinides.[9,110–112] Despite

the generally small overlap of lanthanide f orbitals with the ligand orbitals, the nature of the metal-benzene bonding was shown to be significantly covalent and these molecules have therefore an unexpected thermodynamic stability. Not only did the quantum mechanical analysis reproduce the stability of the lanthanide complexes, but it predicted that the analogous actinide complexes would be stable.[110] Moreover it traced the metal-ligand interaction to a promotion of an electron from the metal $4f$ to $5d$ orbital and a consequently strong metal to ligand back donation through the occupied metal d orbital.

Quantum mechanical calculations are therefore a powerful tool in the investigation of the geometric and electronic structure of heavy metal systems.

Chapter 3

Computational Investigation of an unsupported Pt-Tl bond.

3.1 Introduction

The first compound containing a direct covalent Pt-Tl bond was synthesised by Nagle and Balch and consisted of a square pyramidal $[Pt(CN)_4]^{2-}$ unit with two Tl^+ ions occupying the axial positions of an octahedron.[113] Other compounds containing a Pt-Tl bond were later synthesised, but they were always prepared in the solid state and were not stable in solution.[114–116]

Recently Glaser at al. reported the synthesis in aqueous solution of a series of cyanide species containing a strong unsupported Pt-Tl bond. The complexes, $[(CN)_5Pt\text{-}Tl(CN)_n]^{n-}$ (with n = 0, 1, 2, 3 for complexes **I**, **II**, **III**, and **IV**, respectively) differ from one another by the number of thallium coordinated cyanide ligands and the charge, and were characterised by multinuclear NMR (^{13}C, ^{195}Pt and ^{205}Tl) and Raman spectroscopy.[117,118] The Pt-Tl distances in the series of complexes have subsequently been determined by the same team using EXAFS spectroscopy.[119,120] The structures proposed by Glaser et al.[117] for complexes **I-IV** are shown in Fig. 3.1.

Quantum mechanical calculations on an analogous platinum cyanide compound, $[Pt^{II}(CN)_4]_2$,[121] have shown that the HOMO in this molecule has a strong contribution (~91%) of Pt orbitals, in particular d_{z^2}. Hence the metal-metal bonding in the Pt-Tl cyanide complexes has been interpreted[117] as a donor-acceptor interaction with a donation from the filled Pt^{II} d_{z^2} orbital to the formally empty Tl^{III} $6s$ orbital.

One interesting aspect related to these complexes is the extremely high value of the Pt-Tl coupling constants, 71 kHz for complex **I** decreasing steadily to 38 kHz for complex **IV**. These values are in fact among the highest measured between two nuclei, being also much higher than previously reported Pt-Tl coupling constants in complexes containing Tl(I), which are around 3 kHz.[114,122] The high values of

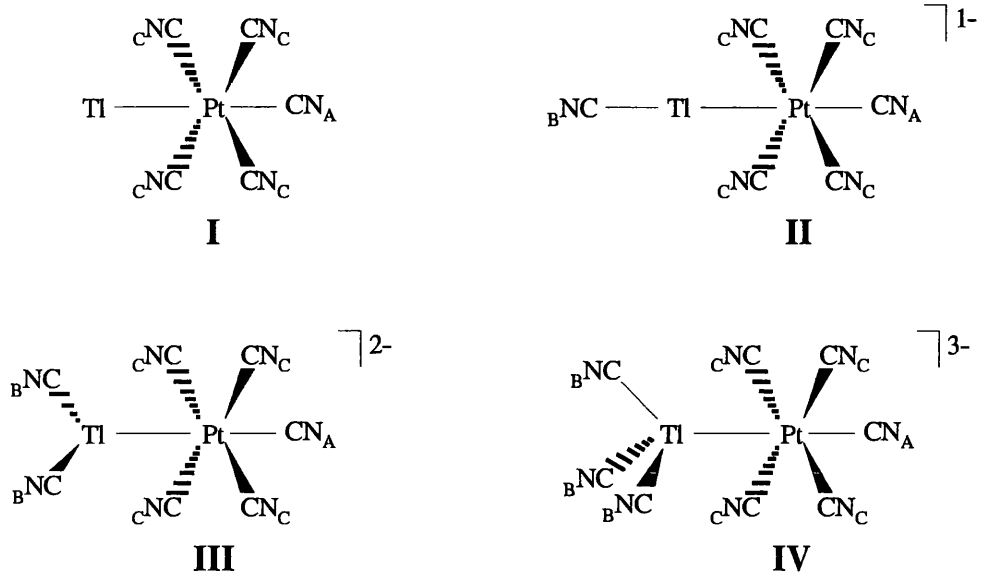

Figure 3.1: Proposed structures for complexes **I-IV**. These structures were used as starting points in our geometry optimisations.

J_{Pt-Tl} have been explained in term of participation of the thallium $6s$ electrons in the Pt-Tl bond. Because of relativistic effects the thallium $6s$ orbital is stabilised and contracted; this results in an increased electron density at the nucleus which contributes to the Fermi contact term for spin-spin coupling.[123] When changing the oxidation state of the thallium from +1 to +3, the participation of $6s$ electrons in the bond results in a large amplification of the coupling.[124]

It is interesting that the Raman and NMR data of Glaser et al. are apparently inconsistent as regards the position of cyanide CN_A. The values of the C-N stretching bands in the Raman spectra are consistent with terminal cyanides and rule out the possibility of bridging ligands. The NMR data however suggest a strong interaction between C_A and the thallium atom therefore supporting the idea that CN_A occupies a bridging position between the two metals (or even that it is fully bound to the thallium). Although the chemical shift of C_A and the Pt-C_A coupling constant are

consistent with platinum bound carbon, the assignement of CN_A as Pt axial does not explain the high values of the Tl-C_A coupling constant.

In this chapter the computational investigation of complexes **I-IV** is reported. It is my aim to establish if the proposed structures in Fig 3.1 are supported computationally, via a comparison of the experimentally determined spectroscopic data with theoretical results.

3.2 Computational Details

All calculations were performed on a DEC 433au workstation using Amsterdam density functional (ADF) program suite (version 2.3).[125,126] The basis sets employed are valence-only Slater type orbitals of double zeta quality plus one polarisation function (ADF type III) for H, C, N and O, and triple zeta without polarisation function (ADF type IV) for Pt and Tl. Quasi relativistic[127] scalar corrections, Darwin and mass-velocity, were included via the Pauli formalism, in which the first order scalar relativistic Pauli Hamiltonian is diagonalised in the space of non relativistic basis sets. The frozen core approximation was employed, and quasi-relativistic frozen $1s$ and $4f$ cores (calculated by the ADF auxiliary program 'DIRAC') were used, respectively for light (C, N, and O) and heavy (Pt and Tl) elements. The local density parametrisation of Vosko, Wilk and Nusair[82] was employed in conjunction with Becke's gradient correction[67] to the exchange part of the potential and the correlation correction due to Perdew.[87]

3.3 Results and discussion

3.3.1 Unsolvated Complexes

Geometry optimisations have been performed on complexes **I-IV**, and the resulting minimum structures have been characterised by harmonic vibrational analysis. The optimised complexes **I-IV** are presented in Fig 3.2, and selected experimental[119,120] and calculated bond lengths and vibrational wavenumbers are collected in tables 3.1 and 3.2 respectively.

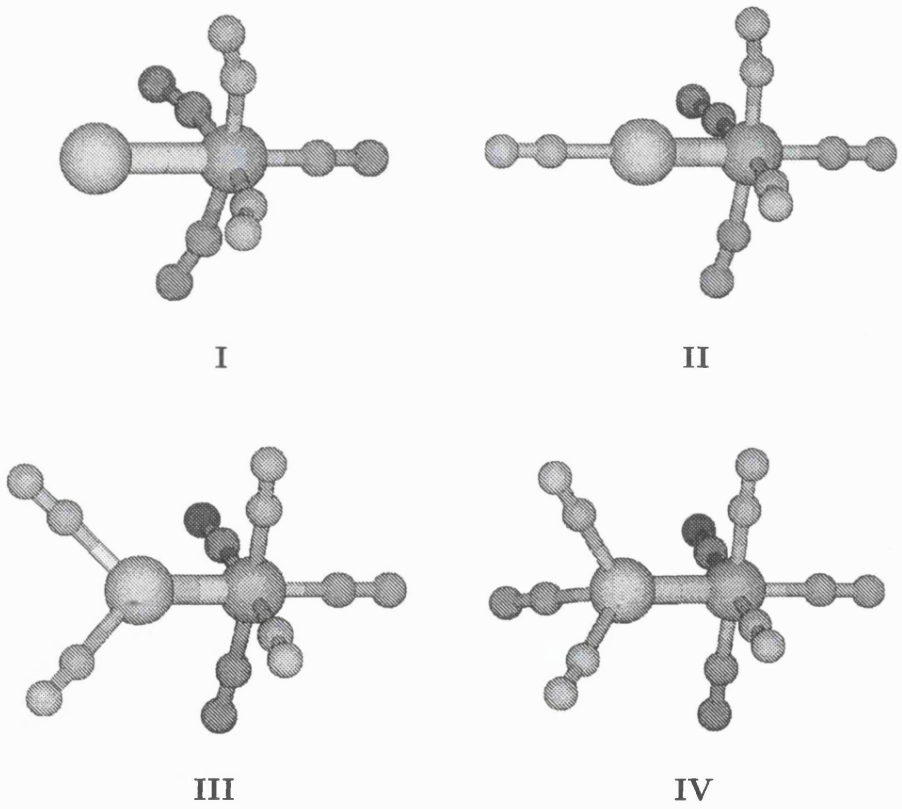

Figure 3.2: Calculated structures for complexes **I-IV**

The agreement between the experimental and calculated vibrational wavenumbers in the CN stretching region is excellent. Good agreement is also found between theory and experiment for the Pt-Tl stretching, with the exception of complex **I** for

Table 3.1: Selected bond lengths in optimised complexes **I-IV** and comparison with experimental Pt-Tl distance.

	I	**II**	**III**	**IV**
Calculational symmetry	C_{4v}	C_{4v}	C_{2v}	C_s
Pt-Tl_{exp} (Å)[119,120]	2.63	2.60	2.62	2.64
Pt-Tl_{calc} (Å)	3.10	2.60	2.63	2.70
Pt-$C_{A\ calc}$ (Å)	1.94	1.98	2.02	2.08
Pt-$C_{C\ calc}$ (Å)	2.01	2.03	2.03	2.03
Tl-$C_{B\ calc}$ (Å)	—	2.24	2.30	2.34

which the calculated value is much lower than the experimental. The calculated and experimental Pt-Tl distances are also consistent with this result, i.e. the agreement is excellent for complexes **II-IV** while the calculated Pt-Tl bond length is overestimated by almost 0.5 Å. These data suggest that while the proposed structures of complexes **II-IV** might be plausible the structure proposed for complex **I** is not supported by our calculations.

Further evidence for the difference between proposed and calculated geometries of complex **I** comes from the analysis of its electronic structure. As mentioned above, the high Pt-Tl coupling constant experimentally observed implies the participation of the thallium 6*s* electrons in the bond, and therefore an oxidation state of +3 for the thallium ion in complexes **I-IV**. Mulliken analyses[128] of the electronic structures of complexes **I-IV** at their optimised geometries showed that for complexes **II-IV** the MO with Pt-Tl bonding character has a significant contribution from the thallium 6*s* orbital (i.e. the oxidation state on thallium is best described as +3), while for complex **I** the thallium 6*s* orbital is essentially localised on thallium, and

Table 3.2: Selected experimental and calculated vibrational wavenumbers for complexes **I-IV**.

Wavenumbers	I	II	III	IV
Pt-Tl_{exp} (cm^{-1})[117]	160	161	157	157
Pt-Tl_{calc} (cm^{-1})	73	138	146	139
C-N_{exp} (cm^{-1})[117]	CN_A not obs.	2210_{CN_A}	2210_{CN_A}	2210_{CN_A}
	2200_{CN_C}	2175_{CN_B}	2162_{CN_B}	2161_{CN_B}
		$2199\text{-}2188_{CN_C}$	$2191\text{-}2179_{CN_C}$	$2191\text{-}2179_{CN_C}$
C-N_{calc} (cm^{-1})	2205_{CN_A}	2210_{CN_A}	2202_{CN_A}	2156_{CN_A}
	2167_{CN_C}	2179_{CN_B}	2164_{CN_B}	2152_{CN_B}
		$2195\text{-}2188_{CN_C}$	$2184\text{-}2179_{CN_C}$	$2191\text{-}2174_{CN_C}$

the thallium is therefore in a formal oxidation state of +1. The different oxidation state observed for complex **I** explains the higher Pt-Tl distance compared to the other complexes, Pt-Tl(I) bond lengths being typically in the range[122] of 2.9-3.1 Å. Thus the optimised geometry obtained for complex **I** is not only at odds with the EXAFS and Raman data of Glaser et al., but it is also inconsitent with their NMR results.

In order to find a more plausible structure for complex **I**, additional geometry optimisations were carried out with no symmetry constraints, tighter gradient and structural convergence criteria, and differing initial Pt-Tl distances. However, the calculations converged in all cases to geometries with metric parameters and electronic structures very similar to those found previously.

3.3.2 Solvated complexes

One possible reason for the discrepancy observed between computational and experimental data is the presence of the solvent. The experimental data on which our comparison is based were obtained in aqueous solution, and in such conditions it is very unlikely that the complexes exist as isolated molecules. Co-ordination of the thallium by one or more water molecules will certainly occur and this might strongly affect the properties of the complexes. I have therefore conducted a series of geometry optimisations on the corresponding hydrated complexes, where only the first coordination sphere of water molecules has been considered. The number

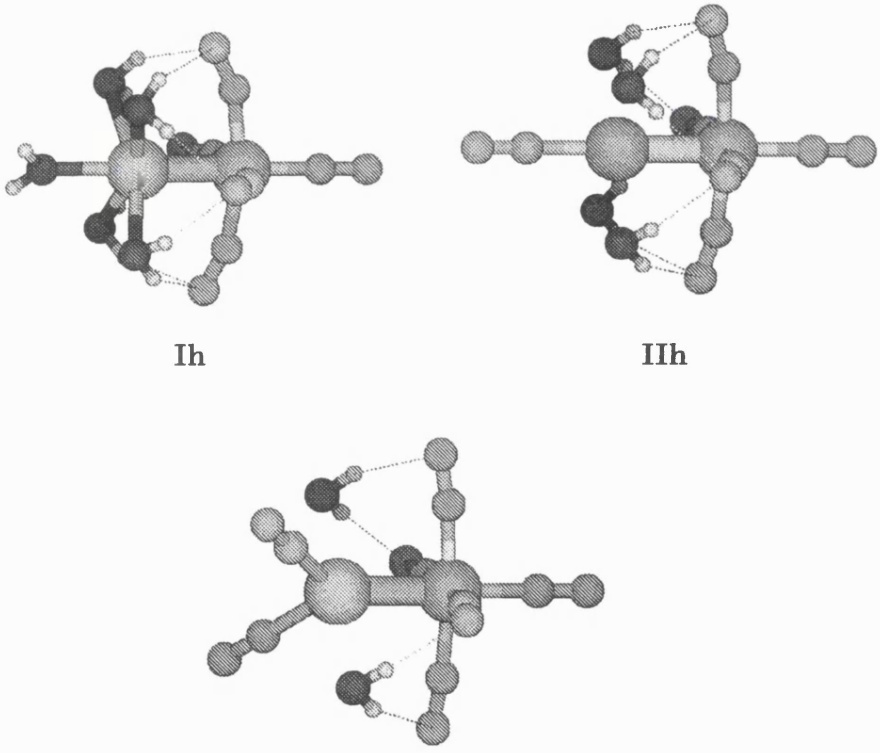

Ih **IIh**

IIIh

Figure 3.3: Calculated structures for solvated complexes **Ih-IIIh**

and position of coordinated water molecules were chosen according to literature in-

Table 3.3: Selected bond lengths for optimised complexes **Ih-IIIh** and vibrational wavenumbers for complex **Ih**.

	Ih	**IIh**	**IIIh**
Calculational symmetry	C_{2v}	C_{4v}	C_{2v}
Pt-Tl_{calc} (Å)	2.60	2.62	2.65
Pt-$C_{A\ calc}$ (Å)	2.00	2.05	2.07
Pt-$C_{C\ calc}$ (Å)	2.02	2.02	2.02
Tl-$C_{B\ calc}$ (Å)	—	2.17	2.26
Wavenumbers			
Pt-Tl_{calc} (cm^{-1})	156	not calculated	not calculated
C-N_{calc} (cm^{-1})	2205_{CN_A}	not calculated	not calculated
	2178_{CN_C}		

formation[129] and preliminary quantum mechanical calculations, and the optimised hydrated complexes **Ih-IIIh** are shown in Fig. 3.3. Owing to the high number of cyanides on the thallium atom in complex **IV** and its pseudo tetrahedral environment, no first shell co-ordination by water molecules has been considered to occur for this complex.

Key bond lengths and vibrational wavenumbers for the optimised solvated molecules are summarised in Table 3.3. Comparison of the data in Table 3.3 with those in Tables 3.1 and 3.2 shows that the effect of co-ordinating water molecules in complexes **II** and **III** is not large. By contrast, a very significant shortening of the Pt-Tl distance is observed on co-ordination of water to complex **I**. Indeed, the agreement between the experimental and calculated Pt-Tl bond length and ν(Pt-Tl) for complex **Ih** is extremely good.

Examination of the optimised geometries (Fig 3.3) for the solvated molecules shows a crucial point, as intramolecular hydrogen bonds are formed between the hydrogen of the coordinated water molecules and the nitrogen atoms of the platinum equatorial cyanides (CN_C). In all three complexes, **Ih-IIIh**, the H···N distance is approximately 2.2 Å, but while in complexes **II** and **III** the Pt-Tl distance is already sufficiently short to allow the hydrogen bonding to occur with minimum distortion of the complexes, the Pt-Tl distance in complex **I** is too large to allow efficient hydrogen bonding on coordination of water, and a significant reduction of the Pt-Tl bond length occurs.

Mulliken analysis of complex **Ih** reveals a significant participation of the thallium $6s$ atomic orbital in Pt-Tl bonding. Hence the coordination by water molecules results in a shortening of the Pt-Tl bond and a modification of the electronic structure of complex **I** which becomes consistent with a thallium oxidation state of +3, and therefore in agreement with the observed NMR data.[117] It is worth noting that for complexes **II-IV** the presence of thallium coordinated cyanide ligands requires the thallium $6s$ electrons to participate in bonding, thereby shortening the Pt-Tl distance. In complex **I**, however, it is energetically more favourable for the thallium $6s$ electrons to remain as an inert pair. This energetic preference for Tl(I) is overcome in complex **Ih** by coordination of water molecules.

To separate the effects of water coordination and intramolecular hydrogen bonding on the Pt-Tl distance, a calculation was performed in which the hydrogen atoms on the coordinating equatorial water molecules were constrained to point away from the platinum axial cyanides so that hydrogen bonding is "turned off". In this case the calculated Pt-Tl distance was significantly larger compared to complex **Ih**, with a value of 2.84 Å. I therefore suggest that the large decrease in the Pt-Tl bond length

observed for complex **I** upon solvation is mainly driven by intramolecular hydrogen bond formation.

3.3.3 Other Factors affecting the Pt-Tl Bond Length

Calculations on the solvated complexes, **Ih-IIIh**, have shown that coordination by water molecules significantly affects the Pt-Tl bond length for complex **I**. Since the observed Pt-Tl bond length of complex **I** has been measured by EXAFS experiments in the solid state,[120] it might be that coordination by neighbour atoms in the crystal lattice is responsible for a shortening of the Pt-Tl bond length. I was therefore interested in analysing the effect of intermolecular interactions (due to nearest neighbours in the solid state) on the Pt-Tl distance in complex **I**.

Since no structural characterisation is at present available for complex **I**, the packing of the complex in the solid state is taken to be similar to that observed for $Tl_2Pt(CN)_4$,[113] where the nearest neighbours of each thallium atom are five cyanides in approximately D_{4h} symmetry. The effect of neighboring cyanide ligands in the crystal lattice has been modelled by five HCN molecules positioned so as to mimic the arrangement of cyanide ligands around the thallium atom in the solid (i.e. four in the equatorial plane and one in the axial position). The geometry and calculated metric parameters for this optimised complex, **Is**, are shown in Fig. 3.4 and Table 3.4 respectively. Previously reported calculations on the $Tl_2Pt(CN)_4$ complex, containing Tl(I), suggested that solid state coordination by cyanide ligands (which were modelled by five point charges and kept at a fixed distance of 3 Å) results in lengthening of the Pt-Tl bond length compared to the isolated molecule.[130] In the system under study however, the effect of coordination by HCN molecules is a marked decrease of the Pt-Tl distance compared to the isolated molecule. Cal-

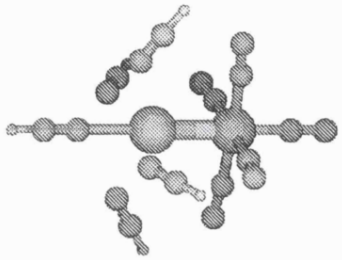

Is

Figure 3.4: Calculated structures for complexes **Is**

culations with only one HCN molecule in the axial position suggest that the effect of the axial ligand is comparable to the equatorial ones, with a Pt-Tl distance of 2.87 Å compared to 2.74 Å whith five HCN molecules.

Table 3.4: Selected bond lengths in optimised complex **Is** and comparison with experimental Pt-Tl distance.

	Is
Calculational symmetry	C_{4v}
$Pt\text{-}Tl_{exp}$ (Å)[120]	2.63
$Pt\text{-}Tl_{calc}$ (Å)	2.74
$Pt\text{-}C_{A\ calc}$ (Å)	1.97
$Pt\text{-}C_{C\ calc}$ (Å)	2.02
$Tl\text{-}N_{ax\ calc}$ (Å)	2.57
$Tl\text{-}N_{eq\ calc}$ (Å)	2.66

Mulliken analysis of the electronic strucure for the optimised complex **Is** showed, similarly to what was observed for water coordination, that the effect of HCN coordinating to the thallium atom is an increased participation of the thallium 6*s*

electrons in the Pt-Tl bond, with a consequent shortening of the Pt-Tl distance.

3.3.4 Position of CN_A

The good agreement obtained between experiment and calculations for the solvated complexes suggests that the assignment on the cyanide sites proposed by Glaser et al. is correct. However, as mentioned in section 3.1, the NMR and Raman data are apparently not in full agreement as to the position of CN_A. Although the chemical shift of C_A is in all four complexes closer to the chemical shift of C_C (the carbon atom bound equatorially to the platinum), the high values of the Tl-C_A coupling constants in all the complexes (higher than those for Tl-C_B), and the fact that C_A couples with C_B while no coupling has been detected with C_C, argue against CN_A being purely platinum terminal.

I therefore decided to investigate alternative sites for CN_A in complex **I** (chosen as it is the smallest, and therefore computationally the least consuming, of the four complexes). Since the Raman spectra preclude the possibility of bridging cyanides, I considered only a modified geometry in which CN_A occupies the thallium axial position. Geometry optimisations were performed for this modified complex **I'** and the corresponding solvated molecule **Ih'**. In the latter complex I assume that four water molecules coordinate to the thallium in the equatorial position and a fifth water molecule coordinates the platinum axially (see Fig. 3.5 for a schematic representation of complexes **I'** and **Ih'**) . The total molecular bonding energies and Pt-Tl bond lengths in the four complexes **I**, **I'**, **Ih** and **Ih'** are collected in Table 3.5.

Although complex **I** is significantly more stable than complex **I'** (by approximately 100kJ mol^{-1}), coordination by five water molecules results in relative stabilisation of the modified complex, so that the solvated complex **Ih** is less than 20 kJ

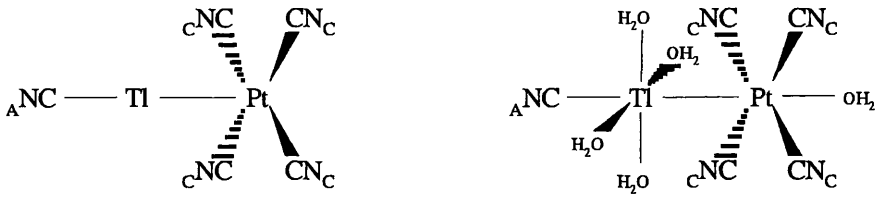

I' Ih'

Figure 3.5: Schematic representation of complexes **I'** and **Ih'**.

mol^{-1} more stable than the solvated modified complex **Ih'**. Furthermore, while the Pt-Tl bond lengths in **I** and **I'** are very different from one another (and significantly different from experiment), the Pt-Tl bond lengths in the two solvated complexes **Ih** and **Ih'** are very similar both to each other and to experiment.

This suggests that there might be an equilibrium between the two species **Ih** and **Ih'** in solution. If the rate of exchange of the axial cyanide between the platinum and the thallium is fast on the NMR time scale, then the resulting signal would be an average of the two different positions, in agreement with the experimental observation that the chemical shift of C_A is intermediate between that of carbon bonded to platinum and carbon bonded to thallium. This would also explain the high values of Tl-C_A coupling constants. That the intermediate with a bridging cyanide is

Table 3.5: Calculated bond lengths and total molecular bonding energies for complexes **I**, **Ih**, **I'** and **Ih'**.

	I	**I'**	**Ih**	**Ih'**
Calculational symmetry	C_{4v}	C_{4v}	C_{2v}	C_{2v}
Pt-Tl_{calc} (Å)	3.10	2.47	2.60	2.63
Molecular bonding energy (kJ mol^{-1})	-8254.6	-8157.4	-15369.7	-15351.3

not detectable by Raman spectroscopy may well be due to low concentration and/or a short lifetime compared with the experimental time scale, properties which are not atypical of intermediate species. On the basis of these findings it is thus not possible to exclude that fast intramolecular rearrangements involving the axial cyanide can take place in solution, resulting in equilibrium between the two different isomers **Ih** and **Ih'**.

3.4 Conclusions

Geometry optimisations have been performed using the density functional approach on the four complexes **I-IV** $[(CN)_5PtTl(CN)_n]^{n-}$ (with n = 0-3) using the previously proposed structures[117] shown in Fig. 3.1 as starting points. Good agreement between the experimental EXAFS and Raman data and the computational results is obtained for complexes **II-IV**, but calculation significantly overestimates the Pt-Tl bond length and underestimates ν(Pt-Tl) for complex **I**.

The addition of coordinating water molecules to the thallium atom in complexes **I-III** (to form **Ih-IIIh**, Fig. 3.3) has little effect on complexes **II** and **III**, but significantly shortens the Pt-Tl bond in complex **I**, bringing it into excellent agreement with experiment. The bond length shortening is traced down to intramolecular hydrogen bonding. A similar effect on the Pt-Tl distance was also obtained for complex **I** upon coordination by five HCN molecules (to form **Is**). The decrease in the Pt-Tl bond length, although not as pronounced as for **Ih**, suggests that coordination by the nearest cyanide ligands in the crystal lattice can also affect the structure of complex **I**.

The total molecular bonding energies of **Ih** and an alternative isomer **Ih'** (in which the axial ligands on the thallium and platinum atoms are interchanged) are found to be very similar to one another. This leads us to suggest that complex **I** might exist in solution as a mixture of two isomers (**Ih** and **Ih'**), a conclusion that furnishes a rationalisation of the ^{205}Tl NMR data obtained for this complex.

Part of the work described in this chapter has been published in:

Russo, M. R.; Kaltsoyannis, N. *Inorg. Chim. Acta* **2001**, *312*, 221.

Chapter 4

Bonding and Bending in Lanthanide Chalcogenolate Complexes.

4.1 Introduction

Molecular lanthanide chemistry presents a series of synthetic challenges due to the unusual combination of high charge-to-radius ratio, large size, and lability of the metal ions. Hence the isolation of well-defined compounds depends in many cases on careful choice of ligands and in particular their donor atoms.[6,7] A key paradigm underlying this choice is Pearson's Hard-Soft principle,[131] the lanthanides behaving as fairly typical hard Lewis acids. Thus the isolation of complexes containing oxygen and nitrogen donor ligands has traditionally been fairly routine. By contrast, although a number of complexes containing, for example, neutral phosphine donors have been prepared,[34–36] the ligands tend to be labile and significant dissociation occurs.

A key conclusion from the above observations, together with the absence of geometrical preferences and extremely small ligand field effects, is that by contrast to the majority of the d-block transition elements, complexes of the lanthanides can be regarded as essentially ionic. However, a number of observations have pointed towards a limited degree of covalency influencing the behaviour of rare earth ion complexes.[60,112] It has, for example, long been known that certain *f-f* transitions show an enhanced sensitivity to the ligand environment, and it is common in the literature to encounter estimates of the percentage covalency in such complexes. Furthermore, the anomalous Mössbauer shift in a trivalent europium cyclopentadienyl complex has been interpreted as implying a substantial *f* orbital contribution to the bonding.[132] Nugent *et al.*[133] concluded that the bonding in $[Ln(\eta^5\text{-}C_5H_5)_3]$ (Ln = Pr, Nd, Er) consists of ~3% or less covalent character, based on a study of solid-state UV-visible spectra. Subsequently Hazin *et al.* used luminescence spec-

troscopy on a range of Ce compounds to suggest that the bonding in $[Ce(\eta^5\text{-}C_5H_5)_3]$ is approximately 10% covalent and is due largely to the $5d$ orbitals.[134]

Computationally, the degree of covalency in lanthanide complexes has been investigated by many groups. For example, in their seminal contribution on the electronic structure of cerocene, $[Ce(\eta^8\text{-}C_8H_8)_2]$, Dolg *et al.*[12] concluded that the metal-ring bonding is largely ionic, with small covalent contributions arising mainly from the metal 5d orbitals. Kaltsoyannis and Bursten[135] found an average of 12% metal character in the Ce-ring bonding MOs of $[Ce(\eta^5\text{-}C_5H_5)_3]$, in good agreement with the experimental results of Hazin *et al.*,[134] coming from both the $5d$ and the $4f$ levels. Li[136] has concluded that the metal $5d$ AOs are the most important in the limited covalent bonding in lanthanide trihalides, with negligible $4f$ participation. Eisenstein[137] has recently shown that the $4f$ electrons do not participate in the lanthanide ligand bonding in $[Ln(NR_2)_3]$. The consensus from these, and other, studies, is clearly that there is at most limited covalency in lanthanide complexes, and that this arises primarily from the Ln $5d$ AOs.

In recent years it has become increasingly common for synthetic chemists to prepare complexes which are mismatched in Pearson terms. The use of *anionic* soft donors has grown rapidly,[138] and a large number of complexes containing silyls,[139,140] germyls,[141,142] phosphides,[31–36] thiolates, selenolates and tellurolates[37–47] have been prepared. Brennan in particular has been instrumental in developing the chemistry of discrete chalcogenolates.[41,42] In the course of this work he and his colleagues have observed subtle differences in metal-ligand bond lengths which they attribute to *trans* influences analogous to, but an order of magnitude smaller than, those seen in the d-block.[42–44] These observations may also point to covalency playing some role in these complexes, and it has been suggested that the vacant $5d$ orbitals might act

as acceptor orbitals serving to stabilize the metal-ligand interactions.[42] Such donor-acceptor interactions have been invoked many times to account for the behaviour of the neighbouring group 4 metals with, for example, alkoxide and imido ligands and, given the spectroscopic and computational results described above, are not an implausible source of covalent effects in lanthanide systems.

A key part of any investigation of these systems requires a direct comparison of the behaviour of a hard donor ligand (such as an alkoxide) with a more polarizable analogue (such as a thiolate). Numerous mixed ligand chalcogenolates have been prepared using cyclopentadienyl ancillaries in particular, which have provided a useful database of structural parameters.[37,38,45–47] In addition, Sella *et al.* have recently prepared a series of 7-coordinate complexes containing pyrazolylborate ligands as ancillaries (see Fig. 4.1) which contain only terminal chalcogenolates and therefore form a directly comparable series.[39,40] Comparison of these complexes as a function

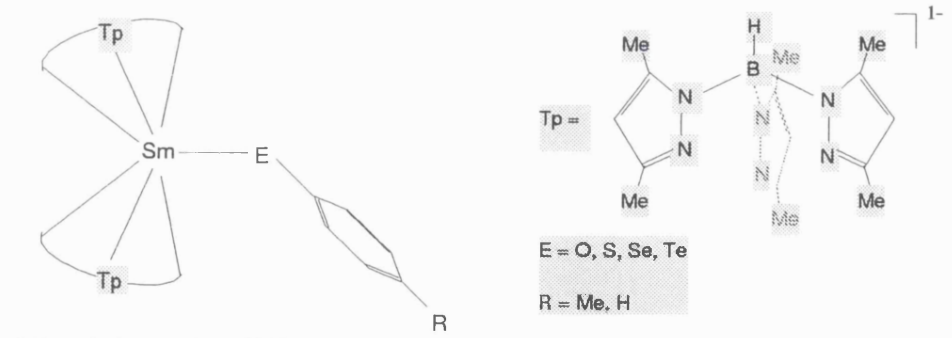

Figure 4.1: Schematic representation of the bis-trispyrazolylborate-lanthanide-chalcogenolate complexes (ref 39).

of chalcogen donor atom reveals some striking differences (all of which have been noted previously for d-block metals[143–147]). The Ln–O–C angle in the alkoxides is essentially linear (150-180°), while the heavier group 16 analogues all display a more acute angle at the donor atom (100-120°). Such behaviour has been discussed in

some detail in the case of analogous zirconium complexes by Parkin[143] who pointed out that the bending in the compounds of the heavier group 16 elements mirrors the behaviour of the hydrides, H_2E, for which the angle decreases down the group. The alkoxides are, however, striking in their deviation from that model. The linearity for transition metal alkoxo systems has previously been attributed to π donation from the oxygen lone pairs to empty metal orbitals,[148] an overlap which is less likely to occur for the heavier elements of group 16 because of their rather more diffuse p orbitals. On the basis of simple comparisons Parkin argued that the M-O-R angle was controlled by an extremely soft potential and therefore strongly subject to steric influences from the other ligands in the coordination sphere of the metal.

A second key issue, the M-O bond distance, has also been the subject of much debate. In both the transition metal and lanthanide cases the M-O distance is significantly shorter than would be expected on the basis of ionic radii. Although multiple bond character due to π overlap has been invoked, the electrostatic contribution arising from the enhanced polarization in the bond can be expected to shorten the distance considerably. This is in line with the predictions of the Shomaker-Stevenson equation which is based on electronegativity considerations.[149]

Since π overlap would be expected to have geometrical consequences while electrostatics should not, Parkin[143] and Rothwell[146,147] have plotted the bond angle at oxygen against M–O distance with a view to finding a correlation. No obvious relationship was found for either group 4 or group 5 metals. An analogous plot based on the structures of samarium alkoxides[39] has, similarly, failed to show any connection between the two parameters suggesting that in these systems also, π interactions are probably of negligible importance.

In this chapter I report the results of density functional theory studies of model

complexes of the type [$LnCp_2ER$] (Cp = η^5-C_5H_5; Ln = La, Lu; E = O, S, Se, Te; R = H, Me, Ph; see Fig. 4.2). The general aim is to address the nature of the lanthanide-chalcogen bond in order to assess the relative extent of ionicity and covalency and hence to faciliate comparison with previous rationalisations of the Ln–E interaction. A more specific goal is an explanation for the apparently anomalous structural behaviour of the alkoxides.

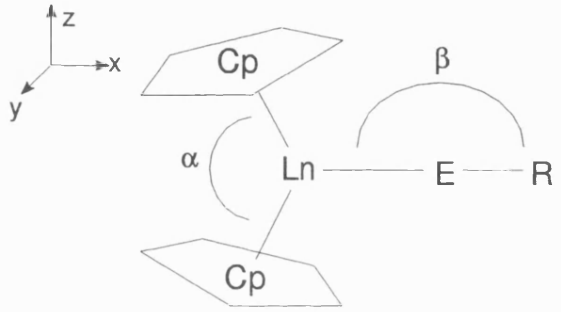

Figure 4.2: Schematic representation of the bis-cyclopentadienyl-lanthanide-chalcogenolate complexes. α is the Cp ring centroid-lanthanide-ring centroid angle; β is the angle subtended by the lanthanide, the chalcogen and the carbon atom bound to the chalcogen (or the hydrogen atom bound to the chalcogen for the model compounds with terminal EH). Potential energy curves were calculated for vertical (v) and horizontal (h) bending of the R group in the x-z and x-y planes respectively.

4.2 Computational Details

All calculations were performed on a DEC 433au workstation using the Amsterdam Density Functional (ADF) program suite (versions 2.3 and 2000).[126,150–152] The basis sets employed are uncontracted, valence-only, Slater type functions of triple zeta quality. Two polarisation functions (one *d* and one *f*) are included for carbon, oxygen, sulfur and selenium (ADF basis type V); one *p* function is added for H (ADF basis type IV). Due to the lack of experience in the use of polarisation functions for heavy elements, no polarisation functions are included in the ADF release for lanthanum, lutetium and tellurium (ADF basis type IV was used for these atoms).* Quasi-relativistic scalar corrections – Darwin and mass-velocity – were included via the Pauli formalism, in which the first-order scalar relativistic Pauli Hamiltonian is diagonalised in the space of non-relativistic basis sets.[127] The frozen core approximation was employed, and quasi-relativistic frozen 1s (C, O), 2p (S), 3d (Se) and 4d (Te, La, Lu) cores were calculated by the ADF auxiliary program 'Dirac'. The local density parametrisation of Vosko, Wilk, and Nusair[82] was employed in conjunction with Becke's gradient correction[67] to the exchange part of the potential and the correlation correction due to Perdew.[87] The convergence criteria in the calculation of the equilibrium structures were as follows: change in total bonding energy $\leq 10^{-4}$ Hartrees; change in energy gradient $\leq 10^{-3}$ Hartrees/Ångstrom. The ADF default values for these criteria (10^{-3} and 10^{-2} respectively) were employed in the calculation of the bending potential curves.

Mulliken analysis[128] was used for the investigation of the Ln–E bonding character and for the assignment of atomic charges. Other charge analysis methods available

*The choice of chalcogen basis set was driven primarily by the desire to ensure triple-zeta quality for all four atoms. The difference in the number of polarisation functions follows automatically from this choice, i.e. from the constraints of the ADF basis sets.

in ADF were also used for comparison. The Hirshfeld[153] analysis produces a charge value per atom, computed as the integral of the SCF charge density over space, in each point weighted by the relative fraction of the initial density of that atom in the total initial density of the molecule. The Voronoi[154] charge analysis assigns the charge density at a point in space to the nearest atom. However it has been noted that this partitioning of space, using mid-way separation planes, is inappropriate to produce useful absolute numbers when neighbouring atoms have very different sizes.

Molecular orbital plots were generated using the program MOLDEN.[155] The ADF output files (TAPE21) were converted to MOLDEN format using the programs ADFrom and ADFrom99 written by F. Mariotti.[†]

[†]"For details of MOLDEN, ADFrom and ADFrom99 programs, see the following URL's:
http://www.cmbi.kun.nl/~schaft/molden/molden.html
http://www-chem.unifr.ch/ac/phd/fmariotti/ADFrom.html

4.3 Results and Discussion

The experimentally characterised complexes referred to in this study have been synthesised using bulky ancillary ligands (pentamethylcyclopentadienyl or trispyrazolylborates) which sterically stabilise the metal centre. In the present calculations, however, the less computationally demanding cyclopentadienyl ligands have been used. Analogously the R group bound to the chalcogen is usually a bulky substituted phenyl group, while I have used an unsubstituted phenyl group, and also methyl or hydrogen for comparison.

I have considered two metals, lanthanum and lutetium, respectively at the beginning and the end of the lanthanide series, in order to represent the general behaviour of lanthanides. They also offer the advantage of being closed shell ions in the trivalent state. Preliminary calculations on the target systems of the present work as well as calculations on related lanthanide complexes[156] showed that the gradient corrections of Becke and Perdew give better results than the local density approximation, and such corrections have therefore been used in the present calculations.

I have carried out geometry optimisations on a series of $[LnCp_2ER]$ complexes, and have investigated the resulting equilibrium structures by means of MO and Mulliken analysis. In order to find an explanation for the anomalous linear structure of the alkoxo complexes I also calculated the potential energy curves for the bending of the Ln–E–R angle, and have analysed the factors which are most likely to affect the preferred angle β (Fig. 4.2).

4.3.1 The equilibrium structures

Geometry optimisations were carried out in C_s symmetry for $[LaCp_2ER]$ (E = O, S, Se, Te and R = Me; E = O, S and R = Ph) and $[LuCp_2ER]$ (E = O, S; R = Me,

Table 4.1: Optimised geometric parameters for the calculated equilibrium structures. See Fig. 4.2 for definition of α and β. d is the metal-Cp ring centroid distance.

Complex	α (°)	*d* (Å)	*Ln–E* (Å)	*E–C* (Å)	β (°)
$LaCp_2OMe$	130.3	2.60	2.15	1.42	179.4
$LaCp_2SMe$	136.8	2.57	2.73	1.85	119.5
$LaCp_2SeMe$	136.2	2.57	2.90	2.02	110.4
$LaCp_2TeMe$	138.1	2.55	3.14	2.23	108.3
$LuCp_2OMe$	133.9	2.32	1.99	1.41	165.1
$LuCp_2SMe$	136.8	2.29	2.54	1.84	118.1
$LaCp_2OPh$	131.4	2.58	2.19	1.35	179.9
$LaCp_2SPh$	134.2	2.56	2.78	1.79	110.6
$LuCp_2OPh$	135.7	2.30	2.01	1.34	179.8
$LuCp_2SPh$	137.0	2.27	2.56	1.79	114.0

Ph) and selected optimised bond lengths and angles are shown in Table 4.1. The optimised structures of the alkoxo complexes all feature essentially linear Ln–O–C angles. By contrast, the complexes of the heavier chalcogens show a bent Ln–E–C angle. For [$LaCp_2EMe$] the La–E–C angle β decreases going down group 16, as is observed experimentally for a series of tris-pyrazolylborate lanthanide chalcogenolates which differ only in the coordinating chalcogen atom.[39]

Experimental values for selected complexes taken from the Cambridge Crystallographic Database are shown in Table 4.2. The choice of samarium and ytterbium chalcogenolates in this table arises from the lack of experimental data on relevant lanthanum and lutetium complexes. Comparison of the data in Tables 4.1 and 4.2 shows that there is acceptable agreement between theory and experiment, particu-

Table 4.2: Experimental bond lengths and angles for some selected bis-cyclopentadienyl-lanthanide-chalcogenolate complexes.

Complex	*α (°)*	*d (Å)*	*Ln–E (Å)*	*E–C (Å)*	*β (°)*
$SmCp^*_2O(Me_4\text{-}C_6H_1\text{-}2,3,5,6)$[45]	133	2.42	2.13	1.295	172
$YbCp^*_2S(C_6H_5)(NH_3)$[47]	133	2.37	2.68	1.79	114
$SmCp^*_2Se(^tBu_3\text{-}C_6H_2\text{-}2,4,6)(thf)$[37]	129	2.48	2.92	1.90	126
$YbCp^*_2Te(C_6H_5)(NH_3)$[38]	131	2.37	3.04	2.12	113

larly given the different metals in the experimental and computational systems. The replacement of Cp* by Cp and substituted phenyl by either phenyl or methyl are also expected to contribute to the differences between the data in Tables 4.1 and 4.2. The values of α and the Ln–E bond length are closely matched between theory and experiment. d is found computationally to be larger for lanthanum and smaller for lutetium than the experimental values for samarium and ytterbium, reflecting the lanthanide contraction.[7] The E–C distances for the E–Me systems are calculated to be around 0.1Å longer than experimental values, possibly due to both sp^2 hybridization of the carbon atom and partial E-C π interaction in the experimental E–Ph systems. Crucially, and as noted above, the experimental β value for the Sm-O complex is between 50 and 60° larger than for the sulfur, selenium and tellurium systems, and this is well reproduced by the present calculations. Indeed this suggests not only that the experimental structures are mainly a result of intramolecular effects, but also that the electronic and steric influence of the substituents on the Cp's and on the phenyl group are not a major factor in determining the geometric properties of the complexes. This provides further justification of the (largely computationally-driven) choice of unsubstituted ligands.

Table 4.3: Calculated Mulliken charges on the lanthanide and chalcogen atom, and Mulliken overlap populations for the Ln–E bond.

Complex	Q*Ln*	Q*E*	*Ln–E*(e)
$LaCp_2OMe$	1.59	-0.77	0.41
$LaCp_2SMe$	1.39	-0.38	0.63
$LaCp_2SeMe$	1.46	-0.56	0.45
$LaCp_2TeMe$	1.24	-0.12	0.51
$LuCp_2OMe$	1.53	-0.85	0.63
$LuCp_2SMe$	1.12	-0.33	0.92
$LaCp_2OPh$	1.58	-0.82	0.34
$LaCp_2SPh$	1.38	-0.40	0.60
$LuCp_2OPh$	1.54	-0.90	0.60
$LuCp_2SPh$	1.08	-0.35	0.91

Having established that it is possible to satisfactorily reproduce the experimental geometric data, I turn now to examination of the Ln–E bond via Mulliken analysis of the electronic structure at the optimised geometries. The results are summarised in Table 4.3, which shows the Mulliken charges for the lanthanide and chalcogen atoms and Mulliken overlap populations of the Ln–E bond.[‡] It is evident that all the complexes have a significant degree of ionicity with a positively charged lanthanide and a negatively charged chalcogen. The Ln–E charge difference, which may be taken as a measure of the ionic character of the bond, is larger for the alkoxo complexes than for the heavier chalcogen complexes, as would be expected given the

[‡]It should be noted that the differences in the polarisation functions available in ADF for oxygen, sulphur, selenium and tellurium (see Computational Details) will inevitably affect the Mulliken analyses to a greater extent than they affect the equilibrium geometries. Thus the fine details of comparison between the data for different chalcogens in Table 4.3 may be open to question, but the key points (e.g. greater ionicity in the oxo-complexes) are more reliable.

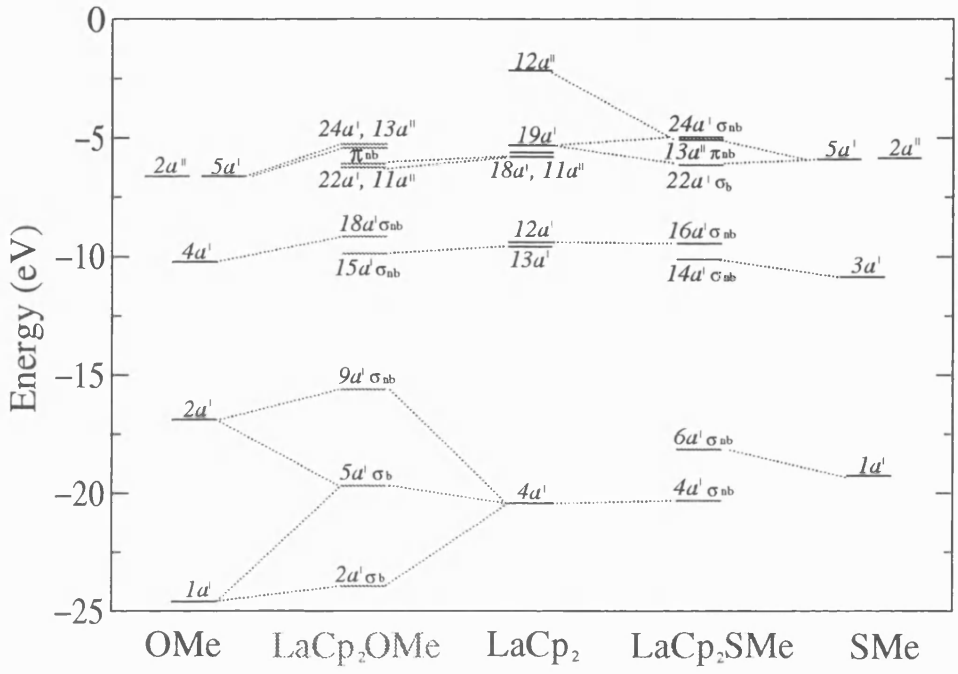

Figure 4.3: Valence molecular orbital energy level diagram for [$LaCp_2EMe$] (E =O, S).

greater electronegativity of oxygen. The overlap population of the Ln–E bond is in general not large, consistent with the expected ionicity in the complexes; however it is slightly larger for the heavier chalcogenolate complexes, confirming the view of a somewhat higher degree of covalency for these elements.

Valence molecular orbital energy level diagrams are presented in Fig. 4.3 for [$LaCp_2EMe$] (E = O, S) at their optimised geometries. The molecules have each been broken down into $LaCp_2$ and EMe fragments. In order to simplify the diagrams, only those MOs of the full molecules which contain at least 5% contribution from both the $LaCp_2$ and EMe fragments have been included. It should be noted that the extent of mixing of the fragment orbitals is generally small and, with few exceptions, the MOs on Fig. 4.3 are typically made up of approximately 10%-90% mix of fragment

orbitals. The assignment of orbitals as σ or π, bonding (b) or non bonding (nb) comes from detailed visual inspection of three dimensional pictures of each MO (not shown), and refers to the character of each MO with respect to the La–E bond.

Figure 4.3 shows that in both cases there is a small La–E σ-bonding interaction. For the alkoxo complex the main interaction is found in the $2a'$ and $5a'$ MOs which have oxygen s and p_x character with some La p_x (axis system shown in Fig. 4.2), while the highest occupied σ orbitals are non bonding. For the thiolate complex the lower lying orbitals ($4a'$ and $6a'$) remain non bonding, while a σ-bonding interaction is found in the $22a'$ MO arising from a mixing of an SMe orbital with sulfur p_x-p_z character with La $d_{x^2-y^2}$.

By contrast to the molecular orbitals of σ symmetry with respect to the Ln–E vector, those of π symmetry ($24a'$, $13a''$, $22a'$, $11a''$ for the alkoxo complex and $13a''$ for the thiolate complex) are entirely non bonding.[§] To confirm this additional calculations on [$LaCp_2OPh$] were performed in which the OPh fragment was rotated around the La–O axis in 10^o steps. Figure 4.4 indicates that the potential energy curve for this rotation is essentially flat, providing further evidence against La–O π bonding.

Therefore although a small La–E σ interaction has been found, the bonding between the lanthanum and the chalcogen is indeed mainly ionic and that there is no evidence for La–E (E = O, S) π interactions. Hence I suggest that the experimentally observed difference between the geometry of the alkoxo complexes and those of the heavier chalcogens is not due to Ln–O π bonding and arises from other factors.

[§]The reason why there are seemingly fewer π orbitals in the thio-complex is because of the different equilibrium structures of the complexes. With a bent structure, the sulphur p_x-p_z orbitals are mixed and are of σ symmetry with respect to the La–S bond and the only π orbital is the sulphur p_y. For the linear oxygen complex both p_y and p_z have π symmetry with respect to the La–O bond.

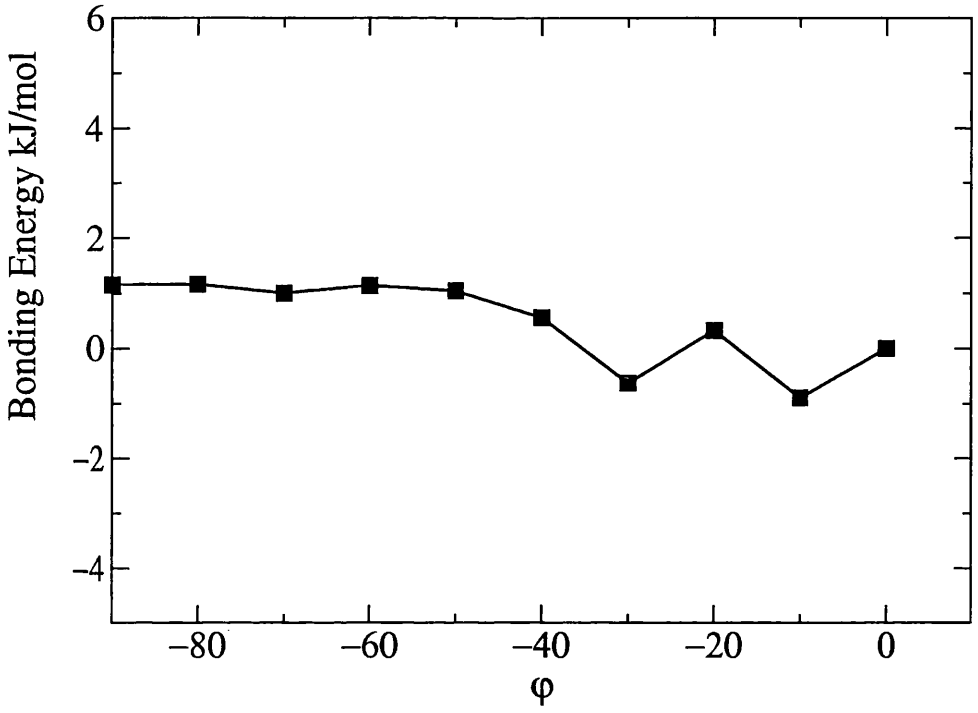

Figure 4.4: Total molecular bonding energy for [$LaCp_2OPh$] as a function of the torsional angle φ, corresponding to rotation of the OPh fragment around the La–O axis. Energy curve is scaled to an arbitrary value of 0 kJ/mol at 0^o.

4.3.2 Analysis of bending at the chalcogen atom in [$LaCp_2ER$] (E = O, S; R = H, Me, Ph)

I now address the effect of varying the Ln–E–R angle β on the energy and electronic structure of the complexes. The analysis of this bending process was carried out by "linear transit" calculations. These consist of a series of constrained geometry optimisations in which the angle β was varied from 180^o to 100^o in steps of 20^o and the rest of the molecule was optimised at each value of β in C_s symmetry. This method allows the evaluation of the potential energy curve for the bending of the R group either in the plane between the two Cp rings (horizontal bending), or towards one of the Cp rings (vertical bending). Analysis of the X-ray crystallographic data shows that vertical bending is most commonly observed for these complexes, and

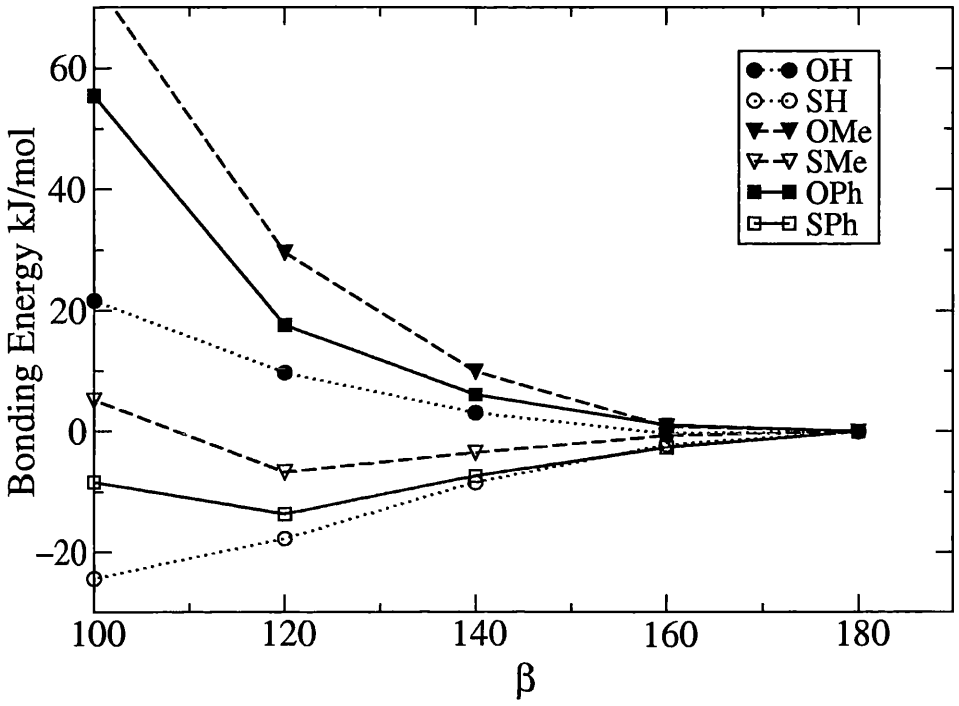

Figure 4.5: Total molecular bonding energy as a function of the La–E–C(H) angle β for [$LaCp_2ER$] (E = O, S; R = H, Me, Ph). Energy curves are scaled to an arbitrary value of 0 kJ/mol at 180°.

preliminary calculations showed that for all the complexes vertical distortion was energetically more facile than horizontal distortion. Therefore only vertical distortions (i.e. with the R group moving in the xz plane in Fig. 4.2) will be discussed here. Because it was found that the sulfur, selenium and tellurium complexes of lanthanum all behave similarly to one another upon vertical distortion, in this section I will compare only the alkoxo and thiolate complexes. The effects of bending in the lutetium complexes are discussed in section 4.3.3.

The calculated potential energy curves for the vertical bending process are given in Fig. 4.5, where bonding energies are normalised to an arbitrary value of 0 kJ/mol at $\beta = 180°$. The plot shows that the alkoxo complexes exhibit an almost flat region between 180 and 160°, with, if anything, a slight destabilization. This becomes

more pronounced at angles smaller than 140°. This is in excellent agreement with experimental findings, as the flat potential region can easily account for the range of angles (180-150°) observed for the alkoxo complexes. On the other hand the thiolate complexes show a small but significant stabilisation as the angle is decreased, with a minimum energy around 120°. This reinforces the conclusion in section 4.3.1 that the bent structure is indeed the most stable for the thiolate complexes.

What, then, is the cause of the energetic changes with alterations in β? Initially I examined the effect of changing β upon the energies of the valence MOs of the alkoxo and thiolate complexes (i.e. by constructed Walsh diagrams) but it was found that none of the valence MOs experienced any significant energy change. This is perhaps unsurprising, in view of the mainly ionic nature of the bonding in these systems. Given that there are no significant orbital factors which influence β I therefore turned to alternative explanations, and these are now discussed.

Steric aspects of the bending process

An obvious structural difference between the alkoxo and thiolate complexes is that the La–E and E–C bond lengths are smaller in the case of oxygen than sulfur. This implies that if the values of α and β are the same for the two complexes, the Cp···R distance in the alkoxo complexes will be smaller than in the corresponding thiolate complex. It is therefore possible that the linear structure of the alkoxo complexes is due to steric repulsion between the Cp and the R group, an effect which is much reduced in the thiolate complexes because of the larger La–E and E–C distances.

Analysis of the calculated geometric structures showed that there is no significant variation of the bond distances during the bending process, and that the only structural parameter (apart, of course, from β) which undergoes significant variation

Table 4.4: Values of the Cp–La–Cp angle α at β = 180 and 120°, in [$LaCp_2ER$] (E = O, S; R = H, Me, Ph)

Complex	α (β=180°)	α (β=120°)
$LaCp_2OH$	137.5	134.0
$LaCp_2SH$	128.8	133.8
$LaCp_2OMe$	137.7	127.8
$LaCp_2SMe$	129.0	135.9
$LaCp_2OPh$	135.9	128.5
$LaCp_2SPh$	134.8	136.5

is the Cp–La–Cp angle (α). The values of α at $\beta = 180^o$ and $\beta = 120^o$ are given in Table 4.4. At first glance, the data in Table 4.4 suggest that there may be merit in the steric argument, for not only does α decrease in the alkoxo complexes between $\beta = 180^o$ and $\beta = 120^o$, but it is also significantly smaller in the 120° alkoxo complex with R = Me and Ph than in the thiolate analogues. Could the destabilisation of the alkoxo complex with decreasing β be due, therefore, to reduction in α caused by Cp···R steric repulsions?

In order to test this suggestion I calculated the energetic consequences of reducing α in [$LaCp_2EPh$] (E = O, S). In both cases I took the complexes with $\beta = 180^o$ and, keeping all of the other geometric parameters fixed, performed single point calculations for α varying in 2° steps from ~136° to ~126° (i.e. the range of α seen in Table 4.4). These calculations reveal that the potential curve for varying α is very flat. For the alkoxo complex the total bonding energy changes by less than 1 kJ/mol as α reduces, while for the thiolate system the analogous energy change is ~3 kJ/mol.

It is therefore concluded that the energy changes shown in Fig. 4.5 are not due to steric interactions between the Cp and R groups as β decreases. Furthermore, given the very flat potential energy curve associated with alterations in α in the 126-136^o range, I suggest that there is little to be gained by attempting to rationalise the α values given in Table 4.4; it is clear that within the observed range α can adopt essentially any value at little or no energetic cost.

Electrostatic aspects of the bending process

The linear structure is observed for virtually all of the experimental lanthanide phenolate complexes, regardless of the nature of the different ancillary ligands, the coordination number of the lanthanide, and the substituents on the phenyl group. This suggests that the key difference between the alkoxo and thiolate complexes must be an intrinsic property of the Ln–E–C fragment, and should be common to all types of lanthanide chalcogenolate complexes.

I now address the cause of the linearity of the alkoxo systems. The changes in the Mulliken overlap populations for the La–E–C moiety during the bending process are in general very small. The values for [$LaCp_2ER$] (E = O, S; R = H, Me, Ph) are given in Table 4.5 for $\beta = 180^o$ and $\beta = 120^o$. In all cases there is a small reduction on bending, but as these reductions are typically less than $0.05e^-$, I conclude that there is very little change in the La–E covalent interaction as β decreases. The Mulliken charges (Table 4.6) are also very little affected by the bending process. However the charges in Table 4.6 indicate a significant difference between the alkoxo and thiolate systems. Oxygen is more electronegative than sulfur resulting in a higher La–O and O–C (or O–H when R = H) bond polarisation. This in turn leads to a higher positive charge on the lanthanum and carbon (hydrogen) atoms than is calculated

Table 4.5: Values of the Mulliken overlap population (e) of the La–E bond at $\beta = 180$ and 120°.

Complex	β=180°	β=120°
$LaCp_2OH$	0.35	0.27
$LaCp_2SH$	0.54	0.53
$LaCp_2OMe$	0.42	0.37
$LaCp_2SMe$	0.65	0.62
$LaCp_2OPh$	0.17	0.13
$LaCp_2SPh$	0.31	0.30

Table 4.6: Values of Mulliken charges of the lanthanum, chalcogen and carbon (hydrogen) atom bound to the chalcogen, at $\beta = 180$ and 120°

Complex	β(°)	Q*La*	Q*E*	Q*C(H)*
$LaCp_2OH$	180	1.58	-0.86	0.34
	120	1.58	-0.89	0.36
$LaCp_2SH$	180	1.38	-0.43	-0.05
	120	1.40	-0.42	-0.04
$LaCp_2OMe$	180	1.61	-0.77	0.55
	120	1.59	-0.78	0.57
$LaCp_2SMe$	180	1.35	-0.36	0.12
	120	1.38	-0.39	0.11
$LaCp_2OPh$	180	1.60	-0.81	0.44
	120	1.58	-0.80	0.45
$LaCp_2SPh$	180	1.39	-0.40	0.07
	120	1.38	-0.40	0.01

for the thiolate systems. Indeed the carbon (hydrogen) atom bound to the sulfur in all three thiolate complexes is calculated to have a charge close to zero, while in the alkoxo systems it is significantly more positive. This is important because as the angle β is decreased, the carbon (hydrogen) bound to the chalcogen moves closer to the lanthanum, and this will result in an increased electrostatic repulsion between the two positively charged atoms. Furthermore, the La···C distance is significantly smaller in the alkoxo complexes due to the smaller La–O and O–C bond lengths, and hence the alkoxo complexes should be more electrostatically destabilised than the thiolate in the bending process. This difference between the alkoxo and thiolate systems may be sufficient to influence the equilibrium value of β.

In order to gain an at least semi-quantitative measure of the lanthanum-carbon (or lanthanum-hydrogen) repulsion, I have calculated the energy of the La–C(H) electrostatic interaction for the different complexes as a function of the angle β, using Coulomb's law (Equation 4.1), in which ε_o is the vacuum permittivity, Q_{La} and Q_C are the average of the Mulliken atomic charges at $\beta = 180^o$ and $\beta = 120^o$ (Table 4.6), and r is the La···C(H) distance evaluated at $\beta = 180$, 160, 140, 120 and 100^o from the calculated structures. This approach is perhaps rather simplistic, but should give a feel for the magnitude of electrostatic factors.

$$E_{el} = \frac{1}{4\pi\varepsilon_o} \frac{Q_{La}Q_C}{r} \tag{4.1}$$

It is assumed that the charges on the lanthanum, chalcogen, and carbon (hydrogen) atoms remain constant during the bending process (which is reasonable given the data in Table 6) and that the La–E and E–C distances do not vary.

The resulting electrostatic energy curves (expressed in kJ/mol and normalised to an arbitrary value of 0 kJ/mol at 180^o) are plotted in Fig. 4.6, and clearly indi-

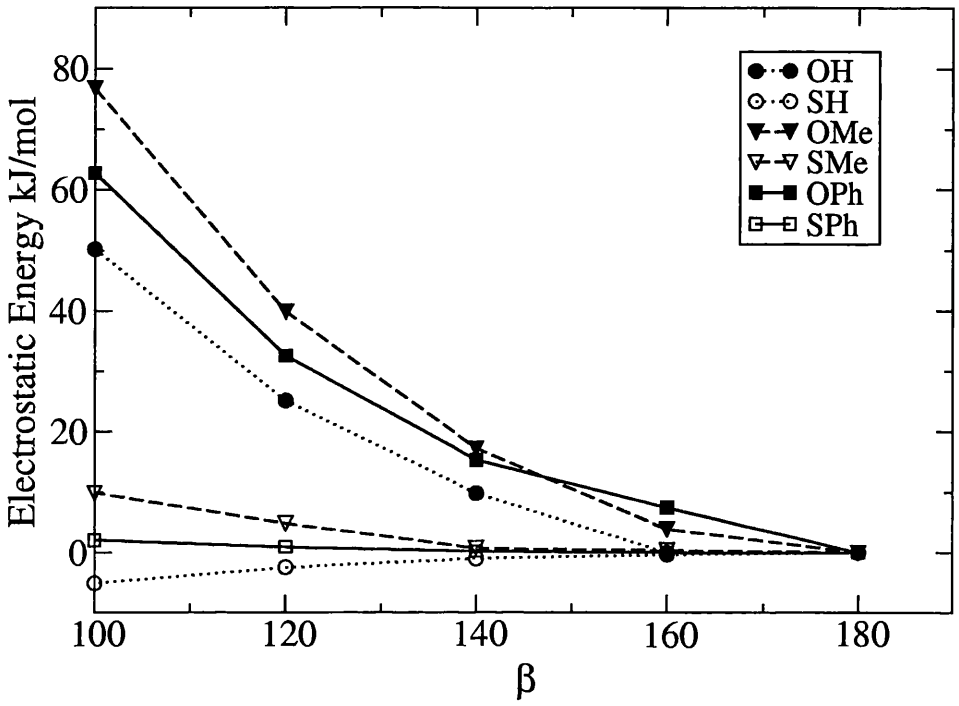

Figure 4.6: La–C(H) electrostatic interaction energy as a function of the La–E–C(H) angle β for [$LaCp_2ER$] (E = O, S; R = H, Me, Ph). Energy curves are scaled to an arbitrary value of 0 kJ/mol at 180°.

cate a significant destabilisation in the alkoxo complexes on going from the linear to the bent structure, while for the thiolate complexes the electrostatic La–C(H) interaction is essentially constant and close to zero throughout the bending process. Furthermore, the ordering of the electrostatic repulsion curves for the different R groups (Me>Ph>H) is the same as that observed for the total bonding energy (see Fig. 4.5), suggesting that the different trends observed for different R groups can also be rationalised in terms of La–C(H) electrostatic repulsion, and are mainly due to the decrease in the carbon (hydrogen) atomic charge in the order Me>Ph>H (see Table 4.6). Both the trends of the curves and the value of the electrostatic energy destabilisation for the alkoxo complexes therefore suggest that this may be a major

factor in determining their linear structure. Also, because of its generality,[¶] the same explanation can be extended to all lanthanide and transition metal chalcogenolate complexes, irrespective of differences in ancillary ligands and coordination number.

Mulliken charges are known to be influenced by the basis sets used. I therefore performed a series of single point calculations on [$LaCp_2ER$] (E = O, S; R = Me, Ph), in which ADF basis set IV (the only one available for lanthanides except II) was used for La, and either ADF basis set type III (double zeta basis sets with one polarisation function) or IV (triple zeta basis sets with one polarisation function) were used for carbon, oxygen, and sulfur (instead of V used in the calculations to this point). The Mulliken charges obtained for calculations with basis set IV are very similar to those previously calculated with basis set V (Q differences less than 0.1), i.e. the removal of the *f* polarization function for carbon, oxygen and sulfur makes very little difference to the calculated charges. On the other hand the charges obtained with basis set III show a significant discrepancy (~0.4) from previous values. Figure 4.7 shows the electrostatic energy curves for calculations with basis set type III. Comparison of Fig. 4.6 with Fig. 4.7 shows that the alkoxo complexes in Fig. 4.7 are slightly less destabilised at bent angles than those in Fig. 4.6, while the thiolate complexes are much more stabilised. Hence changing from triple-zeta to double-zeta basis sets emphasises the difference between the alkoxo complexes and the thiolate species, with electrostatic repulsion opposing bending for the alkoxo complexes but not for the thiolate complexes (indeed, a La–S attraction is calculated if using basis set III).

Other charge analysis schemes are also available in ADF (see Computational Details) and were applied to [$LaCp_2EPh$] (E = O, S) with basis set type V for the O, S and C atoms, in order to probe the generality or otherwise of the electrostatic

[¶]i.e. because it relies solely on the properties of the metal, chalcogen and ipso carbon (hydrogen) atom.

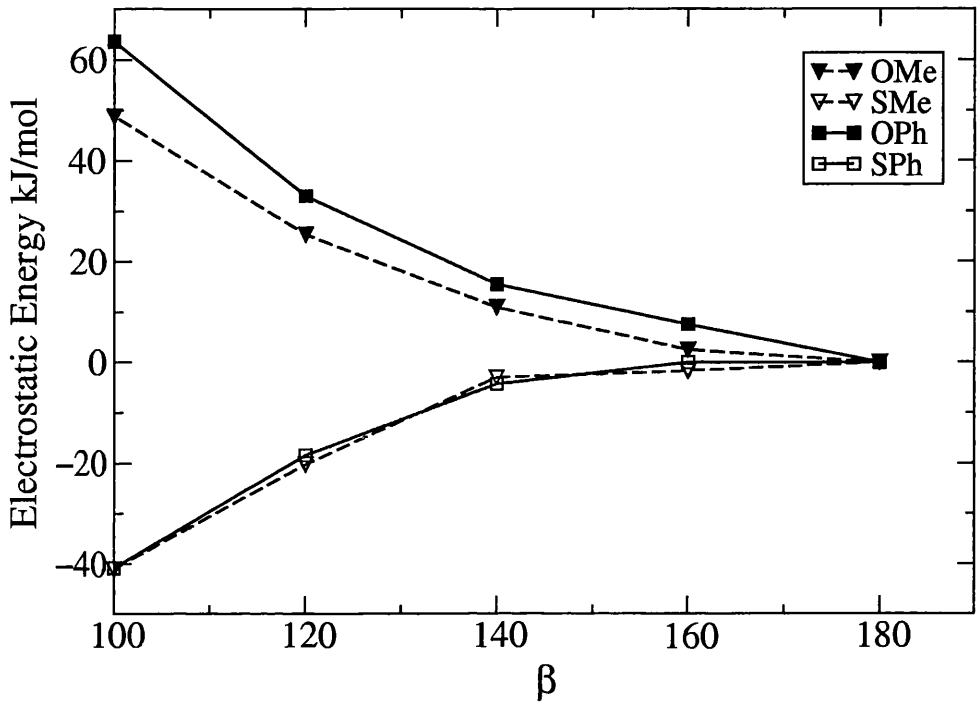

Figure 4.7: La–C(H) electrostatic interaction energy as a function of the La–E–C(H) angle β for [$LaCp_2ER$] (E = O, S; R = Me, Ph), where all atoms have basis set III except La which has basis set IV. Energy curves are scaled to an arbitrary value of 0 kJ/mol at 180°.

argument. Hirshfeld analysis produced charges for La (~0.6), E (~-0.3) and C (~0) which I believe to be too small considering the strongly ionic character of the La–E bond (a suggestion supported by a recent paper in which metal charges calculated for similarly ionic lanthanide systems using natural bond order analysis were found to be in the range + 1.5-1.8[157]). On the other hand Voronoi analysis generally produced charges which were slightly higher than those obtained by Mulliken analysis, with the only exception of the carbon atom bound to the chalcogen, which had a lower charge. Figure 4.8 illustrates the electrostatic energy curves calculated with Hirshfeld and Voronoi charges. While the Voronoi analysis shows a quantitative electrostatic destabilisation of the alkoxo complex and stabilisation of the thiolate complex with bending, the Hirshfeld analysis shows only small energy changes with

bending, although the qualitative difference between the alkoxo and thiolate systems is still evident.

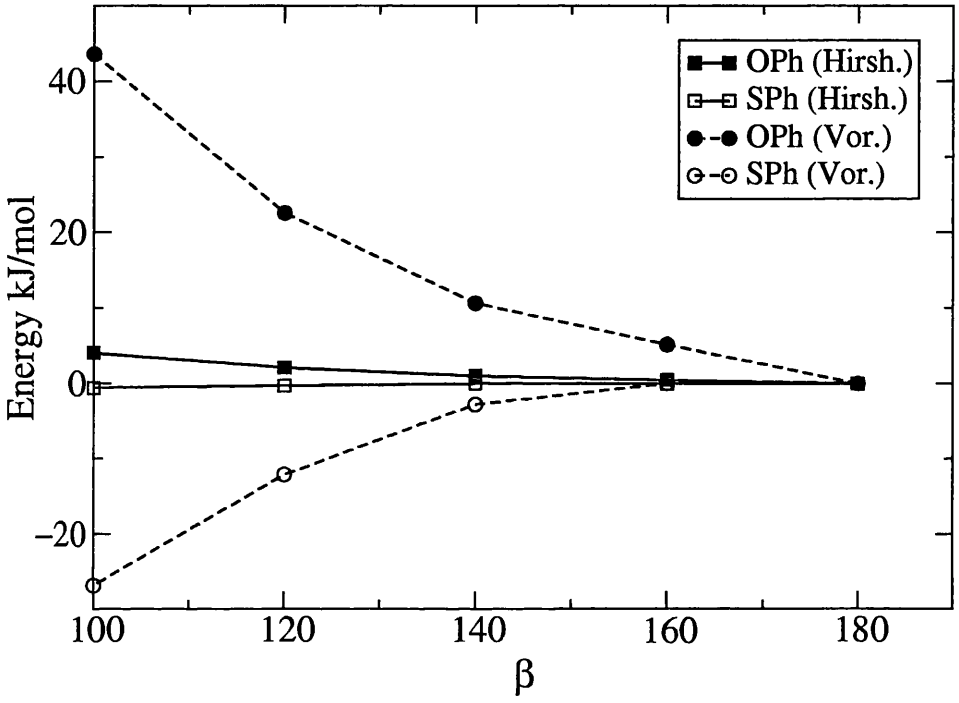

Figure 4.8: La–C(H) electrostatic interaction energy as a function of the La–E–C(H) angle β for [$LaCp_2ER$] (E = O, S; R = Ph), where atomic charges have been evaluated via Hirshfeld and Voronoi analysis. Energy curves are scaled to an arbitrary value of 0 kJ/mol at 180°.

It is therefore concluded that the method employed to calculate the atomic charges used as input to Equation 4.1 does not affect the principal conclusion, i.e. decreasing β is electrostatically destabilising for the alkoxo complexes but neutral (or even stabilising) in the thiolate systems. I also suggest that this electrostatic interaction is the driving force for the linearity observed in the alkoxo systems.

4.3.3 Analysis of bending at the chalcogen atom in [$LuCp_2EPh$] (E = O, S).

In order to investigate possible differences between systems at either end of the $4f$ block, I have performed linear transit calculations on [$LuCp_2EPh$] as described for [$LaCp_2ER$] at the start of section 4.3.2. The plots of the bonding energy vs β (not shown) reveal the same qualitative trends as for [$LaCp_2EPh$] (i.e. the alkoxo complex is destabilised on bending while the thiolate complex is stabilised). However, while the lutetium alkoxo system is destabilised by about the same amount as the lanthanum alkoxo species, the [Cp_2LuSPh] complex is 30 kJ/mol more stabilised than the lanthanum one at $\beta = 120^o$. Given that M–C electrostatic effects play such an important role in the La complexes, it was first thought that the difference in the depth of the $\beta = 120^o$ potential energy minimum between [$LuCp_2SPh$] and [$LaCp_2SPh$] results from a difference in electrostatic energies. However, the plot of Lu–C electrostatic energy in the thiolate complex (not shown) is almost superimposable on the analogous lanthanum one shown in Fig. 4.6. Further analysis reveals that this is due to two self-cancelling effects. Analysis of the calculated electronic and geometric structures at $\beta = 120^o$ shows that the charge on the lutetium atom in [$LuCp_2SPh$] is smaller than its lanthanum equivalent, see Table 4.3, but the Lu–*ipso* C distance is ~0.3Å less than the La–*ipso* C distance (reflecting the shorter Lu–S distance compared to La–S). The net result of these two differences between the lanthanum and lutetium systems is an almost identical metal-carbon electrostatic interaction.

Given that the Lu–S system is much more stabilised on bending than the lanthanum analogue, and that this is not due to differences in electrostatic effects, I turned to an examination of the valence MO structures of the two systems. In gen-

eral, the Lu–S complex has molecular orbitals which are even more localised than in the lanthanum species, and there is virtually no mixing between the fragment orbitals. This is not surprising given that the valence AOs of lutetium are expected to be more contracted than those of lanthanum, an effect emphasised by the formal charge of +3 on the metal. Comparison of orbital energies as a function of β, however, shows that the HOMO of the [$LuCp_2SPh$] system is significantly stabilized by bending ($\Delta_{180-120^o}$ = 50kJ/mol), more than any other MO and also an order of magnitude more than the HOMO of the analogous lanthanum system (indeed, as noted earlier, in the La–S system none of the valence MOs experiences any significant energy change on reduction in β). This orbital is in both complexes π antibonding between the sulfur and the e_1 p_π orbital of the phenyl ring, with much smaller contributions from the Cp rings and the metal atom.

What, then, is the reason for the significant stabilisation of the Lu–S HOMO on decreasing β? In both molecules the character of the HOMO does not appear to change, at least on visual inspection, between $\beta = 180^o$ and 120^o. In order to probe this further the AO composition of this orbital was examined in both systems at 180^o and 120^o. This analysis supports the visual one in that the composition of the HOMOs is very similar in both molecules at both angles. The only significant difference is that there is a small ($\sim$3%) contribution from the Lu $6s$ AO at $\beta = 120^o$, which is not present at 180^o or in the lanthanum molecule at either angle. Given that at 180^o the HOMO of [$LuCp_2SPh$] has an energy of -4.60 eV and that the Lu $6s$ AO in the lutetium atomic fragment used in the molecular calculation has an energy of -4.84 eV, I suggest that small admixture of $6s$ character as β decreases is sufficient to cause the stabilization of the [$LuCp_2SPh$] HOMO.

By contrast, in [$LaCp_2SPh$] at $\beta = 180^o$ the HOMO has an energy of -4.89 eV

while the La $6s$ AO in the atomic fragment has an energy of -3.84 eV. Hence, while in the lutetium system the metal $6s$ AO is more stable than the HOMO at $\beta = 180^o$, for the lanthanum complex the metal $6s$ AO is over 1 eV less stable than the HOMO. It may well be this energy mismatch that prevents the La $6s$ AO mixing into the HOMO as β decreases.

4.4 Conclusions

The work presented here has produced a number of significant results, some well-precedented and some unexpected. In the first place, DFT calculations successfully reproduce the structures of a series of lanthanide complexes and, crucially, confirm that the difference between the geometries of the alkoxo systems and those of complexes containing the heavier members of group 16 are intramolecular in origin. Detailed examination of the electronic structures at these optimized geometries indicates that the forces binding these complexes together are primarily electrostatic in origin. The shortness of the Ln–O bond may therefore be attributed simply to the additional polarity arising from the enhanced electronegativity difference compared with the elements lower in the group. This is in line with predictions based on the Shomaker-Stephenson equation.[149]

At the same time, the present calculations effectively rule out π donation from the oxygen to the vacant $5d$ orbitals of the metal in these systems. Such interactions have long been claimed for the early transition metals in high oxidation states, and have always been assumed to be present for the lanthanides also. My calculations rule this out for the lanthanides at least.

A second key point concerns the origin of the linearity at oxygen in the alkoxides. This has often been interpreted, again, as resulting from a π overlap of the kind excluded above. The present work shows that a much simpler and more obvious effect, the electrostatic repulsion between the metal centre and the *ipso* carbon of the phenoxide group, accounts for the increase of this angle compared with, for example, water and alcohols. Thus a second-order electrostatic effect contributes significantly to the arrangement of the ligands around the metal centre. The in-

triguing possibility therefore exists, that for highly electronegative donor atoms, such as oxygen or nitrogen, bound to high oxidation state metal centres, a simple electrostatic reason underlies the observed geometries. Thus the disagreements in the literature over the electron count of linear vs. bent imido groups as being 1- or 3- electron donors, may need to be reevaluated. While π donation may be a factor in such systems, the electrostatic repulsion between the metal centre and the nitrogen-bound carbon may also play a role in determining the geometry. It may also be the case that electrostatics can account for the bent geometry of the sulfur, selenium and tellurium compounds. I have shown that the energetic preference of [$LaCp_2SMe$] and [$LaCp_2SPh$] for the bent structure is not large ($\sim$5 and 10 kJ/mol respectively). Given the lack of any clearly identifiable orbital reason for the bent structure, it is possible that an attractive electrostatic force between the metal and the *ipso* carbon atom drives the molecules away from 180°. My calculations are much less clear cut on this issue than for the alkoxo systems, the La–*ipso* C electrostatic energy being very basis set dependent. Nevertheless, the possibility exists that the differing geometries of both the alkoxo and thiolate systems are driven exclusively by electrostatics.

How then to test these conclusions experimentally? It would be an intriguing experiment to attempt to correlate data from the Cambridge Database with calculated M–C electrostatic interaction energy. The large amount of data available in the database may be sufficient to negate the complications of packing forces etc. At the same time, it should be possible to prepare a set of identical compounds of the type [Tp^*_2LnOR] (Tp^* = dimethyl-trispyrazolylborate, R = C_6H_4-4-X) such that the X can be varied to modulate the charge buildup at the *ipso* carbon. It may then be possible to observe subtle changes in structure by X-ray crystallography. Con-

versely, it is intriguing to speculate on the possibility of "straightening" the sulfur in thiolate complexes by increasing the positive charge on the appropriate carbon atom. Unfortunately recent experiments by Brennan and coworkers[158] give little comfort in this direction since the structures of lanthanide pentafluorophenyl thiolates are stabilized by Ln–F–C interactions involving the ortho-fluoro substituents. Nevertheless it may be possible to construct systems in which the ortho interactions are suppressed.

Part of this work has been communicated in:

Russo, M. R.; Kaltsoyannis, N.; Sella, A. *Chem. Commun.*, "in press".

Chapter 5

Exploratory studies on the synthesis of functionalizable trivalent lanthanide complexes with calix[4]arene ligands

5.1 Introduction

5.1.1 The Calixarenes

In recent years the growing interest in supramolecular and host-guest chemistry has drawn attention to a new class of easy to synthesise and versatile macrocycles, the calixarenes. These interesting beaker-shaped molecules are obtained by condensation of p-alkylphenols with formaldehyde in alkaline conditions (Fig 5.1). The number of phenolic units in the ring can be varied depending on the reaction conditions, which in the case of p-tert-butylphenol have been optimized by the work of Gutsche.[159] However, the mechanisms which lead to the formation of the different oligomers are not fully understood, though it seems clear that calix[4]arene (n = 4) is the thermodynamically most stable product.

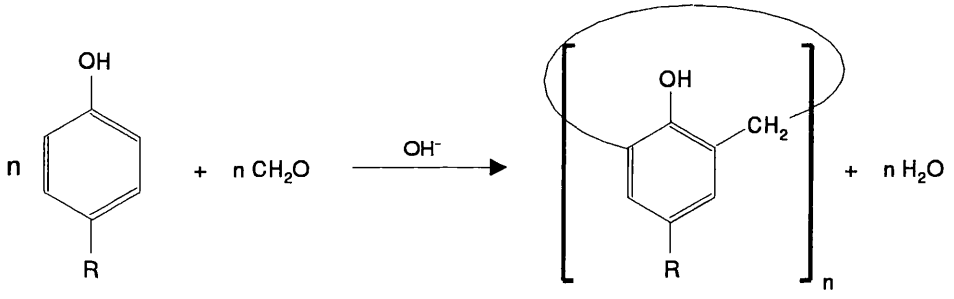

Figure 5.1: One pot synthesis of calixarenes (n = 4-8).

Due to the relatively low barrier for rotation about the σ bonds of the methylene groups, calixarenes also exhibit an intriguing conformational flexibility. The cone conformation of the t-butylcalix[4]arene (all oxygens on the same side of the molecular plane defined by the methylene groups) is shown in Fig 5.2. This is the preferred conformation for many calix[4]arenes and calix[5]arenes, being also stabilised by intramolecular hydrogen bonding between the hydroxyl groups.[159–161]

The strong affinity of the phenolic oxygens for Lewis acids and their preordered

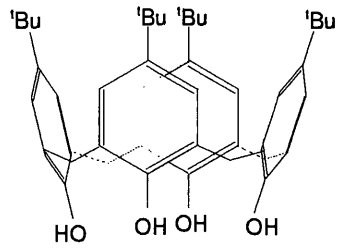

Figure 5.2: Cone conformation of t-butylcalix[4]arene (R = ^{t}Bu). The phenolic oxygens constitute the lower rim of the cone, while the ^{t}Bu groups are at the upper rim.

arrangement within the calixarene macrocycle has led these molecules to be used as metal binding ligands in coordination chemistry, and they have proved to bind efficiently both main group[162–164] and transition metals.[165,166] The facility of functionalizing both phenolic groups (lower rim) and substituents on the aromatic ring (upper rim) offers the advantage of tailoring the binding properties and solubility of the calixarenes as needed, and has recently given these molecules an ever increasing importance in technological applications. It has also been noted that the calixarenes have the ability to bind aromatic molecules and metal cations within their cavity. This characteristic has opened up a series of possibilities in host-guest chemistry and molecular recognition processes.[167]

In lanthanide chemistry, the search for selective complexing agents for the treatment of nuclear waste has often pointed to the use of macrocyclic, chelating ligands.[168,169] Another research area in which the use of effective macrocyclic complexing agents for lanthanide metals has been explored is the study and technological development of optical devises based on the electronic properties of the rare earth metals.[170,171] Being bulky, polydentate, hard ligands the calixarenes can satisfy the electronic and steric requirement of the large, and rather hard lanthanide cations. The binding capacity of calixarene derivatives towards lanthanide ions has been

widely investigated, and their use in lanthanide chemistry seems promising.[172–176]

5.1.2 Coordination chemistry of the calixarenes

Reports on the first metallo-calixarene complexes appeared about ten years ago, when Harrowfield[177,178] and Floriani[179,180] respectively presented the first lanthanide and transition metal complexes with calixarene ligands. In 1990 Floriani[179] reported the synthesis and structural characterization of a molybdenum complex with the t-Bu-calix[4]arene tetraanion, L^{4-}. The calixarene retains its cone conformation resulting in an almost planar array of the four oxygens which coordinate an oxomolybdenum unit (M=O). Similar mononuclear complexes have been obtained with the same ligand and differently functionalized molybdenum[181] and tungsten[182] moieties.

The t-Bu-calix[4]arene tetraanion also proved to be capable of coordinating bimetallic units, and interesting complexes supporting doubly and triply bonded tungsten[183,184] and di-molybdenum units[183,185] have been synthesised. However the formation of more complicated polynuclear complexes with bridging calixarenes has also been reported, especially when the metal atom is in a low oxidation state (such as group 12, 13 and *f*-group metals) or with calixarene ligands containing 6 or more phenolic rings.[163,164,180,186–188]

Comparing both the unsubstituted t-Bu-calix[4]arene (H_4L) and the 1,3-dimethyl t-Bu-calix[4]arene ether (H_2L^{Me}), Raston et al. noticed that the mononuclear Al(III) complex was readily accessible using the partially alkylated ligand,[163] while a binuclear complex was obtained with the unsubstituted ligand. This alkylated calixarene also leaves more possibility for functionalization at the metal centre, so that the 1,3 methylated ligand (H_2L^{Me}), has recently been used to synthesize calixarene

supported zirconium alkyls and to explore the insertion of CO and CN^- on the metal carbon bond.[187] Because of the almost planar array of the phenolic oxygens, calix[4]arene metal complexes have also been used as a model to study the reactivity of metals bound to oxo-surfaces.[189–191]

Another characteristic feature of the calixarenes is their capacity to bind neutral molecules and metal ions inside their cavity leading to an even richer chemistry.[167] Because of their propensity to host aromatic molecules, one can for example achieve self-assembly of metallo-calixarenes in organized supramolecular structures by appropriate functionalization of the metal atom.[182] Calix[4]arene has also shown a remarkable affinity for metal cations, which are bound into the cavity through π interactions with the aromatic rings and coordination by some of the phenolic oxygens.[160,192,193]

Based on this property, a calix[4]tube (i.e. two calix[4]arene molecules interconnected at the lower rim through ethylene linkages) has been synthesized and used as a model for the study of selective protein transport of potassium through cell membranes, a biological process in which π bonding is believed to play a significant role.[194]

Further studies were carried out on the inclusion of cationic species inside the calixarene cavity, and it was shown that the presence of alkali metal ions inside the cavity can influence the coordination of transition metals at the phenoxo binding sites,[195] and vice versa (i. e. the presence of coordinated transition metals affects the π basicity of the calixarene cavity).[186]

With regard to the lanthanides there exist a relatively small number of complexes with calixarene ligands. The first report dates back to 1987 when Harrowfield *et al.* synthesized a bimetallic lanthanide calixarene complex, with two Eu(III) coor-

dinated by the t-butylcalix[8]arene hexa-anion.[177] Soon after, the analogous lanthanide complex with a triply deprotonated t-butylcalix[4]arene anion, HL^{3-}, was synthesized. The complex, $[Eu_2(\mu\text{-}\eta^2\text{-}\eta^2\text{-}HL)_2(dmf)_4]\cdot 7(dmf)$, was shown to be a dimer with the calix[4]arene ligands bridging between the two trivalent europium ions.[178]

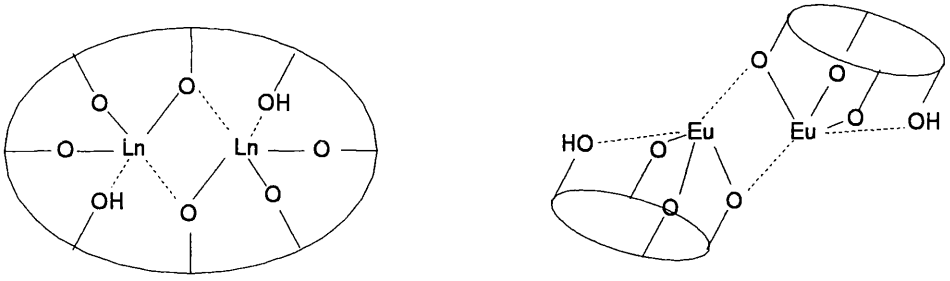

Harrowfield et al., *Inorg. Chem.*, **1987**

Harrowfield et al., *Dalton*, **1989**

Figure 5.3: Schematic representation of the first reported lanthanide calixarene complexes, ref 177 and 178 (the drawing is simplified by omitting coordinating solvent molecules and the phenolic units of the ligand).

Thanks to the work of Bünzli, it was soon understood that calixarenes could enhance the luminescence of coordinated lanthanide ions by acting as an absorption unit and transferring energy to the metal.[172,196] In fact a great deal of attention has been devoted to the synthesis of lanthanide luminescent probes using calixarenes and calixarene derivatives as ligands.[172–174,196–202] Furthermore it was shown that upper rim functionalization of the calixarene ligands affects the photophysical properties of the resulting lanthanide complex and therefore offers a way of tuning the properties of the encapsulated metal.[173] As a result an attempt has recently been made to introduce lanthanide-binding units (such as different pyridine-2,6-dicarboxylates) into the calix[4]arene skeleton by lower rim substitution. This was done in the hope of providing highly luminescent lanthanide complexes and devise a mechanism for

luminescence control in such complexes. However, as shown in Fig 5.4, the binding properties of these neutral pendant arms proved relatively poor.[202]

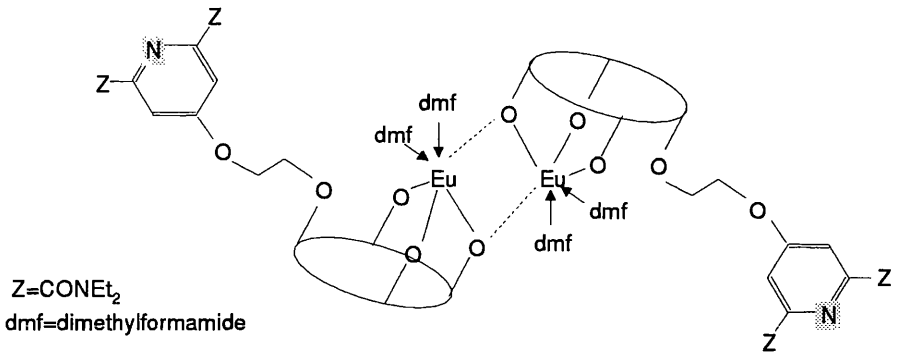

Harrowfield et al., *Inorg. Chem.*, **2000**

Figure 5.4: Schematic representation of a lower rim substituted calix[4]arene bimetallic complex (ref 202). Note that the pendant tridentate groups are rejected by the metal in favour of bridging phenoxide and solvent o-donors. (The drawing is simplified by omitting the phenolic units of the ligand.)

More generally, lower-rim substitution of calixarenes, particularly with functional groups containing coordinating atoms such as oxygen,[199,200,203,204] nitrogen[176,197,198,201] and phosphorus,[174,175,205] has proved highly effective as a strategy to increase the binding and selectivity of the ligand towards lanthanide ions. The binding properties of the calixarenes towards the *f*-elements were also shown to be significantly influenced by the presence of alkali metals. The inclusion of different alkaline metal ions in the cavity of calixarene carboxylate derivatives does affect the extraction selectivity of lanthanide ions from aqueous solution.[204] Similarly the binding capacity of calix[6]arene towards uranyl ion was shown to be influenced by the presence of Cs^+ inside the calixarene cavity.[206]

Despite the consistent number of reports on lanthanide complexes with calixarenes and calixarene derivatives, these molecules are mostly isolated as dimeric species with bridging ligands, or as 2:1 bimetallic complexes when the calixarene is

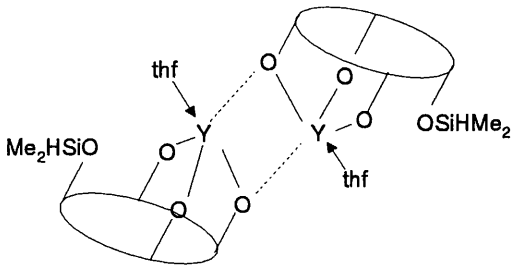

Anwander et al., *Inorg. Chem.*, **2000**

Figure 5.5: Typical lanthanide bimetallic complex with bridging calixarene ligands (ref 190). (The drawing is simplified by omitting the phenolic units of the ligand.)

made by more than 6 phenolic units (see Fig 5.3, Fig 5.4, Fig 5.5 for typical examples). This is partly due to the ionic nature of the rare earth metals and also to the high number (usually 4 or more) of binding sites in the ligands. A monomeric 1:1 complex has recently been synthesised (although not structurally characterized) using a lower rim substituted calix[4]arene with strongly coordinating phosphoryl pendant arms, so as to completely encapsulate the metal ion and prevent it from interaction with anything else in the solution.[174] Similar 1:1 complexes have been obtained using the 1,3-bis(diethylamide)-substituted calix[4]arene, with the lanthanide ion being further coordinated by a picrate trianion to a total coordination number of 8.[203] Although these 1:1 complexes (see Fig 5.6) can prove useful for certain purposes where complete shielding of the lanthanide ion is required (such as selective extraction of lanthanide ions or exploitation of their luminescence properties), the synthesis of more reactive mononuclear lanthanide complexes with calixarene ancillaries might offer a better chance to explore the reactivity at the coordinated lanthanide metal center.

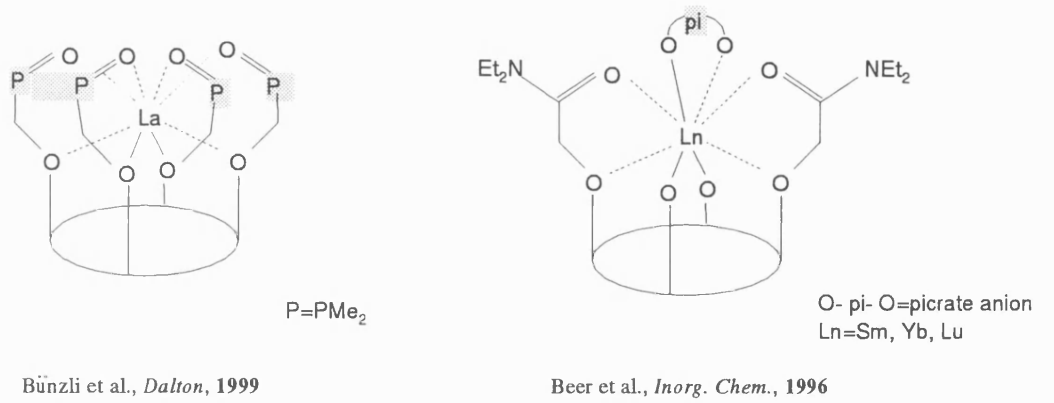

Bünzli et al., *Dalton*, **1999**

Beer et al., *Inorg. Chem.*, **1996**

Figure 5.6: Schematic representation of mononuclear lanthanide calixarene complexes (ref 174 and 203) (the drawing is simplified by omitting the phenolic units of the ligand).

A few years ago Bochkarev *et al.* reported the synthesis of an interesting mononuclear complex of trivalent thulium with the partially alkylated 1,3-dimethoxy t-Bu-calix[4]arene, $[Tm(L^{Me})I(OEt_2)]$. This molecule, illustrated in Fig. 5.7, is the first reported example of a mononuclear, lanthanide calix[4]arene complex, with the iodide leaving scope for further functionalization at the metal centre. The reaction used for its synthesis however, was rather costly as it involved reduction of the phenolic groups to phenoxide by two equivalents of divalent thulium iodide:[207]

$$H_2L^{Me} + 2TmI_2 \longrightarrow [Tm(L^{Me})I(OEt_2)] + TmI_3 + H_2 \qquad (5.1)$$

Furthermore this route seems to be viable only with the strongly reducing TmI_2 and does not proceed with the less reducing SmI_2.

The coordination of lanthanide on to a calixarene ligand has very recently been achieved by reaction of a lanthanide triflate, $Ln\{O_3SCF_3\}_3$, with calix[6]arene (H_6L) using pyridine as solvent.

$$H_6L + 2Ln\{O_3SCF_3\}_3 + 8pyridine \longrightarrow [Ln\{(O_3SCF_3)(pyridine)_4\}_2H_2L] \qquad (5.2)$$

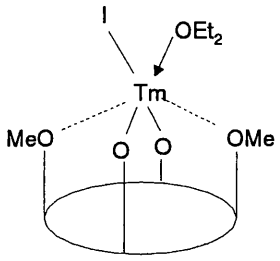

Bochkarev et al., *Z. Naturforsch. (B)*, **1999**

Figure 5.7: Schematic representation of the first mononuclear functionalizable lanthanide cali[4]xarene complex, ref 207 (the drawing is simplified by omitting the phenolic units of the ligand).

The resulting lanthanum, and samarium complexes (see Fig 5.8) were isolated and structurally characterized. These complexes would also lend themselves to functionalization at the lanthanide metal through loss of the triflate ion, however they decompose completely (within a few hours) when isolated as solids, even if kept under argon or nitrogen, and in the absence of light.[208]

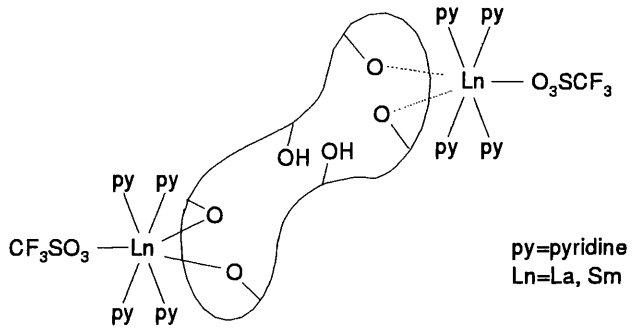

Leverd et al., *Eur. J. Inorg. Chem.*, **2001**

Figure 5.8: Schematic representation of a 2:1 functionalizable lanthanide calix[6]arene complex, ref 208 (the drawing is simplified by omitting the phenolic units of the ligand).

A more satisfactory synthetic route to functionalizable lanthanide calixarene

complexes is therefore needed. In this chapter we describe the synthesis of a series of trivalent functionalizable lanthanide complexes using differently substituted calix[4]arene as ancillary ligands.

5.1.3 Aspects of the coordination and organometallic chemistry of lanthanides

Due to their physical and chemical properties the synthesis of monomeric, homoleptic lanthanide complexes is rather challenging and there are few such complexes reported in the literature, especially when compared to analogous transition metal complexes. In order for the lanthanide metal to attain steric saturation, the formation of oligomers, adducts with solvent, and/or lanthanide -ate complexes is often encountered, the particular type depending on the size of the metal, the nature of the ligand, the type of solvent, and the presence of suitable counter-ions.

Our project aims at the synthesis of functionalizable calixarene complexes of trivalent lanthanides, and for this task homoleptic lanthanide amides and organometallic complexes would be ideal starting materials in protonolysis reactions with the calixarene (see Fig 5.10). A brief description of known lanthanide amides and organometallic complexes and their synthetic routes is therefore provided in the next two sections.

Lanthanide amides

The synthesis of lanthanide amides involves the reaction of an anhydrous lanthanide halide with the alkali metal salt of the amine:

$$LnX_3 + 3MNR_2 \longrightarrow Ln\{NR_2\}_3 + 3MX \text{ (M = Li, Na, K; X = Cl, I)} \qquad (5.3)$$

Although the synthetic route described above is quite simple, it often leads to the formation of undesired products. Reaction of lanthanide trichloride with dimethyl-

and diethyl- lithium amides results in fact in the formation of insoluble products probably due to the aggregation in polymeric chains.[209]

By reaction of lanthanide trichloride with 3 equivalents of the slightly bulkier di-isopropyl lithium amide, a mixture of the thf adduct of the tris amide and the tetrakis lanthanide -ate complex are formed.[22]

$$LnCl_3 + 3LiN^iPr_2 \longrightarrow [Ln\{N^iPr_2\}_3(thf)] + [(thf)Li(\mu\text{–}N^iPr_2)_2Ln(N^iPr_2)_2] \quad (5.4)$$

The proportion of the tetrakis amide is usually very small but difficult to separate, however the reaction of lanthanide trichloride with 2.5 equivalents of isopropyl amide, was reported to give the pure thf adducts of the tris-amide.[22] Similarly Gambarotta *et al.*[23] reported the synthesis of the thf adduct of the cyclohexyl amide, $Sm\{NCy_2\}_3(thf)$, by reaction of $SmCl_3$ with 2.85 equivalent of the lithium cyclohexyl amide.

In order to increase the steric shielding, and therefore the stability of the central metal atom bulkier amides have been used. With lithium diphenylamide the tetrakis complex $[Li(thf)][Ln\{NPh_2\}_4]$ (Ln=Er[210] and Yb[211]) were reported.

$$LnCl_3 + 3LiNPh_2 + thf \longrightarrow [Li(thf)][Ln\{NPh_2\}_4] \quad (5.5)$$

The tetrakis $Sm\{NPh_2\}_4[Na(TMEDA)]_2$ and the thf adduct $Sm\{NPh_2\}_2(thf)_4$ were also obtained[23] by reaction of divalent samarium iodide with sodium and potassium diphenylamide respectively, in the presence of TMEDA/thf.

$$SmI_2(TMEDA)_2 + 4NaNPh_2 \longrightarrow Sm\{NPh_2\}_4[Na(TMEDA)]_2 \quad (5.6)$$

$$SmI_2(thf)_2 + 2KNPh_2 \longrightarrow Sm\{NPh_2\}_2(thf)_4 \quad (5.7)$$

The synthesis of lanthanide complexes with other aromatic amides have been described by Evans.[24] Starting from the potassium salt of aniline, 2,6-dimethylaniline,

and 2,6-diisopropylaniline a whole series of lanthanide arylamido complexes including dimers, thf adduct, and -ate complexes were reported. By reaction of $LnCl_3$ (Ln = Y, Nd, Yb) with 3 equivalent of potassium diisopropyl arylamide, the thf adduct of the tris amide was isolated in good yields.

$$LnCl_3 + 3KNHC_6H_3\ ^iPr_2 \longrightarrow Ln\{NHC_6H_3\ ^iPr_2\}_3(thf)_n \qquad (5.8)$$

The number of coordinating thf molecules in the above adduct was found to vary with the metal (n = 2 for Y, Yb; 3 for Nd).

By use of the even bulkier bis-trimethylsilyl-amide, $-N(TMS)_2$,[21] and the pentafluorophenyl-trimethylsilyl-amide, $-N(C_6F_6)(TMS)$,[212] where TMS = $Si(CH_3)_3$, the corresponding tris homoleptic lanthanide complexes have been obtained without contamination by other products. These complexes where also shown to be stabilised by agostic interactions through the Me groups in the TMS, and by Ln–F interactions.[212]

Lanthanide organometallics

The first reported molecules containing carbon-lanthanide bonds were the cyclopentadienyl complexes,[213] and for many years the complexes with cyclopentadienyl and substituted cyclopentadienyl ligands have been the most used and most studied lanthanide organometallics.[25] Their synthesis involves the reaction of a divalent or trivalent lanthanide halide with NaCp (Cp = C_5H_5), with the Cp coordinating the metal in η^5 fashion.

$$LnCl_3 + 3NaCp \longrightarrow LnCp_3 + 3NaCl \qquad (5.9)$$

$$LnI_2 + 2NaCp \longrightarrow LnCp_2 + 2NaI \qquad (5.10)$$

These molecules exist as monomeric thf adducts in solution. In the solid state they attain steric saturation by bridging Cp ligands, the number of which and the

particular mode of bonding, depend on the size of the metal.[3]

Despite initial attempts at the synthesis of σ bonded methyl[214] and ethyl[215] lanthanides, simple monomeric complexes with these ligands have not unambiguously been characterized. However in the presence of excess MeLi the $[LnMe_6][Li(dme)]_3$ -ate complex was isolated (Ln = Y, Ce, Nd, Sm, Gd, Tb, Dy, Er, Lu).[216]

$$LnCl_3 + 6MeLi + 3dme \longrightarrow [LnMe_6][Li(dme)]_3 + 3LiCl \qquad (5.11)$$

By reaction of a lanthanide chloride with t-butyl lithium the corresponding lanthanide tetrakis salt was isolated (Ln = Tb, Er, Yb, Lu).[217,218] By the same reaction route, the tetrakis σ bonded aryls $Li[LnPh_4]$ (Ln = La, Pr) were isolated but not structurally characterized.[214] Using the bulkier xylyl (2,6-dimethylphenyl) group however, the corresponding tetrakis salt was obtained and structurally characterized, showing a tetrahedral environment of the lanthanide ion.[29]

$$LuCl_3 + 3Li(2,6\text{–}C_6H_3\text{–}Me_2) + thf \longrightarrow [Li(thf)_4][Ln\{2,6\text{–}C_6H_3\text{–}Me_2\}_4] \qquad (5.12)$$

Despite the high steric hindrance of the t-butyl, phenyl and xylyl groups, the corresponding complexes were obtained as tetrakis salts. This problem, which often arises when metathesis reactions are involved, can be avoided by using alternative reaction routes. Transmetallation reactions proved to be successful. Reaction of europium and ytterbium metals with bis(pentafluorophenyl) mercury lead to the corresponding bis homoleptic aryls:

$$Ln + Hg\{C_6F_5\}_2 \longrightarrow Ln\{C_6F_5\}_2 + Hg \quad (Ln = Eu,\ Yb) \qquad (5.13)$$

Structural analysis proved that these molecules are stabilized by intramolecular metal-fluorine interactions, explaining why decreasing the number of fluorine on the ring resulted in significant destabilization of the complexes.[219–221]

In an exciting development Bochkarev[28] has reported the synthesis of tris phenyl lanthanides, using catalytic amounts of LnI_3 to activate the metal.

$$2Ln + 3HgPh_2 + thf + LnI_3 \longrightarrow 2LnPh_3(thf)_3 + Hg \quad (Ln = Er, Tm) \qquad (5.14)$$

These molecules are stabilized by the formation of adducts with thf and were isolated as highly air sensitive crystals.

The first structurally characterized lanthanide neutral homoleptic alkyl was reported by Lappert by use of the bulky bis(trimethylsilyl)methyl ligand, -$CH(TMS)_2$.[30]

$$Ln\{OAr\}_3 + 3LiCH(TMS)_2 \longrightarrow Ln\{CH(TMS)_2\}_3 + 3LiOAr \qquad (5.15)$$

With the same ligand the corresponding divalent lanthanide alkyl was isolated as adduct with diethyl ether:[222]

$$YbI_2 + 2NaCH(TMS)_2 + Et_2O \longrightarrow [Yb\{CH(TMS)_2\}_2(Et_2O)_2] + 2NaI \qquad (5.16)$$

while using the even bulkier tris(trimethylsilyl)methyl, -$C(TMS)_3$, the bis homoleptic alkyl was obtained.[223]

$$YbI_2 + 2KC(TMS)_3Et_2O \longrightarrow Yb\{C(TMS)_3\}_2 + 2KI \qquad (5.17)$$

The metal centre in these molecules was shown to be stabilised by agostic interactions with the TMS groups. A recent comparison of the Si-C and C-H bond lengths obtained by neutron diffraction analysis, has proved that the main interaction with the metal is by the β (Si-C) bond rather than the γ (C-H) bonds.[48]

5.2 Results and Discussion

Since our ultimate aim was to develop the reactivity of the metal centre in the lanthanide calixarene complexes, the unsubstituted ^{t}Bu-calix[4]arene (H_4L) with four acidic phenolic groups would be an unsuitable starting material for the synthesis of trivalent, functionalizable lanthanide complexes. Protonolysis reactions of H_4L with a basic lanthanide compound, LnX_3, (X = amide, alkyl) would result in triple deprotonation of the calixarene and formation of a complex with strong, inert metal-oxygen bonds which would then be difficult to replace, leaving little scope for further functionalization at the metal. Furthermore the presence of four acidic hydrogens on the calixarene is likely to result in formation of dimers or oligomers with bridging calixarene ligands through deprotonation by a second lanthanide-based starting material.[164,178,180,186]

A good strategy to avoid formation of oligomers and allow for further functionalization at the metal centre is to substitute two phenolic protons with alkyl groups, giving a 1,3-dialkyl-tBu-calix[4]arene ether, H_2L^{R}.[163,187,207] The 1,3 calixarene diethers also offer the possibility to control the steric saturation at the metal centre by altering the steric hindrance of the alkyl substituent on the ether oxygen atoms. Therefore in our syntheses, only the 1,3-dialkyl substituted -tBu-calix[4]arenes were used as ligands.

The synthesis of lanthanide complexes is usually achieved by a limited number of synthetic routes, namely metathesis, protonolysis and transmetallation reactions (see Table 1.2). Although transmetallation has been previously used for the synthesis of lanthanide alkoxo- and aryloxo-complexes,[224–226] it is not a viable route for the synthesis of functionalizable lanthanide calixarene complexes. Transmetal-

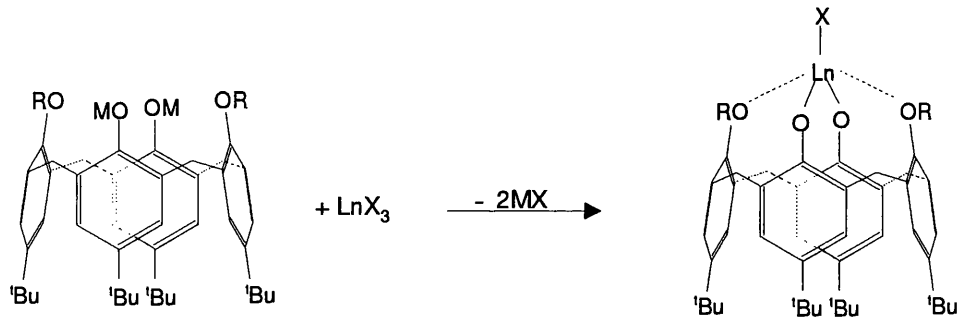

Figure 5.9: Metathesis reaction of an alkaline metal salt of the calix[4]arene ether with a lanthanide halide (M = Na, K; X = Cl, Br, I).

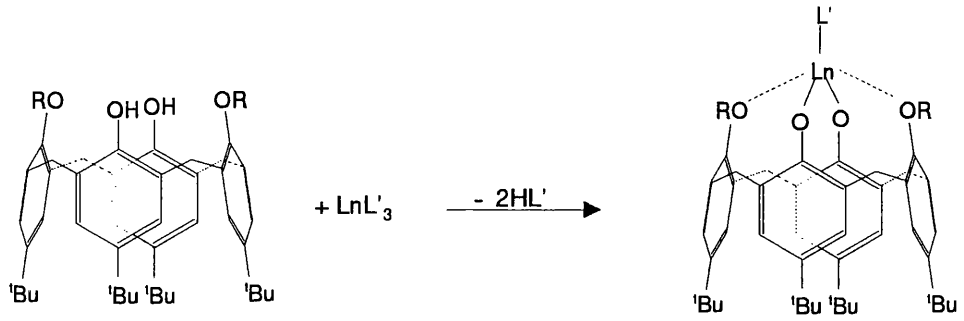

Figure 5.10: Protonolysis reaction of protonated calix[4]arene ether with lanthanide complex (L′ = amide, alkyl, aryl).

lation reaction of lanthanide metal with the divalent dialkyl substituted calixarene H_2L^R, would in fact result in complexes with a 2:3 metal to ligand ratio, $Ln_2L^{R_3}$, leaving little scope for further functionalization at the metal centre. Metathesis and protonolysis reactions are therefore better alternatives (at least in principle) for the synthesis of 1:1 lanthanide calixarene complexes. The two possible reaction pathways are illustrated in Fig 5.9 and 5.10 One problem which could arise when attempting metathesis reactions of the type described in Figure 5.9 is given by the propensity of calix[4]arenes to host alkali metal ions in their cavity. In fact, it has been recently reported that the sodium salt of H_2L^{Me} has a rather more complicated structure than depicted in Fig 5.9, as it was shown to be a dimeric species, $Na_4L_2^{Me}$, with one sodium ion inside the cavity of each calixarene and the remaining two placed in between the two calixarenes.[192] It is therefore possible that the pres-

ence of the alkali metal inside the calixarene cavity might vary the reactivity of the sodium ligand with a lanthanide halide, as will be discussed in section 5.2.3.

5.2.1 Synthesis of tBu-calix[4]arene and calix[4]arene derivatives

The synthesis of tBu-calix[4]arene from tBu-phenol and formaldehyde is a simple condensation reaction which leads to the desired product in quite high yields (see Fig 5.11).[227] The specific formation of the cyclic tetramer is accomplished via the templating effect on the sodium ion, so that in the presence of Na^+ the calix[4]arene is the thermodynamically most stable product. In order to achieve thermodynamic control, high temperatures are needed (~250 °C). The tBu-calix[4]arene was prepared on a big scale reaction and isolated in ~60% yield as a dirty white solid, and was characterized by ^1H NMR spectroscopy.

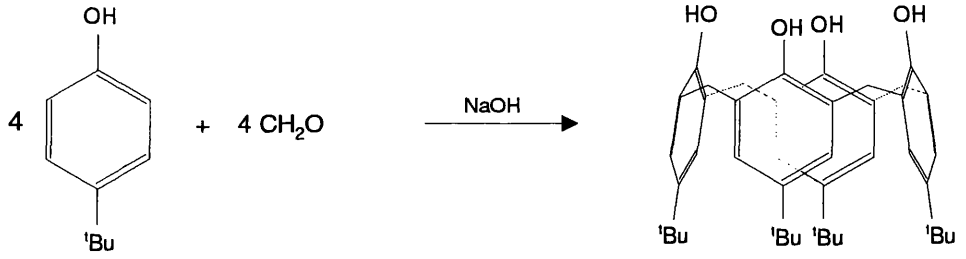

Figure 5.11: Synthesis of tBu-calix[4]arene.

The synthesis of such calix[4]arene ethers is described in Fig 5.12 and is achieved by nucleophylic attack of the calixarene phenoxide on the desired alkyl iodide. Following this procedure the dimethyl and diisopropyl ethers of calix[4]arene have been isolated as yellowish solids in good yields (89 and 82% respectively), and characterized by ^1H NMR spectroscopy and elemental analysis.

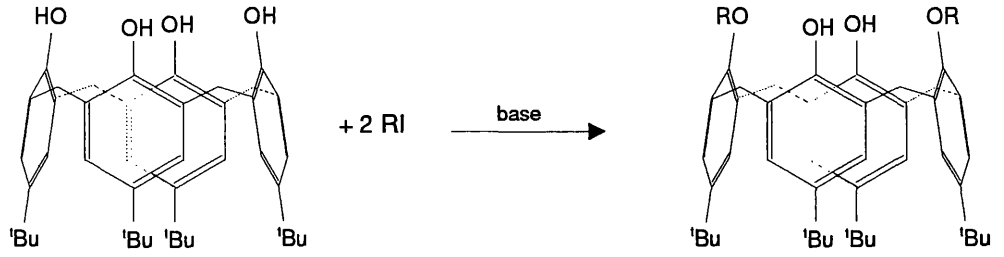

Figure 5.12: Synthesis of 1,3-dialkyl-tBu-calix[4]arene ether (R = Me, ^{i}Pr).

5.2.2 Synthesis of lanthanide starting materials

Synthesis of Lanthanide Amides

Several attempts were made to prepare new homoleptic lanthanide amides. In particular we sought amides easy to prepare from low cost starting materials, sterically saturated (so as to prevent the formation of adducts and -ate complexes) and basic enough to react readily with the protonated calixarene ligand.

The general reaction scheme for their preparation involved refluxing the selected amine with sodium hydride and adding the resulting sodium amide to a suspension of lanthanide chloride in thf:

$$HNRR' + NaH \longrightarrow NaNRR' + H_2 \tag{5.18}$$

$$3NaNRR' + LnCl_3 \longrightarrow Ln\{NRR'\}_3 + 3NaCl \tag{5.19}$$

Synthesis of Lanthanide tris bis-trimethylsilyl Amides

The yttrium and samarium homoleptic bis-trimethylsilyl amides were prepared in thf from the corresponding sodium amide. To reduce contamination by sodium amide and sodium chloride, the yttrium amide was purified by sublimation, while the samarium amide was recrystallized twice from 40-60° petrol. The products were isolated as colorless and pale yellow needle crystals respectively in 26 and 45% yields,

and were characterized by ^{1}H NMR spectroscopy.

$$LnCl_3 + 3NaN(TMS)_2 \longrightarrow Ln\{N(TMS)_2\}_3 + 3NaCl \tag{5.20}$$

Synthesis of Yttrium tris diphenylamide

Despite previous reports showing that the reaction of erbium and ytterbium chlorides with lithium diphenylamide gave the corresponding tetrakis lanthanide-ate salt,[210,211] we decided nevertheless to attempt the synthesis of the tris homoleptic diphenylamide. With two relatively bulky phenyl groups on the nitrogen and being fairly cheap, diphenylamine is an ideal starting material for the synthesis of lanthanide amides. Diphenylamine ($HNPh_2$) was refluxed with sodium hydride in thf, and the correponding sodium amide was isolated as a white solid in 95% yield.

$$HNPh_2 + NaH \longrightarrow NaNPh_2 + H_2 \tag{5.21}$$

A solution of the sodium amide in thf was then added to a suspension of yttrium chloride in thf, and after work-up, the tris homoleptic yttrium diphenylamide was isolated as colorless cubic crystals in 35% yield.

$$3NaNPh_2 + YCl_3 \longrightarrow Y\{NPh_2\}_3 + 3NaCl \tag{5.22}$$

The product, which proved highly air sensitive both in the solid state and in solution, was characterized by ^{1}H NMR spectroscopy and elemental analysis.

The ^{1}H NMR spectrum of $Y\{NPh_2\}_3$ showed a set of 8 closely spaced multiplets (ratio 1:2:1:2:1:1:1:1) in the region typical of aromatic protons, and two additional signals which could be assigned to thf. On the basis of ^{1}H NMR evidence it seems a complex of the type $Y\{NPh_2\}_3(thf)_3$ is formed. However, elemental analysis is consistent with a base free complex (see Table 5.1) suggesting that thf should not

Table 5.1: Elemental microanalysis found and calculated for $Y\{NPh_2\}_3$, $Y\{NPh_2\}_3(thf)_2$ and $Y\{NPh_2\}_3(thf)_3$.

Found	C 72.49; H 5.31; N 7.09
$Y\{NPh_2\}_3$	C 72.85; H 5.09; N 7.08
$Y\{NPh_2\}_3(thf)_2$	C 71.63; H 6.28; N 5.70
$Y\{NPh_2\}_3(thf)_3$	C 71.19; H 6.72; N 5.19

be too tightly bound to the metal and is easily removed by pumping under vacuum.

By comparison of the trivalent ionic radii of yttrium (0.901 Å) with those of erbium (0.890 Å) and ytterbium (0.868 Å) (see Table 1.1), it is clear that the tetrakis coordination previously observed for erbium and ytterbium is not due simply to their sizes, which is in fact comparable (or even smaller) than that of yttrium. A possible reason for the isolation of the tris homoleptic yttrium diphenylamide, may be due to use of sodium, instead of lithium diphenylamide as starting material. Lithium has become notorious in lanthanide chemistry for the formation of complex anions such as $[Ln\{NR_2\}_4]^-$. The use of the larger sodium ion results in the formation of the rather less soluble sodium chloride, an effect in large measure associated with the reduced polarizing power of lithium which results in a much reduced enthalpy of solvation. The successful synthesis of $[Ln\{NR_2\}_3]$ is significant in view of the simplicity of the procedure and the cheapness of the reagents, making this a particularly valuable starting material for further chemistry.

The only limitation associated with the diphenyl amides is the comparatively low pK_a of $HNPh_2$ (~23) compared with alkyl amine (36-30), somewhat reducing the range of protonolysis substrates for which this reagent would be useful. In

the hopes of preparing a more basic and therefore more useful starting material , the analogous reaction was attempted using N-methylaniline (HNMePh), tert-butyl-amine (H_2N^tBu), and cis-2,6-dimethylpiperidine (HN-2,6-Me_2-C_5H_8)

Attempt to the Synthesis of Yttrium tris methylanilide

Changing one of the phenyl substituent on the nitrogen with a methyl group should result in a more basic, though less bulky ligand. Using smaller substituents on the nitrogen however, increases the chance of bridging as opposed to terminal coordination, thus favouring the formation of polynuclear species. The reaction was carried out as described for diphenylamine (see Eq. 5.21 and 5.22), however after work-up only a very small amount of white solid was isolated, possibly due to poor solubility of the product. The ^1H NMR spectrum showed many signals some of which were broad, suggesting the formation of low symmetry species -possibly oligomers- with some dynamic behaviour at room temperature.

Attempt to the Synthesis of Yttrium alkyl amides

We attempted to prepare lanthanide homoleptic amides starting from tert-butyl amine (H_2N^tBu), and cis-2,6-dimethylpiperidine (HN-2,6-Me_2-C_5H_8). In the first case it was noticed that after refluxing with sodium hydride and addition to yttrium chloride, the latter did not seem to react significantly. Possible reasons are that either this less acidic amine does not react with the relatively weak H^- and need a stronger Lewis base to be deprotonated, or the resulting sodium amide is too insoluble.

In the case of cis-2,6-dimethylpiperidine, ^{n}BuLi was used to deprotonate the amine and although the lithium amide seemed to react with the yttrium chloride, we could not isolate the resulting product. Mulvey has since crystallized a close

analogue , sodium tetramethylpiperidide, which he prepared indirectly by lithiation followed by lithium/sodium exchange using NaO^{rmt}Bu. The considerable congestion around the nitrogen may make this a useful ligand for lanthanide chemistry in future.[228]

Synthesis of Neodymium tris(2,6-diisopropyl-arylamide)

Finally following the procedures described by Evans,[24] the neodymium tris(2,6-diisopropyl-arylamide) was prepared and isolated as a very air sensitive white solid in 48% yield.

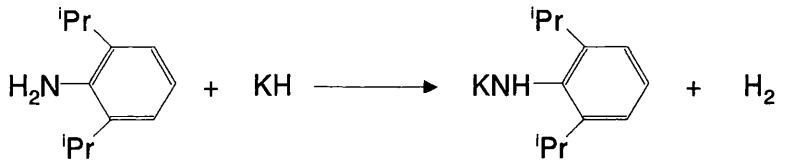

(5.23)

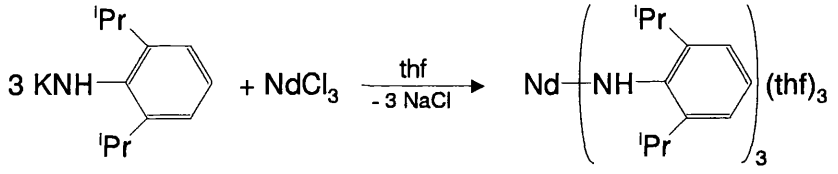

(5.24)

Synthesis of lanthanide organometallics

Among the known homoleptic lanthanide organometallic complexes the most favourable candidate as a starting material for the reaction with calixarenes would be the tris alkyl, Ln{CH(TMS)$_2$}$_3$. The corresponding calixarene-supported lanthanide alkyl, being very basic, could be reacted with a variety of other molecules such as alkynes, amines etc. However, the synthesis of this complex is complicated, involving several steps and requiring quite expensive starting materials.

A cheaper and easier alternative is represented by the tris cyclopentadienyl com-

plexes. Being relatively easy to make, the tris cyclopentadienyls should also be basic enough to react with the protonated calixarene ligand. However, the resulting cyclopentadienyl aromatic anion, being less basic than the bis-trimethylsilyl methyl anion, would not be as effective for protonolysis reactions, therefore reducing the possibility of further functionalization of the corresponding calixarene supported lanthanide cyclopentadienyl complex.

Synthesis of Lanthanide tris Cyclopentadienyl Complexes

The yttrium, lanthanum and samarium tris homoleptic cyclopentadienyl complexes were prepared following a literature procedure.[229]They were isolated as white (orange in the case of samarium) solids, in respectively 68, 28 and 28% yields, and were characterized by ^{1}H NMR spectroscopy (except for the samarium complex).

Attempt to the Synthesis of Lanthanide organometallic complexes *via* transmetallation reactions

In the search for suitable lanthanide organometallics a series of transmetallation reactions were attempted, aiming to the synthesis of tris phenyl lanthanides. Lanthanide aryls are potentially excellent starting materials for protonolysis reactions, the pK_a of benzene being 43, and would be expected to react efficiently with alcohols and amines by virtue of the large pK_a difference. By analogy with the work of Bochkarev[28] neodymium metal powder was stirred for several days with diphenyl mercury in dimethoxy ethane (DME), with the addition of catalytic amount of mercuric iodide. To our surprise no reaction was observed, as evidenced by the fact that no colour appeared in the solution (the Nd complex is reported to be the usual pale blue colour) and the surface of the metal remained unchanged. The supernatant solvent was found to contain unreacted $HgPh_2$. Similar results were ob-

tained when the solvent was changed to thf. Heating the reaction mixture appeared to produce some metallic mercury indicating some decomposition of the $HgPh_2$, but again no lanthanide-containing species were recovered from the supernatant. Similar inertness was also observed for yttrium (see Table 5.2 for a summary of the transmetallation reactions which have been carried out).

Table 5.2: Attempts to transmetallation reactions.

Metal	Alkylating agent	Solvent	Temperature	Catalyst
Nd	$HgPh_2$	DME	room temp.	HgI_2
Y	$HgPh_2$	thf	room temp.	HgI_2/YI_3
Nd	$HgPh_2$	thf	60 °C	I_2
Nd	$BiPh_3$	thf	room temp.	I_2

The failure of these experiments is quite surprising since Bochkarev[28] provides detailed descriptions, full analytical data and a crystal structure of these complexes. It is conceivable that the success of the reaction depends critically on the mesh size of the metal used in the procedure. In the absence of alternative grades of lanthanide metal, further experiments were reluctantly abandoned. Nevertheless, the aryls of the lanthanides remain attractive starting materials and the development of a simple synthetic route would be a significant advance in organolanthanide chemistry.

5.2.3 Synthesis of Calixarene complexes

Synthesis of Alkali Metal Complexes of Calixarene and attempt to Metathesis Reactions with Lanthanide Halides

The reaction of H_2L^{iPr} with excess sodium hydride at 80 °C in thf, afforded after work-up colorless plate crystals which were characterized by ^1H NMR spectroscopy

and single-crystal X-ray diffraction as Na_2L^{iPr}.

$$H_2L^{iPr} + NaH(excess) \longrightarrow Na_2L^{iPr} + 2H_2 \qquad (5.25)$$

The ^1H NMR spectrum shows, at high fields, two singlets for each pair of ^{t}Bu groups in the upper rim, and a doublet for the methyl groups of the ^{i}Pr. At lower fields there are two doublets corresponding to the four methylenic units bridging between the phenolic rings of the calixarene, and a multiplet for the two C-H of the isopropyl groups; finally in the region of the aromatic protons we find two singlets for the hydrogens on the phenolic rings. The spectrum is very similar to that observed for the free ligand, though all the peaks are slightly shifted and the phenolic hydrogen signal is missing, indicating deprotonation of the two phenolic groups.

Crystals suitable for X-ray analysis were obtained from 40-60° petrol; the X-ray structure was collected at low temperature and solved by Dr. Jon Steed of King's College. Although the crystal structure (Fig. 5.13) shows that in the solid state the complex is a dimer with a very low symmetry, the number of peaks in the NMR is consistent with a more symmetric species, suggesting that either the complex is a monomer in solution, or more probably, it undergoes a dynamic behaviour which makes different protons equivalent on the NMR timescale.

The structure consists of two deprotonated calixarene moieties joined at the lower rim by two bridging sodium cations. Each exo sodium is situated in a distorted tetrahedral environment, and is coordinated by one ether O-donor and two phenolate O-donors belonging to one $[L^{iPr}]^{2-}$ unit, and one O-phenolate donor belonging to the second $[L^{iPr}]^{2-}$ unit. The second pair of sodium cations (endo) are situated within the calixarene cavity and are bound by two mutually opposite phenolate O-donors. The short Na-C distances (2.8-3.0 Å) observed for the endo sodium ions are

consistent with a significant metal-π ring interaction.

The two calixarenes exhibit a distorted cone conformation with two opposite phenolic units twisted outward and almost perpendicular to one another, while the other two -i.e. those containing the ethers groups- are twisted inward and almost parallel to one another; this particular conformation probably results in the attempt to minimise the steric repulsion between the isopropyl groups and spatially adjacent atoms, and maximise the metal-π ring interactions.

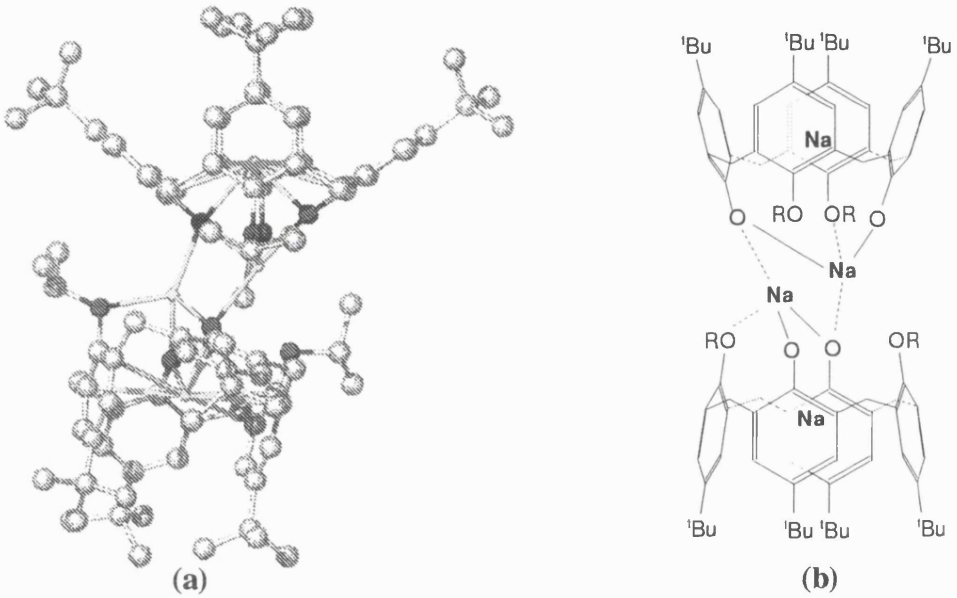

Figure 5.13: a) X-ray crystal structure and b) schematic representation of $[Na_2L^{iPr}]_2$.

The above structure shows many similarities with an analogous one reported by Mountford for $[Na_2L^{Me}]$,[192] the main difference being that, with the bulkier ^{i}Pr substituent, one ethereal oxygen on each calixarene is not coordinating any metal, and the exo sodium cations are therefore tetra- rather than pentacoordinate, as was in fact observed for the methyl substituted calixarene salt. From the difference between the two structures it is clearly shown that steric effects related to the lower

rim substituents of calixarene, can affect its mode of bonding, and that O-alkylation is therefore a useful tool to vary the binding properties of such ligands.

Attempt to Metathesis Reaction of Lanthanide Halides with H_2L^R

The use of alkali metal salts of calixarene as precursors for the synthesis of lanthanide calixarene complexes was investigated (see Fig 5.9). A solution of sodium isopropyl-calixarene salt in thf was prepared as described above and added dropwise to a stirred suspension of yttrium iodide in thf. The crude product obtained after work-up, was analysed by ^{1}H NMR spectroscopy and was shown to be a mixture of Na_2L^{iPr} and the H_2L^{iPr} starting material.

In an attempt to improve the reactivity of the calixarene salt the sodium alkali metal cation was replaced by potassium ion and the isopropyl substituents on the ethereal oxygen replaced by methyl groups. The dimethyl-calixarene ether H_2L^{Me} was therefore refluxed in thf with KC_8 and added dropwise to a suspension of yttrium iodide in thf. Since continuous and vigorous stirring did not result in dissolution of the yttrium iodide suspension, the mixture was refluxed for 12 hours. A crude product was isolated (white powder) but was insoluble in deuterated benzene or in HCl.

Any further attempt to use alkali metal calixarene salt as a starting material for metathesis reactions with lanthanide halides proved unsuccesful. Possible reasons for the failure of such reactions can be traced to the formation of stable oligomers of the calixarene alkali metal salt and the high affinity of the calixarene π cavity for the alkali metal ions, which shifts the equilibrium towards the starting materials.

Protonolysis Reactions of Calixarene with Lanthanide bis trimethylsilyl amides

Following the failure of the metathesis reactions using alkali-metal salts of calixarene as starting materials, an obvious alternative was to attempt protonolysis reactions of lanthanide amides with the calixarene. By reacting a lanthanide tris amide with one equivalent of protonated calixarene ether (H_2L^R) we expected to doubly deprotonate the ligand and obtain a calixarene supported lanthanide amide (see Fig 5.10).

Lanthanide tris (bis-trimethylsilyl) amides were reacted with the protonated H_2L^{Me} and H_2L^{iPr} ligands under different conditions and with different solvents. Lanthanide bistrimethylsilyl amides have been reported to readily deprotonate alkyl-substituted phenols, and they have been successfully used in the synthesis of lanthanide alkoxo complexes.[18] Reaction of calixarene with the lanthanide amides at room temperature was shown to yield the unreacted starting materials, both in saturated hydrocarbons and toluene. However, refluxing the lanthanide amide with one equivalent of anhydrous calixarene in a small amount of toluene, and slowly cooling to room temperature, resulted in the formation of a white microcrystalline product. This might be explained as a steric effect arising from the extremely crowded nature of the metal coordination sphere. In addition, the intramolecular hydrogen bonding between the OH groups of the calixarene may prevent reaction at room temperature.

The protonolysis reaction was carried out with yttrium and samarium bis-trimethylsilyl amides and both H_2L^{Me} and H_2L^{iPr} ligands, in both a 1:1 and a 1:2 ratio. A summary of these reactions is given in Table 5.3

The L^{Me} complexes (i.e. the products of reaction **a**, **b** and **d**) were found to be insoluble in toluene and deuterated benzene at room temperature. However, recording the ^1H NMR spectra at ~60 °C allowed a suffucient amount of the product

Table 5.3: Summary of reactions between lanthanide trimethylsilyl amides and calixarene ligands

Reaction	Calixarene	Amide	Ratio
a	H_2L^{Me}	$Y\{N(TMS)_2\}_3$	1:1
b	H_2L^{Me}	$Y\{N(TMS)_2\}_3$	2:1
c	H_2L^{iPr}	$Y\{N(TMS)_2\}_3$	1:1
d	H_2L^{Me}	$Sm\{N(TMS)_2\}_3$	2:1
e	H_2L^{iPr}	$Sm\{N(TMS)_2\}_3$	1:1

to dissolve and NMR peaks to be detected (with the exception of product **d**, which was unsoluble even at high temperature). Faced with the high unsolubility of the L^{Me} complexes we carried out analogous reactions using H_2L^{iPr}, and indeed the L^{iPr} complexes (i.e. the products of reaction **c** and **e**) were found to be readily soluble in toluene and deuterated benzene at room temperature.

As already seen for the alkali metal calixarene complexes, no signal corresponding to the phenolic protons was observed in the ^1H NMR spectra of these compounds, suggesting that deprotonation has taken place. Furthermore the ^1H NMR spectra of the products of reaction **a** and **b** are identical, suggesting that the same compound was obtained in both cases, irrespective of the stoichiometric ratio between the two starting materials. Since reaction **a** and **b** give the same product, and the yield of reaction **b** is significantly higher than that of **a** (0.205g and 0.160g respectively) it is likely that the compounds isolated have a lanthanide to calixarene ratio smaller than 1:1.

A comparison of the NMR spectra of the dimethyl calixarene ligand and the products of reaction *a* and *b* is shown in Table 5.4. The signals of the product appear

Table 5.4: Comparison of ^{1}H NMR spectra of H_2L^{Me} and the product obtained from reaction **a=b**.

	2OH	4 ring H	4 ring H	$2CH_2$	2OMe	$2CH_2$	2^tBu	2^tBu
H_2L^{Me}	8.64	7.26	6.91	4.48	3.48	3.44	1.45	0.80
a=b	—	7.27	6.89	4.69	3.64	3.36	1.43	0.96

to be sligthly shifted with respect to those of the uncoordinating ligand. Surprisingly however, the ^{1}H NMR spectrum of the product shows no additional signals in the region typical of trimethylsilyl protons (δ ~0 ppm), as it would be expected for L^{Me}-Y-N(TMS)$_2$. In fact, the absence of trimethylsilyl protons is a common feature to all of the compounds (i.e. **a**, **b**, **c** and **e***), suggesting that the course of the reaction is identical. This evidence suggests that upon reaction with the calixarene, the lanthanide ion loses all three coordinated trimethylsilyl amide ligands. Such hypothesis is further supported by elemental analysis carried out on the products of reaction **a** and **d**, for which no nitrogen has been found. The unexpected loss of all amide ligands can be considered as a consequence of the high steric crowding of the lanthanide amide starting material. At room temperature the alkyl substituted calixarene ligands would, in fact, be locked in the cone conformation due to hydrogen bond formation at the lower rim, leaving little possibility for the bulky amide to bind the phenolic protons. At high temperature however, it is likely that the above mentioned hydrogen bond is disrupted and the calixarene becomes more flexible. In this conditions deprotonation can be achieved but, due to the larger size of the tris amide, the protonation rate of the last amide ligand is likely to be much greater than

*As pointed out before, the product of reaction **d** is still mostly unsoluble even at 65 °C and the NMR spectrum is therefore uninformative.

Table 5.5: Comparison of ^{1}H NMR spectra of H_2L^{iPr}, and the products of reactions **c** and **e**.

	2OH	4 ring H	4 ring H	$2CH_2$	2CH (^{i}Pr)	$2CH_2$	2^tBu	$4CH_3$ (^{i}Pr)	2^tBu
H_2L^{iPr}	8.68	7.28	6.96	4.57	4.11	3.40	1.47	1.28	0.82
c	—	7.26	6.89	4.38	4.24	3.17	1.47	1.39	0.97
e	—	8.24 7.89	7.59 3.75	4.28 3.73	4.65 -2.98	3.26 3.17	2.00 1.93	1.26 -2.53	1.42 1.28

that of the second and first, resulting in preferential loss of all coordinated amides. If a less bulky amide is used instead of the trimethylsilyl, it would be expected that the reaction rates of the first, second and third amide ligands be comparable, and therefore that the desired calixarene supported lanthanide amide could be isolated.

The NMR spectrum of the L^{iPr} complex with yttrium resembles that of the uncoordinated ligand, except that no signals are observed for the phenolic hydrogens. However the NMR spectrum of the analogous complex with samarium is rather different, as the calixarene signals appear to be split and spread over a broader range of values. This is not unexpected in view of the paramagnetic properties of the Sm^{3+} ion. A comparison of the NMR spectra of H_2L^{iPr}, and the corresponding yttrium (**c**) and samarium (**e**) complexes is given in Table 5.5 The NMR spectrum of the samarium complex shows 4 singlets of the same intensity (instead of two) for the ^{t}Bu groups and four singlets also for the aromatic hydrogens signals; similarly there are more than two doublets in the region corresponding to the methylenic units. Interestingly, there seem to be two very different isopropyl environments: the signals for one type of isopropyl are in the usual region, i.e. a CH multiplet at 4.47 ppm, and the methyl doublet at 1.26 ppm; the peaks for the other isopropyl are broader and at much higher fields, with the CH signal at -3.03 ppm and the methyl signal at -2.53 ppm. This complicated pattern is consistent with the formation of

Table 5.6: Elemental microanalysis (found and calculated) for the products of reactions **a** and **d** (see Table 5.3)

Reaction	Found	Calculated for $LnHL_2^R$	Calculated for $Ln_2L_3^R$
a	C 75.68; H 8.34	C 76.67; H 8.10	C 75.25; H 7.96
d	C 66.00; H 7.68	C 73.60; H 7.85	C 71.27; H 7.54

an oligomeric complex with lower symmetry compared to the uncoordinated ligand. The different types of isopropyl environment suggest a stronger interaction of one type of isopropyl group with the paramagnetic samarium ion.

Table 5.6 shows the elemental analysis results for the products of reactions **a** and **d**. From the evidences obtained for these series of compounds there are two possible structures which might be associated to the complexes: the 1:2 complex $LnH\{L^R\}_2$ (with a partly protonated calixarene ligand[†]) and the 2:3 complex $Ln_2L_3^R$, which are schematically represented in Fig. 5.14. The elemental analysis calculated for these two complexes can also be found in Table 5.6. From the NMR data of the complexes and the comparison of calculated and obtained elemental analysis in Table 5.6 it is not possible to assign a structure to these compounds. In particular for complex **d**, none of the hypothesized structures seem to fit quite well the elemental analysis results, suggesting that the molecular structure of the complex might be somewhat more complicated than those suggested.

It is unfortunate that although crystals apparently suitable for X ray diffraction had been isolated for the L^{Me} complexes of yttrium and samarium,[‡] the crystallo-

[†]Although no NMR signal corresponding to the phenolic proton has been detected, in a complex of the type $LnH\{L^R\}_2$ the phenolic proton could still not be detected due to fast intramolecular exchange with the remaining phenoxo sites.

[‡]Crystallization of the L^{Me} complexes from hot toluene is relatively easy due to their lower solubility compared to the L^{iPr} complexes.

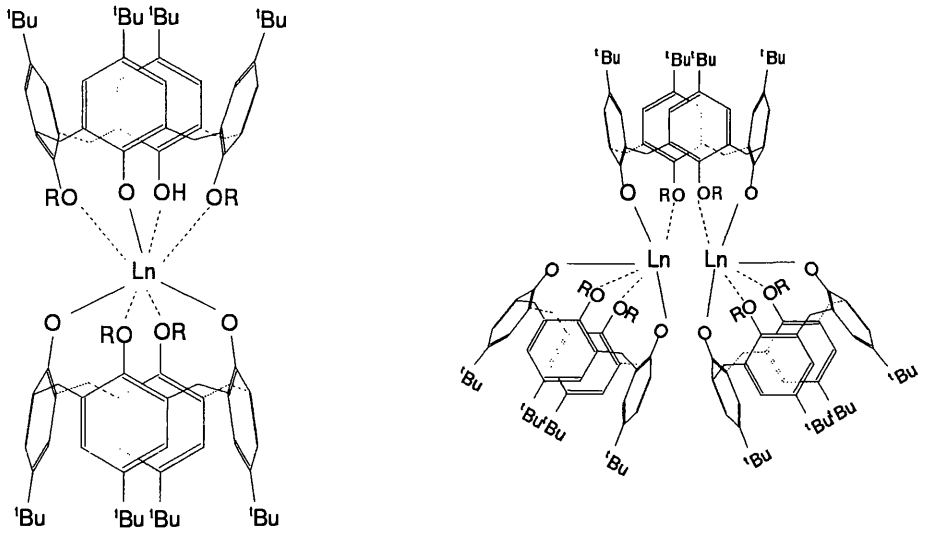

Figure 5.14: Schematic representation of the 1:2 complex $LnH\{L^R\}_2$ and the 2:3 complex $Ln_2L^R_3$.

graphic data could not be obtained due to instrumental reasons.

Protonolysis Reaction of yttrium tris diphenylamide with dimethyl calixarene: Synthesis of calixarene supported yttrium diphenylamide

In order to prove that a less sterically crowded lanthanide amide would help achieving the desired 1:1 product, the less bulky yttrium tris diphenylamide was reacted with H_2L^{Me} in a 1:1 ratio. It would be expected that a more effective contact between the phenolic protons and the nitrogen of the amide results in easier deprotonation of the calixarene ligand and comparable reaction rates for the first, second and third amides. Indeed, immediately after mixing the toluene solutions of the two starting materials a white solid formed, suggesting that the reaction takes place without need of heating. The mixture was stirred at room temperature overnight and the product was isolated as a very air sensitive white powder, which was found to be insoluble in toluene and deuterated benzene at room temperature and only sparingly soluble

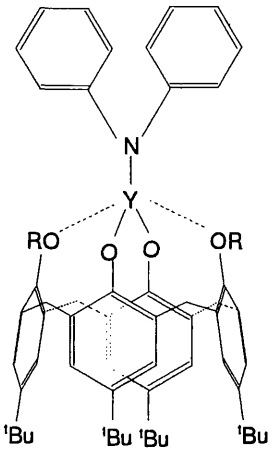

Figure 5.15: Schematic representation of the 1:1 complex $Y\{L^{Me}NPh_2\}$.

at $\sim$ 60 °C.

$$H_2L^{Me} + Y\{NPh_2\}_3 \longrightarrow YL^{Me}NPh_2 \tag{5.26}$$

In the absence of deuterated thf it was not possible to obtain an NMR spectrum of the complex. The elemental analysis of the white powder was consistent with the formulation $L^{Me}YNPh_2$. The extreme insolubility and the absence of a crystal structure prevents us from speculating on the molecularity of the complex since an oligomeric structure with bridging amides is also possible. Nevertheless the observation that the reaction proceeds more smoothly in the case of NPh_2 than for the more basic $N(TMS)_2$ is consistent with the view that sterics play a key role in the protonolysis reactions of these systems.

A schematic rapresentation of a possible structure of the calixarene supported yttrium diphenylamide is given in Figure 5.15

Protonolysis Reactions of Calixarene with Lanthanide tris cyclopentadienyl: Synthesis of calixarene supported lanthanide cyclopentadienyl complex

After the successful isolation of the calixarene supported yttrium amide, a series of protonolysis reactions was carried out, using both H_2L^{Me} and H_2L^{iPr} ligands and $LnCp_3$ (Ln = Y, La) in a 1:1 ratio. The reactions are summarized in table 5.7 With the cyclopentadienyl ligand, the deprotonation of the phenolic protons occurs through the delocalized π electrons of the aromatic ring. As with diphenyl amide we expect that deprotonation of the calixarene ligand should not be hindered by steric crowding of the starting material. However, the lanthanide tris cyclopentadienyl complexes are insoluble in toluene therefore the reaction was carried out at high temperature to aid dissolution of the starting material. After work up the resulting products were isolated as white solids. The complex with the L^{Me} ligand was found to be insoluble even in hot deuterated benzene, confirming that use of L^{iPr} might generally be a better choice.

The ^1H NMR spectra of complex **b** and **c** show the usual pattern observed for the L^{iPr} ligand and an additional peak in the region expected for the cyclopentadienyl ligand. Table 5.8 shows a comparison between H_2L^{iPr} and products **b** and

Table 5.7: Summary of reactions between lanthanide trimethylsilyl amides and calixarene ligands

Reaction	Calixarene	$LnCp_3$
a	H_2L^{Me}	$LaCp_3$
b	H_2L^{iPr}	$LaCp_3$
c	H_2L^{iPr}	YCp_3

c. On the basis of the proton NMR evidence, it seems that the desired calixarene

Table 5.8: Comparison of ^{1}H NMR spectra of H_2L^{iPr}, and the products of reactions **b** and **c**.

	2OH	4 ring H	4 ring H	5H Cp	$2CH_2$	2CH (^{i}Pr)	$2CH_2$	2^tBu	$4CH_3$ (^{i}Pr)	2^tBu
H_2L^{iPr}	8.68	7.28	6.96	—	4.57	4.11	3.40	1.47	1.28	0.82
b	—	7.29	6.75	6.46	4.50	3.99	3.07	1.46	1.28	0.82
c	—	7.24	6.82	6.71	4.64	4.27	3.07	1.49	1.19	0.99

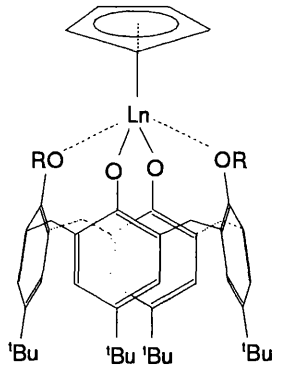

Figure 5.16: Schematic representation of the 1:1 complex LnL^RCp.

supported lanthanide cyclopentadienyl complexes have been obtained (see Fig 5.16 for a schematic representation of the product).

5.3 Conclusions

The novel tris homoleptic yttrium amide, $Y\{NPh_2\}_3$ has been synthesized from the reaction of YCl_3 and $NaNPh_2$. The product has been characterized by ^1H NMR spectroscopy and elemental analysis.

Two disubstituted calixarene ethers, H_2L^{Me} and H_2L^{iPr}, in which two of the phenolic protons are replaced by two Me and ^{i}Pr groups respectively have been successfully prepared.

The sodium salt of the H_2L^{iPr} ligand has been isolated and structurally characterized. The compound turned out to be a dimer in the solid state, with a sodium ion being bound inside the calixarene cavity by π interaction with the aromatic rings. The structure has been compared to a similar one reported in the literature suggesting that a tuning of the steric properties of the alkyl substituent on the phenolic oxygen should result in a different coordination ability of the calixarene ligand.

Several attempts to metathesis reactions of the sodium and potassium salts of calixarene with yttrium iodide proved unsuccessful. Possible reasons are the formation of stable oligomers of the calixarene alkali metal salt starting material, and the high affinity of the calixarene π cavity for the alkali metal ions.

The protonolysis reaction of calixarene ligands, H_2L^{Me} and H_2L^{iPr} with yttrium and samarium tris bistrimethylsilyl amides has been investigated. No reaction is observed at room temperature, while carrying out the reaction at higher temperature results in the complete loss of metal-coordinated amide and possibly in the formation of oligonuclear species. This apparently odd observation is suggested to be an effect of the steric crowding of the amide starting material, and the consequent poor ability to deprotonate the phenol at room temperature. Increasing the temper-

ature, increased flexibility of the calixarene and disruption of the its intramolecular hydrogen bonds are likely to aid deprotonation. However, as a consequence of steric crowding, the protonation rate of the first amide ligand is small compared to the protonation rate of the second and third amide ligands resulting in preferential loss of all the three metal coordinated amides. This hypothesis is supported by the successful synthesis of the less sterically hindered, calixarene supported lanthanide diphenylamide and cyclopentadienyl complexes.

The calixarene supported yttrium diphenylamide complex, $YL^{Me}NPh_2$ has been synthesized from the protonolysis reaction of H_2L^{Me} and $Y\{NPh_2\}_3$. The product has been isolated as a very air sensitive solid and it has been characterized by elemental analysis. As expected for the less sterically crowded diphenylamide, the reaction took place at room temperature, and since the deprotonation rate of the first and subsequent amides should be comparable, the stoichiometric ratio of the starting materials acted as a determining factor in the formation of the preferred product.

The same reasoning applies to the tris cyclopentadienyl lanthanide complexes. A series of calixarene supported lanthanide cyclopentadienyl complexes have been successfully synthesized by reaction of the calixarene ligands H_2L^{Me} and H_2L^{iPr}, with the lanthanide tris cyclopentadienyl complex. The products were isolated as white solids and were characterized by ^1H NMR.

5.4 Experimental

5.4.1 Reagents and apparatus

Unless otherwise stated all reactions and manipulations were carried out under an atmosphere of dry nitrogen, either using standard Schlenck line techniques or in a Braun Lab Star 50 glove-box. $LnCl_3$ was prepared by the NH_4Cl method. YI_3 was prepared by heating of yttrium metal with HgI_2 in a furnace. Reaction solvents were predried over sodium wire, with exception of CH_2Cl_2 which was predried over molecular sieves and CH_3CN which was not predried. They were then dried by refluxing under nitrogen over the appropriate drying agent (Na, K, CaH_2 or 3:1 alloy Na/K), distilled and stored under nitrogen over sodium mirrors or molecular sieves. ^{1}H-NMR spectra were recorded on a Bruker AC400 spectrometer. Spectra were referenced to peaks produced by residual non-deuterated molecules present in the solvent. The following compounds have been prepared according to literature procedures: ^{t}Bu-calix[4]arene (H_4L),[159] H_2L^{Me} and H_2L^{iPr},[227] $Ln\{N(TMS)_2\}_3$,[21] $Nd\{HNC_6H_3\text{-}^iPr_2\text{-}2,6\}_3$,[24] $LnCp_3(thf)_n$.[229]

5.4.2 Synthesis of starting materials

Preparation of ^{t}Bu-calix[4]arene

Para-^{t}Bu-phenol (100 g, 0.665mol), commercial formaldehyde 37% (62.3 ml, 0.83mol), and NaOH solution (1.2 g, 0.03mol in ~10 ml H_2O) were put in a three-necked round-bottom flask equipped with a mechanical stirrer and a thermometer. The mixture was slowly heated to 120 °C and kept at this temperature for 2h turning clear, then orange and finally to a thick yellow paste. After cooling to room temperature the resulting solid was broken to pieces and 1L of diphenyl ether was added. The round-bottom flask was equipped with a gas inlet adaptor and nitrogen was bubbled

through the solution at 120 °C until the mixture stopped foaming and turned clear (~1h). The round-bottom flask was then equipped with a water condenser and the solution was refluxed at ~250 °C for 2h turning brown-black. After cooling to room temperature, 1L ethyl acetate was added to the mixture, stirred for 15′ and allowed to stand overnight. The white solid formed was filtered, washed with ethyl acetate and dried. Yield: 61.53g (57%).

^{1}H NMR ($CDCl_3$): δ = 10.32 (s, 4H, OH), 7.03 (s, 8H, ring H), 4.23 (d, 4H, $2CH_2$), 3.47 (d, 4H, $2CH_22$), 1.19 (s, 36H, ^{t}Bu).

Preparation of 1,3-di-methyl-^{t}Bu-calix[4]arene: H_2L^{Me}

^{t}Bu-calix[4]arene (11.55 g, 17.80 mmol) and oven-dried K_2CO_3 (9.5 g, excess) were put in a round botton flask and added 100 ml acetonitrile and MeI 99% (5.30 g, 36.98 mmol). The white mixture was refluxed in dark at 120°C under nitrogen for 5 days, turning dirty white. Cooled at room temperature, added ~100 ml dichloromethane, stirred for 30′, allowed to settle and filtered. The yellow filtrate was washed twice in a separating funnel with ~75 ml of HCl 3%, dried over $MgSO_4$ (oven-dried and finely ground), filtered and rotoevaporated. The dirty white powder was then dried under vacuum at 120 °C for 24h and stored in the dry box. Yield: 10.72g (89%).

^{1}H NMR ($CDCl_3$): δ = 7.08 (s, 4H, ring H), 6.78 (s, 4H, ring H), 4.32 (d, 4H, $2CH_2$), 3.96 (s, 6H, $2CH_3$ Me), 3.34 (d, 4H, $2CH_22$), 1.31 (s, 18H, ^{t}Bu), 0.95 (s, 18H, ^{t}Bu).

^{1}H NMR (C_6D_6): δ = 8.64 (s, 2H, OH), 7.26 (s, 4H, ring H), 6.91 (s, 4H, ring H), 4.48 (d, 4H, $2CH_2$), 3.48 (s, 6H, $2CH_3$ Me), 3.44 (d, 4H, $2CH_2$), 1.45 (s, 18H, ^{t}Bu), 0.80 (s, 18H, ^{t}Bu).

Elemental microanalysis calculated for

$C_{46}H_{60}O_4$: C 81.61, H 8.93;

found: C 81.79, H 9.07.

Preparation of 1,3-di-isopropyl-^{t}Bu-calix[4]arene: H_2L^{iPr}

^{t}Bu-calix[4]arene (13.47 g, 20.76 mmol) and oven-dried K_2CO_3 (9.16 g, excess) were placed in a round botton flask and $\sim$ 100 ml acetonitrile was added followed by ^{i}PrI (7.15 g, 41.64 mmol). The white mixture was refluxed in the dark at 120°C under nitrogen for 5 days, turning dirty white. After cooling to room temperature, $\sim$ 125 ml dichloromethane were added, stirred for 30 minutes, allowed to settle, and filtered. The yellow filtrate was washed twice in a separating funnel with $\sim$75 ml of 3% HCL, dried over $MgSO_4$ (oven-dried and finely ground), filtered and rotoevaporated. The white-yellowish powder was then dried under vacuum at 160-180° for 24h and stored in the dry box. Yield: 12.50g (82%).

^{1}H NMR ($CDCl_3$): δ = 7.69 (s, 2H, OH), 7.00 (s, 4H, ring H), 6.84 (s, 4H, ring H), 4.33 (d, 4H, $2CH_2$), 4.25 (m, 2H, 2CH ^{i}Pr), 3.27 (d, 4H, $2CH_22$), 1.48 (m, 12H $4CH_3$ ^{i}Pr), 1.25 (s, 18H, ^{t}Bu), 1.00 (s, 18H, ^{t}Bu).

^{1}H NMR (C_6D_6): δ = 8.68 (s, 2H, OH), 7.28 (s, 4H, ring H), 6.96 (s, 4H, ring H), 4.57 (d, 4H, $2CH_2$), 4.11 (m, 2H, 2CH ^{i}Pr), 3.40 (d, 4H, $2CH_2$), 1.47 (s, 18H, ^{t}Bu), 1.28 (m, 12H $4CH_3$ ^{i}Pr), 0.82 (s, 18H, ^{t}Bu).

Elemental microanalysis calculated for

$C_{50}H_{68}O_4$: C 81.87, H 9.28;

found: C 81.91, H 9.32.

Preparation of sodium trimethylsilyl-amide: $NaN(TMS)_2$

NaH 60% in mineral oil (2.62 g, 65.5 mmol) was placed in a Schlenk, washed twice with ~15 ml 40-60° petrol, and ~40 ml toluene were added. $HN(TMS)_2$ 98% (10.00g 60.72 mmol) was placed in a Schlenk, diluted with ~10 ml toluene and added to the NaH. The mixture was refluxed under nitrogen at 120 °C for 24h. The brown-grey mixture was cooled at room temperature, allowed to settle and filtered. The yellow filtrate was pumped-dry to afford a white solid. Yield: 10.3g (93%).

Preparation of sodium cyclopentadienyl: NaCp(thf)

NaH 60% in mineral oil (8 g, 0.33mol) was washed twice with ~30 ml 40-60° petrol, and diluted with~70 ml thf. Freshly cracked cyclopentadiene (15 g, 0.227mol) was added dropwise with stirring to the suspension and stirred under a nitrogen flow for further 2h until effervescence ceased. The excess NaH was filtered off and the resulting pink solution was pumped dry. Yield: 20.1g (55%).

Preparation of sodium diphenylamide

NaH 60% in mineral oil (4.1 g, excess) was washed twice with ~20 ml 40-60° petrol. $HNPh_2$ (9.5 g, 56.15 mmol) was added and ~100 ml thf. The mixture was refluxed under nitrogen for ~20h, allowed to cool at room temperature and filtered. The yellow filtrate was pumped dry giving a creamy white powder. Yield: 10.2g (95%).

Preparation of potassium di isopropyl arylamide: $K(HNC_6H_3\text{-}^iPr_2\text{-}2,6)$

KH (2.00 g, 0.05mol) was suspended in ~100 ml thf and freshly distilled di-isopropyl aniline (8.80 g, 0.049mol) was added dropwise with stirring. The mixture was stirred under a nitrogen flow for further 2h until effervescence disappeared. The excess KH was filtered off and the extremely air sensitive yellow solution was reduced in volume

and put in the freezer. The resulting white precipitate was filtered and pumped dry. Yield: 5.2g (50%).

Preparation of mesityl lithium

^{n}BuLi 2.5M (12 ml, 30 mmol) was added dropwise to a solution of MesBr (5 g, 25 mmol) in ~30 ml 40-60° and refluxed under nitrogen for 3h (bright yellow solution + white precipitate). The supernatant was decanted off and the white solid was washed with 40-60°. Yield: 1.73g (55%).

5.4.3 Synthesis of Lanthanide Amides

Preparation of yttrium tris-bistrimethylsilyl-amide: $Y\{N(TMS)_2\}_3$

YCl_3 (1.71 g, 8.76 mmol) and $NaN(TMS)_2$ (4.82g 26.27 mmol) were placed in a Schlenk, diluted with ~40 ml thf and refluxed under nitrogen at 100 °C over the week-end. The white-grey mixture was cooled at room temperature, allowed to settle and filtered. The pale yellow solution was pumped dry (dirty-white powder), extracted into 40-60° petrol, reduced in volume and placed in the freezer. The first + second crop collected and sublimed at 160 °C to yield a white powder. Yield: 1.5g (26%).

^{1}H NMR (C_6D_6): $\delta = 0.29$ (s, 54H, 6Si-Me_3)

Preparation of samarium tris-bistrimethylsilyl-amide: $Sm\{N(TMS)_2\}_3$

$SmCl_3$ (2.95 g, 11.49 mmol) and $NaN(TMS)_2$ (6.32g 34.50 mmol) were placed in a Schlenk, diluted with ~50 ml thf (exothermic) and refluxed under nitrogen at 100 °C for 36h. The dirty-white mixture was cooled at room temperature, allowed to settle and filtered (adding more thf to extract the product). The pale yellow solution was pumped dry (white yellow powder), extracted into 40-60° petrol, reduced in volume and placed in the freezer. First + second crop collected. The obtained

yellow crystals were extracted in a minimum amount of 40-60° and recrystallised. Yield: 3.25g (45%).

^{1}H NMR (C_6D_6): δ = -1.58 (s, 54H, 6Si-Me_3)

Synthesis of yttrium tris-diphenyl-amide: Y{NPh_2}$_3$

$NaNPh_2$ (1.48 g, 7.74 mmol) was dissolved in thf (lime yellow solution) and added to a suspension of YCl_3 (0.51 g, 2.61 mmol) in thf (previously stirred for 3h). The lime-yellow colour disappeared during the addition, the YCl_3 dissolved, and a fine grey-white powder appeared (NaCl). The mixture was stirred for further 30′, pumped dry and extracted into toluene (~50 ml). The pale yellow solution was reduced in volume until colorless cubic crystals appeared. The solution was placed in the frezeer for 24h, supernatant decanted off, and pumped dry. Yield: 0.53g (35%).

^{1}H NMR (C_6D_6): δ = 7.18 (s, 3H), 7.16 (s, 6H), 7.08 (d, 3H, J = 8 Hz), 7.07 (s, 6H), 7.05 (s, 3H), 6.84 (d, 3H, J = 8 Hz) 6.80 (d, 3H, J = 8 Hz), 6.78 (d, 3H, J = 8 Hz), 3.46 (m, 12H, thf), 0.84 (m, 12H, thf).

Elemental microanalysis calculated for

$C_{36}H_{30}N_3Y$: C 72.86, H 5.06, N 7.08;

found: C 72.49, H 5.31, N 7.09.

Synthesis of neodymium tris diisopropyl-arylamide: Nd{HNC_6H_3-^{i}Pr_2-2,6}$_3$

A solution of K(HNC_6H_3-^{i}Pr_2-2,6) (1.00 g, 4.74 mmol) in ~25 ml thf was added dropwise with stirring to a suspension of $NdCl_3$ (0.39 g, 1.58 mmol) in ~25 ml thf resulting in immediate deep blue (red through torch light) coloration of the supernatant. The mixture was stirred overnight, pumped dry, and extracted into 40-60° petrol. The deep blue/red solution was reduced in volume and placed in the

freezer overnight resulting in the formation of green crystals which were isolated and pumped dry. Yield: 0.68g (48%)

Attempt to the synthesis of yttrium tris N-methylanilide: $Y\{NMePh\}_3$

NaH 60% in mineral oil (excess) was placed in a Schlenk, washed twice with ~15 ml 40-60° petrol, and HNMePh (0.4 g, 3.73 mmol) was added followed by ~20 ml thf. The mixture was refluxed under nitrogen at 80°C overnight, cooled at room temperature, allowed to settle (green-yellow solution) and filtered dropwise into a suspension of YCl_3 (0.26 g, 1.33 mmol) in thf. Work up of the resulting solution resulted in the isolation of very small amount of white powder (0.009g) with a uninterpretable ^1H NMR spectrum.

Attempt to the synthesis of yttrium tris t-butylamide: $Y\{NH^tBu\}_3$

NaH 60% in mineral oil (excess) was placed in a Schlenk, washed twice with ~15 ml 40-60° petrol, and $NH_2{}^tBu$ (0.25 g, 3.42 mmol) was added, followed by ~15 ml thf. The mixture was refluxed under nitrogen at 80°C overnight, cooled at room temperature, allowed to settle (colorless solution) and filtered dropwise into a suspension of YCl_3 (0.24 g, 1.23 mmol) in thf. No visible changes were observed upon the addition, and work up of the resulting solution did not result in the isolation of any useful product.

Attempt to the synthesis of yttrium tris piperidine $Y\{NC_5H_8\text{-}Me_2\text{-}2,6\}_3$

A 2.5M solution of ^{n}BuLi (1.8 ml, 4.5 mmol) was added dropwise at -78°C to a solution of dimethyl piperidine (0.52 g, 4.61 mmol) in Et_2O, stirred at room temperature for 30 minutes. The resulting bright yellow solution was added dropwise to a suspension of YCl_3 (0.30 g, 1.54 mmol) in thf and stirred overnight. The mixture

was filtered and the filtrate pumped dry to obtain a yellow oil, which was found to be insoluble in thf, toluene, and 40-60° petrol.

5.4.4 Synthesis of Lanthanide Organometallics

Preparation of tris cyclopentadienyl yttrium: YCp_3

NaH 60% in mineral oil (1.12 g, excess) was placed in a Schlenk, washed twice with ~15 ml 40-60° petrol, diluted with ~30 ml thf, and cyclopentadiene, C_5H_6, (1.02 g, 15 mmol) dropwise at room temperature, resulting in ready formation of H_2. The mixture was stirred for 30 minutes, and filtered dropwise into a suspension of YCl_3 (1.00 g, 5.12 mmol) in thf (previously stirred for 3h). The pale yellow mixture was allowed to settle and filtered. The filtrate was pumped-dry (white powder) and sublimed at 10^{-2}mm Hg and 180°C overnight. The product was isolated as a white powder. Yield: 0.99g (68%).

^{1}H NMR (C_6D_6): $\delta = 6.19$ (s, 15H, Cp).

Preparation of tris cyclopentadienyl lanthanum: $LaCp_3$

A solution of NaCp(thf) (1.67 g, 10.3 mmol) in ~30 ml thf was added dropwise with stirring to a suspension of $LaCl_3$ (0.85g 3.5 mmol) in ~40 ml thf, stirred for 24h at room temperature, and allowed to settle overnight. The resulting pink solution was pumped dry to a crunchy pink solid and sublimed at 10^{-2}mm Hg and 220°C for 36h giving a white powder. Yield: 0.325g (28%).

^{1}H NMR (C_6D_6): $\delta = 5.93$ (s, 15H, Cp).

Preparation of tris cyclopentadienyl samarium: $SmCp_3$

A solution of NaCp(thf) (1.90 g, 11.7 mmol) in ~30 ml thf was added dropwise with stirring to a suspension of $SmCl_3$ (1.00g 3.9 mmol) in ~40 ml thf, resulting in disappearance of the pink colour and appearance of a yellow colour and a jelly

white ppt. The mixture was stirred for 12h at room temperature, pumped dry, and extracted twice with ~30 ml toluene/thf mixture (5:1). The resulting yellow solution was pumped dry to a yellow solid and sublimed at 10^{-2}mm Hg and 200°C for 48h giving an orange crystalline solid. Yield: 0.380g (28%).

Reaction of mesityl sodium (prepared *in situ*) with YCl_3

Mesityl bromide (0.92 g, 4.61 mmol) was added to a suspension of sodium pieces (~0.5 g, excess) in ~20 ml toluene and stirred at ~80 °C under nitrogen for 2h. The resulting mixture was added dropwise to a suspension of YCl_3 (0.3 g, 1.54 mmol) in ~30 ml Et_2O, stirred overnight and filtered. The filtrate was pumped dry (peach-pink oil), washed with 40-60° (white crystalline solid) and pumped dry. The solid was qualitatively tested for yttrium (positive) and sodium (negative). Yield: 0.17g (25%). Not soluble in C_6D_6.

Reaction of mesityl lithium with YCl_3

A suspension of 4 equivalent of MesLi (0.22g 1.74 mmol) in ~40 ml Et_2O was added dropwise with stirring to a suspension of YCl_3 (0.09 g, 0.46 mmol) in ~20 ml Et_2O. During addition the YCl_3 dissolves and solution turns canary yellow. Stirred for further 30 minutes (orange-red solution), filtered and pumped dry. The resulting orange oil was stirred with ~40 ml 40-60° petrol for 1 day, and the supernatant (red solution) was decanted off leaving a deep orange crystalline solid. Pumped dry. Qualitative tests on the orange solid proved positive for both yttrium and lithium. Yield: 0.08g (30%).

Attempt to transmetallation reaction of neodymium metal with $HgPh_2$ in DME

Finely divided Nd metal (0.07g 0.5 mmol) was suspended in ~15 ml of DME and suspended in a solution of $HgPh_2$ (0.27 g, 0.76 mmol) in DME. The mixture was stirred at room temperature for 1 day, then a catalytic amount of HgI_2 was added and the mixture stirred for 10 days. The supernatant solution did not show the typical lilac colour of Nd^{3+}, suggesting that no reaction took place.

Attempt to transmetallation reaction of neodymium metal with $HgPh_2$ in thf

Finely divided Nd metal (0.32g excess) was suspended in ~25 ml of thf and a crystal of I_2 was added (brown supernatant turning yellow/green upon stirring). The resulting mixture was added $HgPh_2$ (0.50 g, 1.41 mmol) and stirred at room temperature for 6 days. As no colour change occurred the mixture was stirred at 60°C for further 3 days, allowed to settle and the supernatant was decanted off and pumped dry. Qualitative tests for the presence of neodymium in the resulting powder proved negative.

Attempt to transmetallation reaction of yttrium metal with $HgPh_2$ in thf

Yttrium metal pieces (0.24g 2.70 mmol) and $HgPh_2$ (1.43g 4.0 mmol) were mixed in ~25 ml of thf and ~0.05g YI_3 and ~0.05g HgI_2. The mixture was stirred at room temperature for 20 days, filtered and pumped dry. Qualitative tests for the presence of yttrium in the resulting white powder proved negative.

Attempt to transmetallation reaction of neodymium metal with $BiPh_3$ in thf

Finely divided Nd metal (0.30g excess) and $BiPh_3$ (1.56 g, 3.54 mmol) were mixed in ~25 ml of thf and a crystal of I_2 was added. The resulting mixture was stirred

at room T for 5 days (resulting in an increas of black bismuth powder) allowed to settle and the supernatant was decanted off and pumped dry. Qualitative tests for the presence of neodymium in the resulting grey powder proved negative.

Attempt to reaction of neodymium metal with pentafluorophenol

Nd metal powder (0.050g 0.35 mmol) and pentafluorophenol (0.163g 0.89 mmol) were mixed in ~15 ml thf and stirred at room temperature for 24h. As no reaction took place the mixture was refluxed at 80°C for 36h. Still no sign of reaction.

5.4.5 Synthesis of Calixarene Complexes

Synthesis of $(Na_2L^{iPr})_2$

NaH 60% in mineral oil (0.25 g, excess) was placed in a Schlenk, washed twice with ~15 ml 40-60 petrol, and mixed with ~10 ml thf. H_2L^{iPr} (0.3 g, 0.41 mmol) were dissolved in ~20 ml thf and added to the NaH suspension. The mixture was refluxed under nitrogen at 80°C for 4h, cooled at room temperature, allowed to settle and filtered. The pale yellow filtrate was pumped-dry, (yellow oil) dissolved in 40-60° petrol and placed in the freezer. The product was isolated as colorless cubic crystals. Yield: 0.29g (91%).

^{1}H NMR (C_6D_6): δ = 7.34 (s, 4H, ring H), 6.88 (s, 4H, ring H), 4.52 (d, 4H, $2CH_2$), 3.87 (m, 2H, 2CH ^{i}Pr), 3.17 (d, 4H, $2CH_2$), 1.55 (s, 18H, ^{t}Bu), 1.11 (m, 12H $4CH_3$ ^{i}Pr), 0.99 (s, 18H, ^{t}Bu).

Attempt to metathesis reaction of YI_3 and Na_2L^{iPr}

H_2L^{iPr} (0.234 g, 0.32 mmol) was added to a suspension of NaH (excess) in ~ 20 ml thf and refluxed at 80°C for 4h. The yellow supernatant was filtered dropwise into a suspension of YI_3 (0.150 g, 0.32 mmol) in ~30 ml thf (previously stirred for 12h).

The mixture was stirred at room temperature overnight, filtered, pumped dry and extracted into 40-60° petrol. Keeping in the freezer overnight did not result in the formation of any solid, therefore the yellow solution was pumped dry to afford a yellow oil. ^{1}H NMR spectroscopy showed it to be a mixture of $(Na_2L^{iPr})_2$ and H_2L^{iPr}.

Attempt to metathesis reaction of YI_3 and K_2L^{Me}

H_2L^{Me} (0.260 g, 0.38 mmol) and KC_8 (0.200g excess) were dissolved in $\sim$ 30 ml thf and refluxed at 80°C overnight. The yellow supernatant was filtered while hot into a suspension of YI_3 (0.180 g, 0.38 mmol) in $\sim$20 ml thf. The mixture was stirred at room temperature overnight (still unreacted YI_3 at the bottom) and then refluxed at 80°C for further 12h. The mixture was filtered and pumped dry. The crude product is insoluble in hot C_6D_6 and concentrated HCl.

Reaction of $Y\{N(TMS)_2\}_3$ with H_2L^{Me}

$Y\{N(TMS)_2\}_3$ (0.200 g, 0.35 mmol) and H_2L^{Me} (0.237 g, 0.35 mmol) were dissolved in $\sim$20 ml toluene, refluxed at 110°C for 1h, and allowed to cool down slowly (in hot water bath). The resulting colorless cubic crystals were isolated and pumped dry. Yield: 0.160g.

^{1}H NMR (C_6D_6, T=65°): δ = 7.27 (s, 4H, ring H), 6.89 (s, 4H, ring H), 4.69 (d, 4H, $2CH_2$), 3.64 (s, 6H, $2CH_3$ OMe), 3.36 (d, 4H, $2CH_2$), 1.43 (s, 18H, ^{t}Bu), 0.96 (s, 18H, ^{t}Bu).

Elemental microanalysis calculated for

$C_{138}H_{174}O_{12}Y_2$ ($Y_2L_3^{Me}$): C 75.25, H 7.96;

$C_{92}H_{117}O_8Y$ (YHL_2^{Me}): C 76.67, H 8.1;

found: C 75.68, H 8.34.

Reaction of $Y\{N(TMS)_2\}_3$ with 2 H_2L^{Me}

$Y\{N(TMS)_2\}_3$ (0.200 g, 0.35 mmol) and H_2L^{Me} (0.480 g, 0.70 mmol) were added ~30 ml toluene, refluxed at 110°C for 1h, and allowed to cool down slowly (in hot water bath). The resulting colorless cubic crystals were isolated and pumped dry. Yield: 0.205g. ^1H NMR shows the same peaks as for the 1:1 reaction.

Reaction of $Y\{N(TMS)_2\}_3$ with H_2L^{iPr}

$Y\{N(TMS)_2\}_3$ (0.150 g, 0.26 mmol) and H_2L^{iPr} (0.193 g, 0.26 mmol) were dissolved in ~20 ml toluene, refluxed at 110°C overnight. The resulting yellow solution was reduced in volume and placed in the freezer. As no solid appeared, the solution was pumped-dry, and the crude product was isolated as dirty white powder. Yield: 0.125g.

^1H NMR (C_6D_6): δ = 7.26 (s, 4H, ring H), 6.89 (s, 4H, ring H), 4.38 (d, 4H, $2CH_2$), 4.24 (m, 2H, 2CH ^iPr), 3.17 (d, 4H, $2CH_2$), 1.47 (s, 18H, ^{t}Bu), 1.39 (m, 12H $4CH_3$ ^iPr), 0.97 (s, 18H, ^{t}Bu), 0.50 (s, 18H, $2SiMe_3$).

Reaction of $Sm\{N(TMS)_2\}_3$ with 2 H_2L^{Me}

$Sm\{N(TMS)_2\}_3$ (0.125 g, 0.20 mmol) and H_2L^{Me} (0.268 g, 0.40 mmol) were dissolved in ~10 ml toluene, refluxed at 110°C for 1h, and allowed to cool down slowly (in hot water bath). The resulting colorless cubic crystals were isolated and pumped dry. Yield: 0.215g.

^1H NMR (C_6D_6, T=75°): δ = 7.50 (s, 4H, ring H), 7.38 (s, 4H, ring H), 3.23 (b, 6H, $2CH_3$ OMe), 1.50 (s, 18H, ^{t}Bu), 1.39 (s, 18H, ^{t}Bu).

Elemental microanalysis calculated for
$C_{138}H_{174}O_{12}Sm_2$ ($Sm_2L_3^{Me}$): C 71.27, H 7.54;

$C_{92}H_{117}O_8Sm$ ($SmHL_2^{Me}$): C 73.60, H 7.85;

found: C 66.00, H 7.68.

Reaction of $Sm\{N(TMS)_2\}_3$ with H_2L^{iPr}

$Sm\{N(TMS)_2\}_3$ (0.134 g, 0.21 mmol) and H_2L^{iPr} (0.155 g, 0.21 mmol) were placed in an ampoul, and ~20 ml were added. The solution was refluxed at 110°C for two days. The resulting yellow solution was pumped-dry, and the crude product was recrystallised from toluene + few milliliters of 40-60° petrol, affording a white microcrystalline solid. Yield: 0.05g.

^{1}H NMR (C_6D_6): δ = 8.24 (s, 4H, ring H), 7.89 (s, 4H, ring H), 7.59 (s, 4H, ring H), 4.65 (m, 2H, 2CH ^{i}Pr), 4.28 (d, 4H), 3.75 (s, 4H) 3.73 (d, 4H), 3.26 (d, 4H), 3.17 (d, 4H), 2.00 (s, 18H, ^{t}Bu), 1.93 (s, 18H, ^{t}Bu), 1.42 (s, 18H, ^{t}Bu), 1.28 (s, 18H, ^{t}Bu), 1.26 (m, 12H $4CH_3$ ^{i}Pr), -2.53 (s, 12H), -2.98 (b, 4H).

Reaction of $Y\{NPh_2\}_3$ with H_2L^{Me}

$Y\{NPh_2\}_3$ (0.110 g, 0.186 mmol) and H_2L^{Me} (0.118 g, 0.175 mmol) were dissolved in ~10 ml toluene and stirred at room temperature overnight. The resulting white powder was allowed to settle and the pale green supernatant was decanted off. The white solid was pumped dry. Yield: 0.105g (62%). The product is insoluble C_6D_6 at room temperature. Attempts to record the NMR spectrum at 70 °C resulted in a complicate pattern of peaks, probably due to fluxional behaviour at such temperature.

Elemental microanalysis calculated for

$C_{58}H_{68}O_4N$ ($YL^{Me}NPh_2$): C 74.74, H 7.35, N 1.50;

found: C 73.46, H 7.52, N 1.08.

Reaction of $LaCp_3$ with H_2L^{Me}

$LaCp_3$ (0.080 g, 0.24 mmol) and H_2L^{Me} (0.162 g, 0.24 mmol) were mixed with ~20 ml toluene, refluxed at 110°C for 12h, and allowed to cool down slowly (in hot water bath) and placed in the freezer. The resulting white solid was isolated and pumped dry. Yield: 0.115g (54%). The product is insoluble in hot C_6D_6.

Reaction of $LaCp_3$ with H_2L^{iPr}

$LaCp_3$ (0.090 g, 0.27 mmol) and H_2L^{Me} (0.200 g, 0.27 mmol) were mixed with ~20 ml toluene, refluxed at 110°C for 12h. The reaction mixture was evaporated and the white solid was washed with minimum amount of 40-60° petrol and pumped dry. Yield: 0.093g (37%).

^{1}H NMR (C_6D_6): $\delta = 7.29$ (s, 4H, ring H), 6.75 (s, 4H, ring H), 6.46 (s, 5H, Cp), 4.50 (d, 4H, $2CH_2$), 3.99 (m, 2H, 2CH ^{i}Pr), 3.07 (d, 4H, $2CH_2$), 1.46 (s, 18H, ^{t}Bu), 1.28 (m, 12H, $4CH_3$ ^{i}Pr), 0.82 (s, 18H, ^{t}Bu).

Reaction of YCp_3 with H_2L^{iPr}

YCp_3 (0.214 g, 0.75 mmol) and H_2L^{iPr} (0.553 g, 0.75 mmol) were mixed with ~20 ml toluene, refluxed at 110°C for two days (red-orange solution) and pumped-dry. The mixture (white powder + orange oil) was washed with ~10 ml 40-60° petrol and the resulting white solid (1^{st} crop) was pumped dry. The orange washing was reduced in volume and placed in the freezer overnight, resulting in the precipitation of more white solid (2^{nd} crop). Yield: 0.33g (49%).

^{1}H NMR (C_6D_6): $\delta = 7.24$ (s, 4H, ring H), 6.82 (s, 4H, ring H), 6.71 (s, 5H, Cp), 4.64 (m, 2H, 2CH ^{i}Pr), 4.27 (d, 4H, $2CH_2$), 3.07 (d, 4H, $2CH_2$), 1.49 (s, 18H, ^{t}Bu), 1.19 (m, 12H $4CH_3$ ^{i}Pr), 0.99 (s, 18H, ^{t}Bu).

References

1. Edelmann, F. T.; Lorenz, V. *Coord. Chem. Rev.* **2000,** *209,* 99.

2. Evans, W. J. *Coord. Chem. Rev.* **2000,** *206,* 263.

3. Schaverien, C. J. *Adv. Organomet. Chem.* **1994,** *36,* 283.

4. Cloke, F. G. N. *Chem. Soc. Rev.* **1993,** *22,* 17.

5. Evans, W. J. *Polyhedron* **1987,** *6,* 803.

6. Hart, F. A. Scandium, Yttrium and the Lanthanides. In *Comprehensive Coordination Chemistry*; Pergamon Press: Oxford, 1987.

7. Kaltsoyannis, N.; Scott, P. *The f-Elements;* Oxford University Press: Oxford, 1999.

8. Hong, G. Y.; Dolg, M.; Li, L. M. *Chem. Phys. Lett.* **2001,** *334,* 396.

9. Hong, G. Y.; Dolg, M.; Li, L. M. *Int. J. Quantum Chem.* **2000,** *80,* 201.

10. Liu, W.; Dolg, M. *Phys. Rev. A* **1998,** *57,* 1721.

11. Cundari, T. R.; Saunders, L. C. *J. Chem. Inf. Comput. Sci.* **1998,** *38,* 523.

12. Dolg, M.; Fulde, P.; Stoll, H.; Preuss, H.; Chang, A.; Pitzer, R. *Chem. Phys.* **1995,** *195,* 71.

13. Seth, M.; Dolg, M.; Fulde, P.; Shwerdtfeger, P. *J. Am. Chem. Soc.* **1995,** *117,* 6597.

14. Pepper, M.; Bursten, B. E. *Chem. Rev.* **1991,** *91,* 719.

15. Shannon, R. D. *Acta Crystallogr. Sect. A* **1976,** *32,* 751.

16. Quadrelli, E. A. *Inorg. Chem.* **2002,** *41,* 167.

17. Kaltsoyannis, N. *J. Chem. Soc.-Dalton. Trans.* **1997,** 1.

18. Hitchcock, P. B.; Lappert, M. F.; Singh, A. *Chem. Commun.* **1983,** 1499.

19. Schaverien, C. J.; Meijboom, N.; Orpen, G. *Chem. Commun.* **1992,** *2,* 124.

20. Clark, D. L.; Gordon, J. C.; Huffman, J. C.; Vincent, R. L.; Watkin, J. G. *Inorg. Chem.* **1994,** *33,* 5903.

21. Bradley, D. C.; Ghotra, J. S.; Hart, F. A. *J. Chem. Soc.-Dalton Trans.* **1973,** 1021.

22. Aspinall, H. C.; Tillotson, M. R. *Polyhedron* **1994,** *13,* 3229.

23. Minhas, R. K.; Ma, Y. L.; Song, J. I.; Gambarotta, S. *Inorg. Chem.* **1996,** *35,* 1866.

24. Evans, W. J.; Ansari, M. A.; Ziller, J. W.; Khan, S. I. *Inorg. Chem.* **1996,** *35,* 5435.

25. Schumann, H.; Meesemarktscheffel, J. A.; Esser, L. *Chem. Rev.* **1995,** *95,* 865.

26. Cotton, S. A. *Coord. Chem. Rev.* **1997,** *160,* 93.

27. Edelmann, F. T. *Angew. Chem. Int. Ed. Engl.* **1995,** *34,* 2466.

28. Bochkarev, L. N.; Stepantseva, T. A.; Zacharov, L. N.; Fukin, G. K.; Yanovsky, A. I.; Struchkof, Y. T. *Organometallics* **1995,** *14,* 2127.

29. Cotton, S. A.; Hart, F. A.; Hartshouse, M. B.; Welch, A. J. *Chem. Commun.* **1972,** 1225.

30. Hitchcock, P. B.; Lappert, M. F.; Smith, G.; Bartlett, R. A.; Power, P. P. *Chem. Commun.* **1988,** *15,* 1007.

31. Rabe, G. W.; Riede, J.; Schier, A. *Organometallics* **1996,** *15,* 439.

32. Rabe, G. W.; Ziller, J. W. *Inorg. Chem.* **1995,** *34,* 5378.

33. Rabe, G. W.; Yap, G. P. A.; Rheingold, A. L. *Inorg. Chem.* **1995,** *34,* 4521.

34. Tilley, T.; Andersen, R.; Zalkin, A. *Inorg. Chem.* **1983,** *22,* 856.

35. Fryzuk, M.; Haddad, T.; Rettig, S. *Organometallics* **1992,** *11,* 2967.

36. Cary, D.; Ball, G.; Arnold, J. *J. Am. Chem. Soc.* **1995,** *117,* 3492.

37. Recknagel, A.; Noltemeyer, M.; Stalke, D.; Pieper, U.; Schmidt, H. G.; Edelmann, F. T. *J. Organomet. Chem.* **1991,** *411,* 347.

38. Berg, D. J.; Andersen, R. A.; Zalkin, A. *Organometallics* **1988,** *7,* 1858.

39. Hillier, A. C.; Liu, S. W.; Sella, A.; Elsegood, M. R. J. *Inorg. Chem.* **2000,** *39,* 2635.

40. Hillier, A. C.; Liu, S. W.; Sella, A.; Elsegood, M. R. J. *J. Alloys Compds.* **2000,** *303,*.

41. Berardini, M.; Lee, J.; Freedman, D.; Lee, J.; Emge, T. J.; Brennan, J. G. *Inorg. Chem.* **1997,** *36,* 5772.

42. Lee, J.; Brewer, M.; Berardini, M.; Brennan, J. G. *Inorg. Chem.* **1995,** *34,* 3215.

43. Freedman, D.; Melman, J. H.; Emge, T. J.; Brennan, J. G. *Inorg. Chem.* **1998,** *37,* 4162.

44. Kornienko, A.; Emge, T. J.; Hall, G.; Brennan, J. G. *Inorg. Chem.,* in press.

45. Evans, W. J.; Hanusa, T. P.; Levan, K. R. *Inorg. Chim. Acta* **1985,** *110,* 191.

46. Evans, W.; Drummond, D.; Hughes, L.; Zhang, H.; Atwood, J. *Polyhedron* **1988,** *7,* 1693.

47. Zalkin, A.; Henly, T. J.; Andersen, R. A. *Acta Crystallogr., Sect.C (Cr.Str.Comm.)* **1987,** *43,* 233.

48. Klooster, W. T.; Brammer, L.; Schaverien, C. J.; Budzelaar, P. H. M. *J. Am. Chem. Soc.* **1999,** *121,* 1381.

49. Evans, W. J.; Allen, N. T.; Ziller, J. W. *J. Am. Chem. Soc.* **2001,** *123,* 7927.

50. Ganesan, M.; Gambarotta, S.; Yap, G. P. A. *Angew. Chem. Int. Ed. Engl.* **2001,** *40,* 766.

51. Dube, T.; Ganesan, M.; Conoci, S.; Gambarotta, S.; Yap, G. P. A. *Organometallics* **2000,** *19,* 3716.

52. Jubb, J.; Gambarotta, S. *J. Am. Chem. Soc.* **1994,** *116,* 4477.

53. Evans, W. J.; Ulibarri, T.; Ziller, J. W. *J. Am. Chem. Soc.* **1988,** *110,* 6877.

54. Hillier, A. C.; Liu, S. Y.; Sella, A.; Zekria, O.; Elsegood, M. R. J. *J. Organomet. Chem.* **1997,** *528,* 209.

55. Hillier, A. C.; Sella, A.; Elsegood, M. R. J. *J. Chem. Soc.-Dalton Trans.* **1998,** 3871.

56. Dube, T.; Guan, J. W.; Gambarotta, S.; Yap, G. P. A. *Chem.-Eur. J.* **2001,** *7,* 374.

57. Dube, T.; Gambarotta, S.; Yap, G. P. A. *Angew. Chem. Int. Ed. Engl.* **1999,** *38,* 1432.

58. Izod, K. *Angew. Chem. Int. Ed.* **2002,** *41,* 743.

59. Arnold, P. L.; Cloke, F. G. N.; Hitchcock, P. B. *Chem. Commun.* **1997,** *5,* 481.

60. Brennan, J. G.; Cloke, F. G. N.; Sameh, A. A.; Zalkin, A. *J. Chem. Soc., Chem. Commun.* **1987,** *21,* 1668.

61. Fermi, E. *Z. Phys.* **1928,** *48,* 73.

62. Thomas, L. H. *Proc. Cambridge Phil. Soc.* **1927,** *23,* 542.

63. Parr, R. G.; Yang, W. *Density-Functional Theory of Atoms and Molecules;* Oxford University Press: Oxford, 1989.

64. Hohenberg, P.; Kohn, W. *Phys. Rev. B* **1964,** *136,* 864.

65. Kohn, W.; Sham, L. J. *Phys Rev. A* **1965,** *140,* 1133.

66. Dahl, J. P.; Avery, J. *Local Density Approximation in Quantum Chemistry and Solid State Physics;* Plenum: New York and London, 1984.

67. Becke, A. *Phys. Rev. A* **1988,** *38,* 3098.

68. Kohn, W.; Becke, A. D.; Parr, R. G. *J. Phys. Chem.* **1996,** *100,* 12974.

69. Ziegler, T. *Chem. Rev.* **1991,** *91,* 651.

70. Becke, A. D. *J. Chem. Phys.* **2000,** *112,* 4020.

71. Boese, A. D.; Doltsinis, N. L.; Handy, N. C.; Sprik, M. *J. Chem. Phys.* **2000,** *112,* 1670.

72. Perdew, J. P.; Kurth, S.; Zupan, A.; Blaha, P. *Phys. Rev. Lett.* **1999,** *82,* 5179.

73. Ivanov, S.; Hirata, S.; Bartlett, R. J. *Phys. Rev. Lett.* **1999,** *83,* 5455.

74. Gritsenko, O. V.; Schipper, P. R.; Baerends, E. J. *J. Chem. Phys* **1997,** *107,* 5007.

75. Levine, I. N. *Quantum Chemistry;* Prentice Hall: Englewood Cliffs, N.J., 2000.

76. Atkins, P. W.; Friedman, R. S. *Molecular Quantum Mechanics;* Oxford University Press: Oxford; New York, 1997.

77. March, N. H. *Adv. Phys.* **1957,** *6,* 1.

78. Lieb, E. H. *Rev. Mod. Phys.* **1981,** *53,* 603.

79. Cohen, A. J.; Handy, N. H. *Chem. Phys. Lett.* **2000,** *316,* 160.

80. Dirac, P. A. M. *Proc. Cambridge. Phil. Soc.* **1930,** *26,* 376.

81. Ceperley, D. M.; Alder, B. J. *Phys. Rev. Lett.* **1980,** *45,* 566.

82. Vosko, S. H.; Wilk, L.; Nusair, M. *Can. J. Phys.* **1980,** *58,* 1200.

83. Von Barth, U.; Hedin, L. *J. Phys. C* **1972,** *5,* 1629.

84. Gunnarsson, O.; Lundqvist, B. I. *Phys. Rev. B* **1976,** *13,* 4274.

85. Perdew, J. P.; Wang, Y. *Phys. Rev. B* **1986,** *33,* 8800.

86. Lee, C.; Yang, W.; Parr, R. G. *Phys. Rev. B* **1988,** *37,* 785.

87. Perdew, J. P. *Phys. Rev. B* **1986,** *33,* 8822.

88. Perdew, J. P.; Wang, Y. *Phys. Tev. B* **1992,** *45,* 13244.

89. Perdew, J. P.; Burke, K.; Ernzerhof, M. *Phys. Rev. Lett.* **1996,** *77,* 3865.

90. Hammer, B.; Hansen, L. B.; Norskov, J. K. *Phys. Rev. B* **1999,** *59,* 7413.

91. Zhang, Y.; Yang, W. *Phys. Rev. Lett.* **1998,** *80,* 890.

92. Becke, A. D. *J. Chem. Phys.* **1998,** *109,* 2092.

93. Perdew, J. P.; Kurth, S.; Zupan, A.; Blaha, P. *Phys. Rev. Lett.* **1999,** *82,* 2544.

94. Van Voorhis, T.; Scuseria, G. E. *J. Chem. Phys.* **1998,** *109,* 400.

95. Pyykkö, P. *Chem. Rev.* **1988,** *88,* 563.

96. Ziegler, T.; Snijders, J. G.; Baerends, E. J. *Chem. Phys. Lett.* **1980,** *75,* 1.

97. Snijders, J. G.; Pyykkö, P. *Chem. Phys. Lett.* **1980,** *75,* 5.

98. Ziegler, T.; Snijders, J. G.; Baerends, E. J. *J. Chem. Phys.* **1981,** *74,* 1271.

99. van Lenthe, E.; Baerends, E. J.; Snijders, J. G. *J. Chem. Phys.* **1996,** *105,* 2373.

100. van Wüllen, C. *J. Comp. Chem.* **1999,** *20,* 51.

101. Snijders, J. G.; Baerends, E. J. *Mol. Phys.* **1978,** *36,* 1789.

102. Li, J.; Scnreckenbach, G. *J. Am. Chem. Soc.* **1995,** *117,* 486.

103. van Lenthe, E.; Ehlers, A. H.; Baerends, E. J. *J. Chem. Phys.* **1999,** *110,* 8943.

104. Kahn, L. R.; Hay, P. J.; Cowan, R. D. *J. Chem. Phys.* **1978,** *68,* 2386.

105. Dolg, M.; Liu, W.; Kalvoda, S. *Int. J. Quantum Chem.* **2000,** *76,* 359.

106. Wang, S. G.; Schwarz, W. H. E. *J. Phys. Chem.* **1995,** *99,* 11687.

107. Laerdahl, J. K.; Faegri, K.; Visscher, L.; Saue, T. *J. Chem. Phys.* **1998,** *109,* 10806.

108. Kuchle, W.; Dolg, M.; Stoll, H. *J. Phys. Chem. A* **1997,** *101,* 7128.

109. Edelstein, N. M.; Allen, P. G.; Bucher, J. J.; Shuh, D. K.; Sofield, C. D.; Kaltsoyannis, N.; Maunder, G. H.; Russo, M. R.; Sella, A. *J. Am. Chem. Soc.* **1996,** *118,* 13115.

110. Hong, G.; Schautz, F.; Dolg, M. *J. Am. Chem. Soc.* **1999,** *121,* 1502.

111. Li, J.; Bursten, B. E. *J. Am. Chem. Soc.* **1999,** *121,* 10243.

112. King, W. A.; Bella, S. D.; Lanza, G.; Khan, K.; Duncalf, D. J.; Cloke, F. G. N.; Fragala', I. F.; Marks, T. J. *J. Am. Chem. Soc.* **1996,** *118,* 627.

113. Nagle, J. K.; Balch, A. L. *J. Am. Chem. Soc.* **1988,** *110,* 319.

114. Ezomo, O. J.; Mingos, M. P.; Williams, I. D. *Chem. Commun.* **1987,** 924.

115. Hao, L.; Vittal, J. J.; Puddephat, R. J. *Inorg. Chem.* **1996,** *35,* 269.

116. Hao, L.; Xiao, J.; Vittal, J. J.; Puddephat, R. J. *Inorg. Chem.* **1996,** *35,* 658.

117. Maliarik, M.; Berg, K.; Glaser, J.; Sandström, M.; Tóth, I. *Inorg. Chem.* **1998,** *37,* 2910.

118. Maliarik, M.; Glaser, J.; Tóth, I.; da Silva, M. W.; Zekany, L. *Eur. J. Inorg. Chem.* **1998,** 565.

119. Jalilehvand, F.; Maliarik, M.; Sandström, M.; Mink, J.; Persson, I.; Persson, P.; Tóth, I.; Glaser, J. *Inorg. Chem.* **2001,** *40,* 3889.

120. Jalilehvand, F.; Eriksson, L.; Glaser, J.; Maliarik, M.; Mink, J.; Sandström, M.; Tóth, I.; Tóth, J. *Chem. Eur. J.* in press.

121. Ziegler, T.; Nagle, J. K.; Snijders, J. G.; Baerends, E. J. *J. Am. Chem. Soc.* **1989,** *111,* 5631.

122. Balch, A.; Rowley, S. P. *J. Am. Chem. Soc.* **1990,** *112,* 6139.

123. Pyykkö, P.; Wiesenfeld, L. *Mol. Phys.* **1981,** *43,* 557.

124. Jameson, C. J. *Multinuclear NMR;* Plenum Press: New York, 1987.

125. ADF 2.3, Department of Theoretical Chemistry, Vrije Universiteit, Amsterdam, 1997.

126. te Velde, G.; Baerends, E. J. *J. Comput. Phys.* **1992,** *99,* 84.

127. Ziegler, T.; Tschinke, V.; Baerends, E. J.; Snijders, J.; Ravenek, W. *J. Phys. Chem.* **1989,** *93,* 3050.

128. Mulliken, R. S. *J. Chem. Phys* **1955,** *23,* 1833.

129. Blixt, J.; Glaser, J.; Mink, J.; Persson, I.; Persson, P.; Sandström, M. *J. Am. Chem. Soc.* **1995,** *117,* 5089.

130. Dolg, M.; Pyykkö, P.; Runeberg, N. *Inorg. Chem.* **1996,** *35,* 7450.

131. Pearson, R. G. *Chemical Hardness;* Wiley: New York, 1997.

132. Depaoli, G.; Russo, U.; Valle, G.; Grandjean, F.; Williams, A.; Long, G. *J. Am. Chem. Soc.* **1994,** *116,* 5999.

133. Nugent, L.; Laubereau, P.; Werner, G.; van der Sluis, K. *J. Organomet. Chem.* **1971,** *27,* 365.

134. Hazin, P.; Bruno, J.; Brittain, H. *Organometallics* **1987,** *6,* 913.

135. Kaltsoyannis, N.; Bursten, B. E. *J. Organomet. Chem.* **1997,** *528,* 19.

136. Li, L. *Abs. Pap. Am. Chem. Soc.* **2000,** *220,* 317-INOR, Part 1.

137. Maron, L.; Eisenstein, O. *J. Phys. Chem. A* **2000,** *104(30),* 7140.

138. Nief, F. *Coord. Chem. Rev.* **1998,** *180,* 13.

139. Radu, N. S.; Tilley, T. D.; Rheingold, A. L. *J. Am. Chem. Soc.* **1992,** *114,* 8293.

140. Schumann, H.; Meese-Marktscheffel, J. A.; Hahn, F. E. *J. Organomet. Chem.* **1990,** *390,* 301.

141. Zakarov, L.; Struchkov, Y. T. *J. Organomet. Chem.* **1997,** *536,* 65.

142. Schumann, H.; Nickel, S.; Loebel, J.; Pickardt, J. *Organometallics* **1988,** *7,* 2004.

143. Howard, W. A.; Trnka, T. M.; Parkin, G. *Inorg. Chem.* **1995,** *34,* 5900.

144. Ashby, M.; Alguindigue, S.; Khan, M. *Inorg. Chim. Acta* **1998,** *270,* 227.

145. Mountford, P.; Swallow, D. *J. Chem. Soc., Chem. Commun.* **1995,** *22,* 2357.

146. Steffey, B.; Fanwick, P.; Rothwell, I. *Polyhedron* **1990,** *9,* 963.

147. Coffindaffer, T.; Steffey, P.; Rothwell, I.; Folting, K.; Huffmann, J.; Streib, W. *J. Am. Chem. Soc.* **1989,** *111,* 4742.

148. Huheey, J. E. *Inorganic Chemistry: principles of structure and reactivity;* Harper & Row: New York, 1983.

149. Shomaker, V.; Stephenson, D. P. *J. Am. Chem. Soc.* **1941,** *63,* 37.

150. Baerends, E. J.; Ellis, D. E.; Ros, P. *Chem. Phys.* **1973,** *2,* 41.

151. Versluis, L.; Ziegler, T. *J. Chem. Phys.* **1988,** *88,* 322.

152. Fonseca Guerra, C.; Snijders, J. G.; te Velde, G.; Baerends, E. J. *Theor. Chem. Acc.* **1998,** *99,* 391.

153. Hirshfeld, F. L. *Theoret. Chim. Acta* **1977,** *44,* 129.

154. Bickelhaupt, F. M.; van Eikema Hommes, N. J. R.; Fonseca Guerra, C.; Baerends, E. J. *Organometallics* **1996,** *15,* 2923.

155. Schaftenaar, G.; Noordik, J. H. *J. Comput.-Aided Mol. Design* **2000,** *14,* 123.

156. Kaltsoyannis, N.; Russo, M. R., submitted for publication in *J. Nucl. Sci. Tech.*

157. Tobisch, S.; Nowak, T.; Bogel, H. *J. Organomet. Chem.* **2001,** *619,* 24.

158. Melman, J. H.; Emge, T. J.; Brennan, J. G. *Inorg. Chem.* **2001,** *40,* 1078.

159. Gutsche, C. D. *Calixarenes;* The Royal Society of Chemistry: Cambridge, 1989.

160. Böhmer, V. *Angew. Chem. Int. Ed. Engl.* **1995,** *34,* 713.

161. Thondorf, I.; Brenn, J. *Theochem J. Molec. Struct.* **1997,** *398,* 307.

162. Webber, P. R. A.; Chen, G. Z.; Drew, M. G. B.; Beer, P. D. *Angew. Chem. Int. Ed.* **2001,** *40,* 2265.

163. Atwood, J. L.; Gardiner, M. G.; Jones, C.; Raston, C. L.; Skelton, B. W.; White, A. H. *Chem Commun* **1996,** 2487.

164. Gardiner, M. G.; Lawrence, S. M.; Raston, C. L.; Skelton, B. W.; White, A. H. *Chem. Commun.* **1996,** 2491.

165. Wieser, C.; Dieleman, C. B.; Matt, D. *Coord. Chem. Rev.* **1997,** *165,* 93.

166. Roundhill, D. M. *Prog. Inorg. Chem.* **1995,** *43,* 533.

167. Rebek, J. *Chem. Commun.* **2000,** 637.

168. Arnaud Neu, F. *Chem. Soc. Rev.* **1994,** *23,* 235.

169. Arnaud Neu, F.; Browne, J. K.; Byrne, D.; Marrs, D. J.; McKervey, M. A.; O'Hagan, P.; Schwing Weill, M. J.; Walker, A. *Chem. Eur. J.* **1999,** *5,* 175.

170. Korovin, Y.; Rusakova, N. *Rev. Inorg. Chem.* **2001,** *21,* 299.

171. Piguet, C.; Bünzli, J. C. G. *Chem. Soc. Rev.* **1999,** *28,* 347.

172. Froidevaux, P.; Bünzli, J. C. G. *J. Phys.. Chem.* **1994,** *98,* 532.

173. Bünzli, J. C.; Ihringer, F.; Dumy, P.; Sager, C.; Rogers, R. D. *J. Chem. Soc.-Dalton Trans.* **1998,** 497.

174. Le Saulnier, L.; Varbanov, S.; Scopelliti, R.; Elhabiri, M.; Bünzli, J. C. G. *J. Chem. Soc.-Dalton Trans.* **1999,** 3919.

175. Baaden, M.; Burgard, M.; Wipff, G. *Phys. Chem. Chem. Phys.* **2001,** *3,* 1317.

176. de Namor, A. F. D.; Jafou, O. *J. Phys. Chem. B* **2001,** *105,* 8018.

177. Furphy, B. M.; Harrowfield, J. M.; Kepert, D. L.; Skelton, B. W.; White, A. H.; Wilmer, F. R. *Inorg. Chem.* **1987,** *26,* 4231.

178. Furphy, B. M.; Harrowfield, J. M.; Ogden, M. I.; Skelton, B. W.; White, A. H.; Wilmer, F. R. *J. Chem. Soc.-Dalton Trans.* **1989,** 2217.

179. Corazza, F.; Floriani, C.; Chiesi Villa, A.; Guastini, C. *Chem. Commun.* **1990,** 640.

180. Corazza, F.; Floriani, C.; Chiesi Villa, A.; Guastini, C. *Chem. Commun.* **1990,** 1083.

181. Gibson, V. C.; Redshaw, C.; Clegg, W.; Elsegood, M. R. J. *Chem. Commun.* **1995,** 2371.

182. Zanotti Gerosa, A.; Solari, E.; Giannini, L.; Floriani, C.; Chiesi Villa, A.; Rizzoli, C. *Chem. Commun.* **1996,** 119.

183. Chisholm, M. H.; Folting, K.; Streib, W. E.; Wu, D. *Chem. Commun.* **1998,** 379.

184. Giannini, L.; Solari, E.; Zanotti Gerosa, A.; Floriani, C.; Chiesi Villa, A.; Rizzoli, C. *Angew. Chem. Int. Ed. Engl.* **1997,** *36,* 753.

185. Acho, J.; Ren, T.; Sun, J.; Lippard, S. *Inorg. Chem.* **1995,** *34,* 5266.

186. Zanotti Gerosa, A.; Solari, E.; Giannini, L.; Floriani, C.; Chiesi Villa, A.; Rizzoli, C. *Chem. Commun.* **1997,** 183.

187. Giannini, L.; Caselli, A.; Solari, E.; Floriani, C.; Chiesi Villa, A.; Rizzoli, C.; Re, N.; Sgamellotti, A. *J. Am. Chem. Soc.* **1997,** *119,* 9709.

188. Gibson, V. C.; Redshaw, C.; Elsegood, M. R. J. *J. Chem. Soc.-Dalton Trans.* **2001,** 767.

189. Floriani, C. The M-C bond functionalities bonded to an oxo-surface modeled by calix[4]arenes. In *Advances in Organometallic Chemistry,* Vol. 47;.

190. Anwander, R.; Eppinger, J.; Nagl, I.; Scherer, W.; Tafipolsky, M.; Sirsch, P. *Inorg. Chem.* **2000,** *39,* 4713.

191. Floriani, C. *Chem.-Eur. J.* **1999,** *5,* 19.

192. Dubberley, S. R.; Blake, A. J.; Mountford, P. *Chem. Commun.* **1997,** *17,* 1603.

193. Abidi, R.; Baker, M. V.; Harrowfield, J. M.; Ho, D. S. C.; Richmond, W. R.; Skelton, B. W.; White, A. H.; Varnek, A.; Wipff, G. *Inorg. Chim. Acta* **1996,** *246,* 275.

194. Schmitt, P.; Beer, P. D.; Drew, M. G. B.; Scheen, P. D. *Angew. Chem. Int. Ed. Engl.* **1997,** *37,* 1840.

195. Gibson, V. C.; Redshaw, C.; Clegg, W.; Elsegood, M. R. J. *Chem. Commun.* **1997,** 1605.

196. Bünzli, J. C. G.; Froidevaux, P.; Harrowfield, J. M. *Inorg. Chem.* **1993,** *32,* 3306.

197. Hazekamp, M. F.; Blasse, G.; Sabbatini, N.; Ungaro, R. *Inorg. Chim. Acta* **1990,** *172,* 93.

198. Sabbatini, N.; Guardigli, M.; Mecati, A.; Balzani, V.; Ungaro, R.; Ghidini, E.; Casnati, A.; Pochini, A. *J. Chem. Soc. Chem. Commun.* **1990,** 878.

199. Rudkevich, D. M.; Verboom, W.; Vandertol, E.; Van Staveren, C. J.; Kaspersen, F. M.; Verhoeven, J. W.; Reinhoudt, D. N. *J. Chem. Soc. Perkin Trans.* **1995,** *2,* 131.

200. Steemers, F. J.; Verboom, W.; Reinhoudt, D. N.; Vandertol, E.; Verhoeven, J. W. *J. Am. Chem. Soc.* **1995,** *117,* 9408.

201. Casnati, A.; Fisher, C.; Guardigli, M.; Isernia, A.; Manet, I.; Sabbatini, N.; Ungaro, R. *J. Chem. Soc. Perkin Trans.* **1996,** *2,* 395.

202. Froidevaux, P.; Harrowfield, J. M.; Sobolev, A. N. *Inorg. Chem.* **2000,** *39,* 4678.

203. Beer, P. D.; Drew, M. G. B.; Kan, M.; Leeson, P. B.; Ogden, M. I.; Williams, G. *Inorg. Chem.* **1996,** *35,* 2202.

204. Ohto, K.; Yano, M.; Inoue, K.; Nagasaki, T.; Goto, M.; Nakashio, F.; Shinkai, S. *Polyhedron* **1997,** *26,* 1655.

205. Harrowfield, J. M.; Peachey, M. M. B. J. *J. Chem. Soc.-Dalton Trans.* **1996,** 1687.

206. Leverd, P. C.; Berhault, P.; Lance, M.; Nierlich, M. *Eur. J. Inorg. Chem.* **1998,** 1859.

207. Fedushkin, I. L.; Weydert, M.; Fagin, A. A.; Nefedov, S. E.; Eremenko, I. L.; Bochkarev, M. N.; Schumann, H. *Z. Naturforsch. (B)* **1999,** *54,* 466.

208. Leverd, P. C.; Rinaldo, D.; Nierlich, M. *Eur. J. Inorg. Chem.* **2001,** 2021.

209. Evans, W. J.; Anwander, R.; Doedens, R. J.; Ziller, J. W. *Angew. Chem. Int. Ed. Engl.* **1994,** *33,* 1641.

210. Wong, W. K.; Zhang, L.; Xue, F.; Mak, T. C. W. *Polyhedron* **1997,** *16,* 2013.

211. Wong, W. K.; Zhang, L.; Xue, F.; Mak, T. C. W. *Polyhedron* **1997,** *16,* 345.

212. Click, D. R.; Scott, B. L.; Watkin, J. G. *Chem. Commun.* **1999,** *7,* 633.

213. Wilkinson, G.; Birmingham, J. M. *J. Am. Chem. Soc.* **1954,** *76,* 6210.

214. Hart, F. A.; Massey, A. G.; Saran, M. S. *J. Organomet. Chem.* **1970,** *21,* 147.

215. Gilman, H.; Jones, R. G. *J. Org. Chem.* **1945,** *10,* 505.

216. Schumann, H.; Lauke, H.; Hahn, E.; Pickardt, J. *J. Organomet. Chem.* **1984,** *263,* 29.

217. Wayda, A. L.; Evans, W. J. *J. Am. Chem. Soc.* **1978,** *100,* 7119.

218. Evans, W. J.; Drummond, D. K.; Hanusa, T. P.; Olofson, J. M. *J. Organomet. Chem.* **1989,** *376,* 311.

219. Deacon, G. B.; Vince, D. G. *J. Organomet. Chem.* **1976,** *112,* C1.

220. Deacon, G. B.; Raverty, W. D.; Vince, D. G. *J. Organomet. Chem.* **1977,** *135,* 103.

221. Deacon, G. B.; Koplick, A. J.; Raverty, W. D.; Vince, D. G. *J. Organomet. Chem.* **1979,** *182,* 121.

222. Hitchcock, P. B.; Holmes, S. A.; Lappert, M. F.; Tian, S. *Chem. Commun.* **1994,** 2691.

223. Eaborn, C.; Hitchcock, P. B.; Izod, K.; Smith, J. D. *J. Am. Chem. Soc.* **1994,** *116,* 12071.

224. Deacon, G. B.; Feng, T.; Forsyth, C. M.; Gitlits, A.; Hockless, D. C. R.; Shen, Q.; Skeloton, B. W.; White, A. H. *J. Chem. Soc.-Dalton Trans.* **2000,** 961.

225. Hubert Pfalzgraf, L. G.; Daniele, S.; Bennaceur, A.; Daran, J. C.; Vaissermann, J. *Polyhedron* **1997,** *16,* 1223.

226. Mehrotra, R. C.; Singh, A.; Tripathi, U. M. *Chem. Rev.* **1991,** *91,* 1287.

227. Gutsche, C. D. *J. Org. Chem.* **1986,** *51,* 742.

228. Gehrhus, B.; Hitchcock, P. H.; Kennedy, A. R.; Lappert, M. F.; Mulvey, R. E.; Rodger, P. J. A. *J. Organomet. Chem.* **1999,** *587,* 88.

229. Calderazzo, F.; Pappalardo, R.; Losi, S. *J. Inorg. Nucl. Chem.* **1966,** *28,* 987.